#8

AP E4018

Superconductivity Experiment

Superconductivity may become one of the most significant innovations of modern times. This is a result of very recent discoveries of high temperature superconductors which may revolutionize everything from electrical generation and transmission to high-speed computers to controlled fusion generating plants.

In this experiment, you will investigate the superconductivity of the new Y-Ba-Cu-O compound system as a function of temperature and magnetic field. The most important question should should answer is "What is the resistance of the superconductor as the temperature and applied magnetic field are changed?" Other questions which you will not be able to answer are related to the determination of current density which can pass through the material and the mechanical strength and elasticity of the material.

Attached to these notes are some articles which describe aspects of superconductivity and the results of recent measurements of the Y-Ba-Cu-O compound made by Prof. M. K. Wu and co-workers. These will provide background for the experiments that you will be performing. Pay particular attention to Prof. Wu's article. Their measurements are identical to those that you can obtain with the equipment supplied in the laboratory. Next, look over the description of type 1 and type 2 superconductors given by Gennes in *Superconductivity in Metals and Alloys.* and in Eisberg and Resnick Type 1 superconductors have a "correlation length" between conduction electrons (denoted by the symbol, ξ_0) much longer than the magnetic field penetration length (denoted by λ_0). They generally have a very abrupt critical field, H_c, below which the material is superconducting and excludes all magnetic flux. (H_c is a function of temperature.) This "perfect diamagnetism" is characteristic of the superconducting state. Type 2 superconductors have $\lambda_0 > \xi_0$ and have a more gradual transition to this superconducting state. They are described by three critical magnetic fields. Below H_{c1} (the lowest critical field), a type 2 superconductor has no resistance and, like a type 1 superconductor, excludes flux. Between H_{c1} and H_{c2}, the resistance is very low, but finite, and the superconductor partially excludes flux. Between H_{c2} and H_{c3}, the resistance is low, but no flux is excluded. Finally, above the highest of the three critical fields, H_{c3}, the material is no longer superconducting.

Description

The Y-Ba-Cu-O compound becomes superconducting between 77 and 85 °K. This makes the cryogenic aspects of these experiment very easy compared with experiments using more conventional superconductors that require temperatures below 22 °K. Liquid nitrogen is relatively inexpensive and a styrofoam thermos is all that is required to store it for several hours.

We have built three LN_2 containers for you, and these are large enough to hold stainless-steel and copper "sample stands". The sample stands cool the

superconducting sample and provide a stable base to make your measurements. Also, attached to each sample is a calibrated temperature sensor so that you can measure the sample at all times. Be careful to note that if the rate of change of the temperature is too rapid, then a temperature difference will develop between the superconductor and the sample.

The superconductor is provided in two geometries. First, a small disk (with a small hole drilled into its center) can be used to study the Meissner effect. We have provided permanent magnetics which can be levitated and an inductor which can be used to measure changes in the permeability of the superconductor. The second sample is a short rectangular rod onto which four electrical leads are attached in order to measure the electrical resistivity. Finally, a very large solenoid has been made which can provide a 1.2 kG field to the rod enabling measurements of the transition temperature and resistance as a function of applied magnetic field.

Suggested Experiments

The main goal of your experiments will be to characterize the electrical resistance and the magnetic properties of the Y-Ba-Cu-O samples as a function of temperature and applied magnetic field strength. A reasonable schedule for your experiments, accomplishing these goals, is shown below:

WEEK 1: First, familiarize yourself with the experimental setup, diagnostics, power supplies, and the temperature and magnetic field monitors. Then, using the disk-like sample, examine the magnetic properties of Y-Ba-Cu-O. You should monitor the temperature of the sample while, at the same time, determining the ability of the sample to levitate a magnet. Next, place the wire inductor around the sample and determine the change of the coil's inductance as a function of temperature. How do these measurements relate to the Meissner effect? ~~If you have time,~~ You should also measure the ability of the sample to retain flux. This can be done by first passing current through the coil while the sample's temperature is above the critical temperature and then reducing the field below T_c after which you can turn off the current in the coil, retaining flux within the hallow superconductor. Contrast this result with your knowledge of the Meissner effect. What is the role of the sample's geometry?

WEEK 2 → WEEK 3: Setup the experiment to measure the resistance of the sample using the four-point diagnostic. Be sure you understand the principles of what you are doing. Measure the resistance as a function of temperature. Don't forget to measure the properties of the sample at room temperature before you begin. It will probably be best first to cool the sample to 77 °K and then to use the resistive heaters to slowly bring the sample up beyond it's critical temperature.

~~WEEK 3~~: Repeat the above experiments ~~performed in week 2~~ above while at the same time applying increasing magnetic field strength with the large solenoid. How does the critical temperature and resistivity change with applied field?

Superconductivity at 93 K in a New Mixed-Phase Y-Ba-Cu-O Compound System at Ambient Pressure

M. K. Wu, J. R. Ashburn, and C. J. Torng
Department of Physics, University of Alabama, Huntsville, Alabama 35899

and

P. H. Hor, R. L. Meng, L. Gao, Z. J. Huang, Y. Q. Wang, and C. W. Chu[a]
Department of Physics and Space Vacuum Epitaxy Center, University of Houston, Houston, Texas 77004

(Received 6 February 1987; Revised manuscript received 18 February 1987)

A stable and reproducible superconductivity transition between 80 and 93 K has been unambiguously observed both resistively and magnetically in a new Y-Ba-Cu-O compound system at ambient pressure. An estimated upper critical field $H_{c2}(0)$ between 80 and 180 T was obtained.

PACS numbers: 74.70.Ya

The search for high-temperature superconductivity and novel superconducting mechanisms is one of the most challenging tasks of condensed-matter physicists and material scientists. To obtain a superconducting state reaching beyond the technological and psychological temperature barrier of 77 K, the liquid-nitrogen boiling point, will be one of the greatest triumphs of scientific endeavor of this kind. According to our studies,[1] we would like to point out the possible attainment of a superconducting state with an onset temperature higher than 100 K, at ambient pressure, in compound systems generically represented by $(L_{1-x}M_x)_aA_bD_y$. In this Letter, detailed results are presented on a specific new chemical compound system with L=Y, M=Ba, A=Cu, D=O, x=0.4, a=2, b=1, and $y \leq 4$ with a stable superconducting transition between 80 and 93 K. For the first time, a "zero-resistance" state ($\rho < 3\times10^{-8}$ Ω-cm, an upper limit only determined by the sensitivity of the apparatus) is achieved and maintained at ambient pressure in a simple liquid-nitrogen Dewar.

In spite of the great efforts of the past 75 years since the discovery of superconductivity, the superconducting transition temperature T_c has remained until 1986 below 23.2 K, the T_c of Nb_3Ge first discovered[2] in 1973. In the face of this gross failure to raise the T_c, nonconventional approaches[3] taking advantage of possible strong nonconventional superconducting mechanisms[4] have been proposed and tried. In September 1986, the situation changed drastically when Bednorz and Müller[5] reported the possible existence of percolative superconductivity in $(La_{1-x}Ba_x)Cu_{3-\delta}$ with x=0.2 and 0.15 in the 30-K range. Subsequent magnetic studies[6-8] confirmed that high-temperature superconductivity indeed exists in this system. Takagi *et al.*[9] further attributed the observed superconductivity in the La-Ba-Cu-O system to the K_2NiF_4 phase. By the replacement of Ba with Sr,[8,10,11] it is found that the La-Sr-Cu-O system of the K_2NiF_4 structure, in general, exhibits a higher T_c and a sharper transition. A transition width[10] of 2 K and an onset[11] T_c of 48.6 K were obtained at ambient pressure.

Pressure[8,12] was found to enhance the T_c of the La-Ba-Cu-O system at a rate of greater than 10^{-3} K bar^{-1} and to raise the onset T_c to 57 K, with a "zero-resistance" state[13] reached at 40 K, the highest in any known superconductor until now. Pressure reduces the lattice parameter and enhances the Cu^{+3}/Cu^{+2} ratio in the compounds. This unusually large pressure effect on T_c has led to suggestions[8,12] that the high-temperature superconductivity in the La-Ba-Cu-O and La-Sr-Cu-O systems may be associated with interfacial effects arising from mixed phases; interfaces between the metal and insulator layers, or concentration fluctuations within the K_2NiF_4 phase; strong superconducting interactions due to the mixed valence states; or yet a unidentified phase. Furthermore, we found that when the superconducting transition width is reduced by making the compounds closer to the pure K_2NiF_4 phase, the onset T_c is also reduced while the main transition near 37 K remains unchanged. Extremely unstable phases displaying signals indicative of superconductivity in compounds consisting of phases in addition to or other than the K_2NiF_4 phase have been observed by us,[8,14] up to 148 K, but only in four samples, and in China,[15] at 70 K, in one sample. Therefore, we decided to investigate the multiple-phase Y-Ba-Cu-O compounds instead of the pure K_2NiF_4 phase, through simultaneous variation of the lattice parameters and mixed valence ratio of Cu ions by chemical means at ambient pressure.

The compounds investigated were prepared with nominal compositions represented by $(Y_{1-x}Ba_x)_2CuO_{4-\delta}$ with x=0.4 through solid-state reaction of appropriate amounts of Y_2O_3, $BaCO_3$, and CuO in a fashion similar to that previously described.[8] Bar samples of dimensions $1\times0.5\times4$ mm^3 were cut from the sintered cylinders. A four-lead technique was employed for the resistance (R) measurements and an ac inductance bridge for the mag-

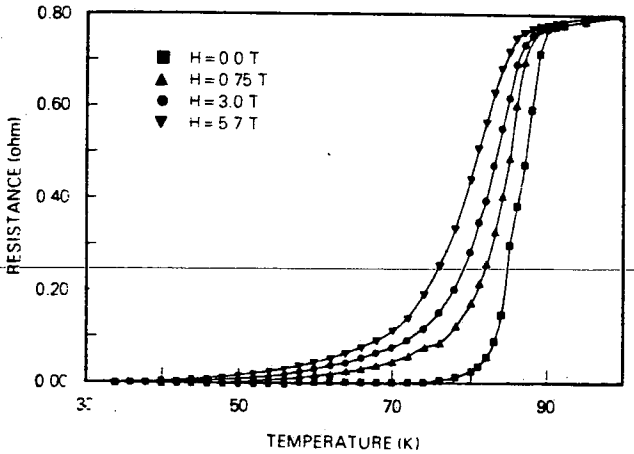

FIG. 1. Temperature dependence of resistance determined in a simple liquid-nitrogen Dewar.

netic susceptibility (χ) determinations. The temperature was measured by means of Au+0.07% Fe–Chromel and Chromel-Alumel thermocouples in the absence of a magnetic field, and a carbon-glass thermometer in the presence of a field. The latter was calibrated against the former without a field. Magnetic fields up to 6 T were generated by a superconducting magnet.

The temperature dependence of R determined in a simple liquid-nitrogen Dewar is shown in Fig. 1. R initially drops almost linearly with temperature T. A deviation of R from this T dependence is evident at 93 K and a sharp drop starts at 92 K. A "zero-R" state is achieved at 80 K. The variation of χ with T is shown in Fig. 2. It is evident that a diamagnetic shift starts at 91 K and the size of the shift increases rapidly with further cooling. At 4.2 K, the diamagnetic signal corresponds to 24% of the superconducting signal of a Pb sample with similar dimensions. In a magnetic field, the R drop is shifted toward lower T. At our maximum field of 5.7 T, the "zero-R" state remains at a T as high as 40 K. Preliminary x-ray powder diffraction patterns show the existence of multiple phases uncharacteristic of the K_2NiF_4 structure in the samples. Detailed analyses are under way.

The above results demonstrate unambiguously that superconductivity occurs in the Y-Ba-Cu-O system with a transition between 80 and 93 K. We have determined the upper critical field $H_{c2}(T)$ resistively. If the positive curvature at very low fields is neglected, one gets a value of dH_{c2}/dT near T_c of 3 T/K or 1.3 T/K, depending on whether $H_{c2}(T_c)$ is taken at the 10% or the 50% drop from the normal-state R. In the weak-coupling limit, $H_{c2}(0)$ is thus estimated to be between 80 and 180 T in the Y-Ba-Cu-O system investigated. We believe that the value of $H_{c2}(0)$ can be further enhanced as the material is improved. The paramagnetic limiting field at 0 K for a sample with a $T_c \sim 90$ K is 165 T. Because of the porous and multiphase characteristics of the samples, it is therefore difficult to extract any reliable information about the density of states from the slope of $H_{c2}(T)$ at T_c on the basis of the dirty-limit approximation.

On the basis of the existing data, it appears that the high-temperature superconductivity above 77 K reported here occurs only in compound systems consisting of a phase or phases in addition to or other than the K_2NiF_4 phase. While it is tempting to attribute the superconductivity to possible nonconventional superconducting mechanisms as mentioned earlier, all present suggestions are considered to be tentative at best, especially in the absence of detailed structural information about the phases in the Y-Ba-Cu-O samples. However, we would like to point out here that the lattice parameters, the valence ratio, and the sample treatments all play a crucial role in achieving superconductivity above 77 K. The role of the different phases present in superconductivity is yet to be determined.

The work at the University of Alabama at Huntsville is supported by NASA Grants No. NAG8-032 and No.

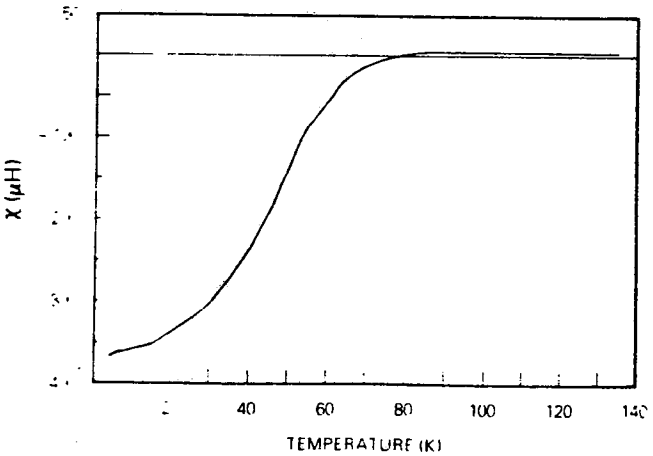

FIG. 2. Temperature dependence of magnetic susceptibility.

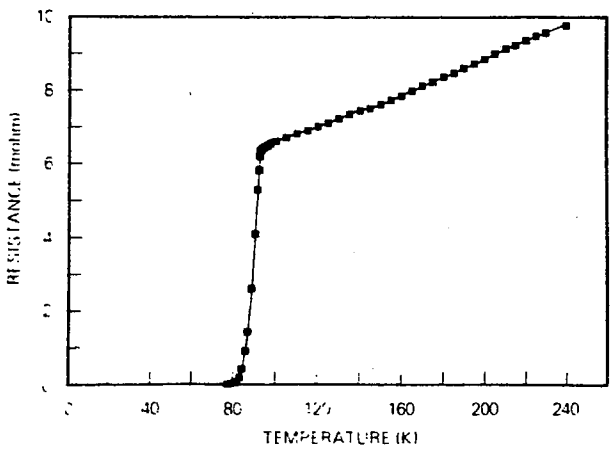

FIG. 3. Magnetic field effect on resistance.

NAGW-A12, and National Science Foundation Alabama EPSCoR Program Grant No. R11-8610669, and at the University of Houston by National Science Foundation Grant No. DMR 8616537, NASA Grants No. NAGW-977 and No. NAG8-051, and the Energy Laboratory of the University of Houston. Technical assistance from D. Campbell, A. Testa, and J. Bechtold is greatly appreciated.

---

[a]Also at the Division of Materials Research, National Science Foundation, Washington, DC 20550.

[1]C. W. Chu, U.S. Patent Application (12 January 1987).

[2]J. R. Gavaler, Appl. Phys. Lett. **23**, 480 (1973); L. R. Testardi, J. H. Wernick, and W. A. Royer, Solid State Commun. **15**, 1 (1974).

[3]See, for example, C. W. Chu and M. K. Wu, in *High Pressure in Science and Technology*, edited by C. Homan, R. K. MacCrone, and E. Whalley (North-Holland, New York, 1983), Vol. 1, p. 3; C. W. Chu, T. H. Lin, M. K. Wu, P. H. Hor, and X. C. Jin, in *Solid State Physics under Pressure*, edited by S. Minomura (Terra Scientific, Tokyo, 1985), p. 223.

[4]See, for example, J. Bardeen, in *Superconductivity in d- and f-Band Metals*, edited by D. Douglass (Plenum, New York, 1973), p. 1.

[5]J. G. Bednorz and K. A. Müller, Z. Phys. B **64**, 189 (1986).

[6]J. G. Bednorz, M. Takashige, and K. A. Müller, to be published.

[7]S. Uchida, H. Takagi, K. Kitazawa, and S. Tanaka, Jpn. J. Appl. Phys. **26**, L1 (1987).

[8]C. W. Chu, P. H. Hor, R. L. Meng, L. Gao, Z. J. Huang, and Y. Q. Wang, Phys. Rev. Lett. **58**, 405 (1987).

[9]H. Takagi, S. Uchida, K. Kitazawa, and S. Tanaka, to be published.

[10]R. J. Cava, R. B. Van Dover, B. Batlogg, and E. A. Rietman, Phys. Rev. Lett. **58**, 408 (1987).

[11]Z. X. Zhao, L. Q. Chen, C. G. Cui, Y. Z. Huang, J. X. Liu, G. H. Chen, S. L. Li, S. Q. Guo, and Y. Y. He, to be published.

[12]C. W. Chu, P. H. Hor, R. L. Meng, L. Gao, and Z. J. Huang, Science **235**, 567 (1987).

[13]P. H. Hor, R. L. Meng, L. Gao, Z. J. Huang, and C. W. Chu, to be published.

[14]C. W. Chu, P. H. Hor, and R. L. Meng, unpublished.

[15]According to a report in Renmin Ribao, 17 January 1987.

THE MEASUREMENT OF TEMPERATURE

Temperature can be accurately measured with thermometers designed and calibrated for use in the temperature range of interest. For all experiments in this manual using Colorado Superconductor Inc.'s family of superconductor kits, a range from room temperature to that of liquid nitrogen is of interest. Sophisticated thermometers typically do not operate over such a wide range. Thermocouple thermometers however are fairly accurate over this great a range of temperature variation.

A thermocouple consists of a mechanical junction of two dissimilar metals. This junction generates a small electrical potential (voltage), the value of which depends upon the temperature of the junction. Thus with calibration, and an appropriate choice of metals, one can obtain a thermometer for the desired temperature range. For our range (300 Kelvin to 77 Kelvin), a type T, or Copper-Constantan thermocouple is used. A -0.16mV reading indicates room temperature (298K), and +6.43mV is 77K.

The thermocouple junction has been carefully attached to the superconductors in our kits, and thermally balanced and calibrated. A simple digital millivoltmeter attached to the leads can be used to determine the voltage of this junction. Note that thermocouple leads must be connected to the voltmeter via wires of the same material and the junction to the thermocouple leads must be at room temperature. This voltage can be converted to the equivalent temperature with the help of the conversion chart below.

Conversion from mV to Kelvin

°K	0	1	2	3	4	5	6	7	8	9	10	°K
60	7.60	7.53	7.46	7.40	7.33	7.26	7.19	7.12	7.05	6.99	6.92	60
70	6.92	6.85	6.78	6.71	6.64	6.56	6.49	6.42	6.37	6.33	6.29	70
80	6.29	6.25	6.21	6.17	6.13	6.09	6.05	6.01	5.97	5.93	5.90	80
90	5.90	5.86	5.83	5.79	5.75	5.72	5.68	5.64	5.60	5.56	5.52	90
100	5.52	5.48	5.44	5.41	5.37	5.34	5.30	5.27	5.23	5.20	5.16	100
110	5.16	5.13	5.09	5.06	5.02	4.99	4.95	4.91	4.88	4.84	4.81	110
120	4.81	4.77	4.74	4.70	4.67	4.63	4.60	4.56	4.53	4.49	4.46	120
130	4.46	4.42	4.39	4.35	4.32	4.28	4.25	4.21	4.18	4.14	4.11	130
140	4.11	4.07	4.04	4.00	3.97	3.93	3.90	3.86	3.83	3.79	3.76	140
150	3.76	3.73	3.69	3.66	3.63	3.60	3.56	3.53	3.50	3.47	3.43	150
160	3.43	3.40	3.37	3.34	3.30	3.27	3.24	3.21	3.18	3.15	3.12	160
170	3.12	3.09	3.06	3.03	3.00	2.97	2.94	2.91	2.88	2.85	2.82	170
180	2.82	2.79	2.76	2.73	2.70	2.67	2.64	2.61	2.58	2.53	2.52	180
190	2.52	2.49	2.46	2.43	2.40	2.37	2.34	2.31	2.29	2.26	2.23	190
200	2.23	2.20	2.17	2.14	2.11	2.08	2.05	2.02	1.99	1.96	1.93	200
210	1.93	1.90	1.87	1.84	1.81	1.78	1.75	1.72	1.69	1.66	1.64	210
220	1.64	1.61	1.59	1.56	1.54	1.51	1.49	1.46	1.44	1.41	1.39	220
230	1.39	1.36	1.34	1.31	1.29	1.26	1.24	1.21	1.19	1.16	1.14	230
240	1.14	1.11	1.09	1.07	1.04	1.02	0.99	0.97	0.94	0.92	0.89	240
250	0.89	0.87	0.84	0.82	0.79	0.77	0.74	0.72	0.69	0.67	0.65	250
260	0.65	0.62	0.60	0.58	0.55	0.53	0.50	0.48	0.45	0.42	0.40	260
270	0.40	0.38	0.36	0.34	0.32	0.30	0.28	0.26	0.24	0.22	0.20	270
280	0.20	0.18	0.16	0.14	0.12	0.10	0.08	0.06	0.04	0.02	0.00	280
290	0.00	-0.02	-0.04	-0.06	-0.08	-0.10	-0.12	-0.14	-0.16	-0.18	-0.20	290
300	-0.20	-0.22	-0.24	-0.26	-0.28	-0.30	-0.32	-0.34	-0.36	-0.38	-0.40	300

Precautions.

1. When pouring liquid nitrogen be careful to prevent any splashing. Read the section on safety & hanc starting page 12 before beginning this experiment.
2. Be careful not to touch the device or wires when they are cold. Follow the safety directions.
3. No more than 0.5 Amp of current should pass through the device or wires at any time.
4. Use a hair dryer to carefully dry the Four Point Probe device after use. Store it with a dessicant.
5. The probe and thermocouple wires are very brittle when cold. Please handle them with care.

Some Questions.

1. What effect would one expect if the Critical Temperature is measured with the device placed insic functioning electromagnet?
2. Why is the transition in resistance gradual at the Critical Temperature?
3. A simple two-probe measurement of device resistance below its Critical Temperature exhibits a non-z value. Why?

Determination of the Critical Temperature

The Critical Temperature, Tc is obtained during the measurement of the electrical resistance as functio the Temperature of the superconductor on the previous page. The Critical Temperature of $Bi_2CaSr_2Cu_2O_9$ superconductor is about 108 Kelvin versus about 95 Kelvin for the $YBa_2Cu_3O_7$ mate These results are shown below in figure 4.

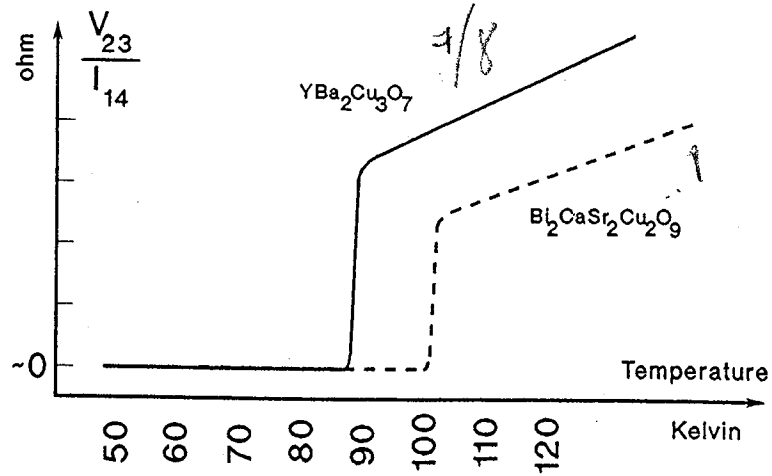

Figure 4: Resistance versus Temperature

14 SOLIDS— SUPERCONDUCTORS AND MAGNETIC PROPERTIES

14-1 SUPERCONDUCTIVITY 484

review of independent electron motion theories of conductivity; temperature dependence of conductivity; resistanceless current in superconductors; critical temperature; Meissner effects and their relation to resistanceless current; critical field; isotope effect evidence for importance of lattice vibrations; attractive electron-electron interactions by means of phonon exchange; conditions for formation of Cooper pairs; ordered pair motion under applied electric field; pair binding energy; origin of energy gap; gap width and relation to critical temperature; estimate of size and density of pairs; applications of superconductivity; Type II superconductors; flux quantization

14-2 MAGNETIC PROPERTIES OF SOLIDS 492

relations between magnetic induction, magnetization, magnetic field strength, and magnetic susceptibility; diamagnetism and Lenz's law; comparison of diamagnetic, paramagnetic, and ferromagnetic susceptibilities

14-3 PARAMAGNETISM 493

role of independent permanent magnetic dipole moments; calculated susceptibility of system of atoms with two spin orientations; Curie's law as an approximation; comparison with experiment; paramagnetic susceptibility in metals

14-4 FERROMAGNETISM 497

Curie temperature; failure of classical dipole-dipole interaction explanation; role of exchange interactions; structure of 3*d* bands in transition elements; partial bands; origin of ferromagnetism; domains; hysteresis; permanent magnetism

14-5 ANTIFERROMAGNETISM AND FERRIMAGNETISM 503

properties; role of exchange interactions

QUESTIONS 503

PROBLEMS 504

14-1 SUPERCONDUCTIVITY

Shortly after the discovery of the electron it was recognized that the high electrical and thermal conductivities of metals could be attributed to the motion of electrons in the metal. Classical theories of metallic conduction treated these electrons as a gas of independent particles within the metals colliding with lattice imperfections. Using methods of the classical kinetic theory, many experimental facts of electrical and thermal conductivity could be explained. With the advent of quantum mechanics, it became possible to take into account the wave nature of electrons and the exclusion principle. A number of phenomena not previously explainable then became clear. For example, the need to use the Fermi distribution for free electrons led to an understanding of the electronic contribution to the specific heats of solids. The further application of wave ideas led to quantization of energy levels and the band theory of solids, which accounted for the wide range in conductivities observed in normal solids. The free-electron model approximation averaged out variations in the interactions of electrons with one another and with the lattice ions, and it could account for resistance to electron flow under normal conditions. A major failure of this independent particle model, however, is its inability to explain superconductivity. To understand that phenomenon requires taking into account the collective behavior of electrons and ions, or the so-called *many-body effects*, in solids. Let us now examine superconductivity.

Many factors contribute to the electrical resistivity of a solid, as we have seen. Electrons are scattered by the deviations from a perfect lattice due to structural defects or impurities in a crystal. In addition, there are vibrations of the lattice ions in normal modes that constitute something like sound waves traveling through the solid; we refer to such waves as *phonons*. The higher the temperature is, the more phonons there are present in the lattice. When phonons are present, there is an electron-phonon interaction which scatters conduction electrons and causes further resistance. Hence, the electrical resistance of a solid should decrease as the temperature decreases, but we expect a residual resistance even near absolute zero due to the crystal imperfections. It therefore seems remarkable that *the electrical resistance of some solids disappears completely at sufficiently low temperatures.*

In 1911, Kammerlingh-Onnes found that the electrical resistance of solid mercury drops to an immeasurably small value when cooled below a certain temperature, called the *critical temperature* T_c. Mercury goes from a normal state to a *superconducting* state as the temperature drops below $T_c = 4.2°K$. Many other elements, and many compounds and alloys, have since been found to be superconductors with critical temperatures as high as 23°K. But not all materials superconduct. Figure 14-1 shows the resistivity at very low temperatures for a superconductor, tin, and a nonsuperconductor, silver. In a superconductor, currents can be set up which persist for years with no detectable decay.

In 1933, Meissner and Oschenfeld found that as a superconducting substance is cooled below its critical temperature in the presence of an applied magnetic field, it expels all magnetic flux from its interior. If the field is applied after the substance has been cooled below its critical temperature, the magnetic flux is excluded from the superconductor. Hence, a superconductor acts like a perfect diamagnet. Both *Meissner effects* are illustrated in Figure 14-2. According to Lenz's law, when the magnetic flux through a circuit is changing, an induced current is established in such a direction as to oppose the change in flux. In a *diamagnetic* atom, the orbital electrons adjust their rotational motion to produce a net magnetic moment opposite to the externally applied magnetic field. We can say analogously that an external magnetic field does not penetrate the interior of a superconducting substance because in a superconductor the conduction electrons, whose motion is as unimpeded as in an

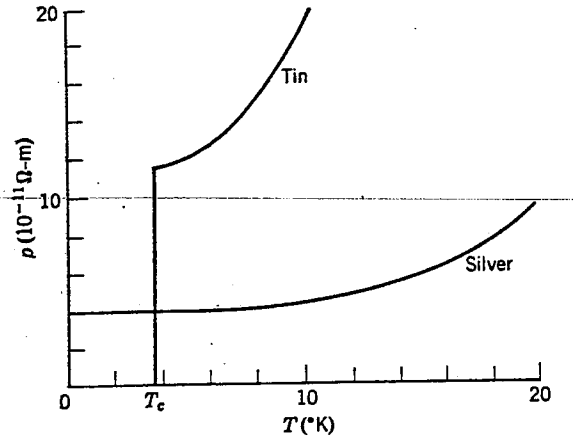

Figure 14-1 A plot of resistivity ρ versus temperature T, showing the drop to zero at the critical temperature T_c for a super-conductor, and the finite resistivity of a normal metal at absolute zero.

atom, adjust their motion to produce a counteracting magnetic field. The entire superconductor behaves like a single diamagnetic atom in this respect. Hence, the two principal characteristics of superconductors, namely the exclusion of magnetic flux and the absence of resistance to current flow, are related to one another. It is necessary to have a persisting (resistanceless) current to maintain the flux exclusion when the external field is on.

Figure 14-3 shows a photograph of superconducting levitation. If a small permanent magnet is placed over a perfectly conducting surface, it will float there. If the magnet is placed on a surface which thereafter is made superconducting (by lowering its temperature), it will rise and float. A repulsive force large enough to overcome the weight of the magnet exists between the magnet and the diamagnetic superconductor, because the superconducting body excludes the magnetic lines of flux associated with the magnet. Serious engineering studies have indicated the feasibility of using this phenomenon to provide very smooth support for high-speed passenger trains.

It is found that if the external field is increased beyond a certain value, called the *critical field* H_c, the metal ceases to be superconducting and becomes normal. The value of this critical field for a given material depends on the temperature, as shown for the case of lead in Figure 14-4. As the external magnetic field increases, therefore, the critical temperature is lowered until when $H > H_c(0°K)$ there is no superconductivity for that material at any temperature. We can understand this as follows. Suppose that at some temperature below T_c we turn on a magnetic field; the superconductor will act to exclude this field (the Meissner effect). The energy decrease of the magnetic field appears as increased energy of the electrons that make up the superconducting current. As the strength of the external magnetic field is increased, the energy acquired by the superconductor also increases. At the critical value of the field, H_c, the energy of the superconducting state becomes higher than the energy of the normal state, so that the material becomes normal.

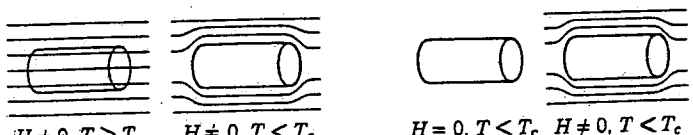

Figure 14-2 *Left:* A schematic illustration of expulsion. *Right:* The exclusion of magnetic flux in a superconductor. Both are called *Meissner effects.*

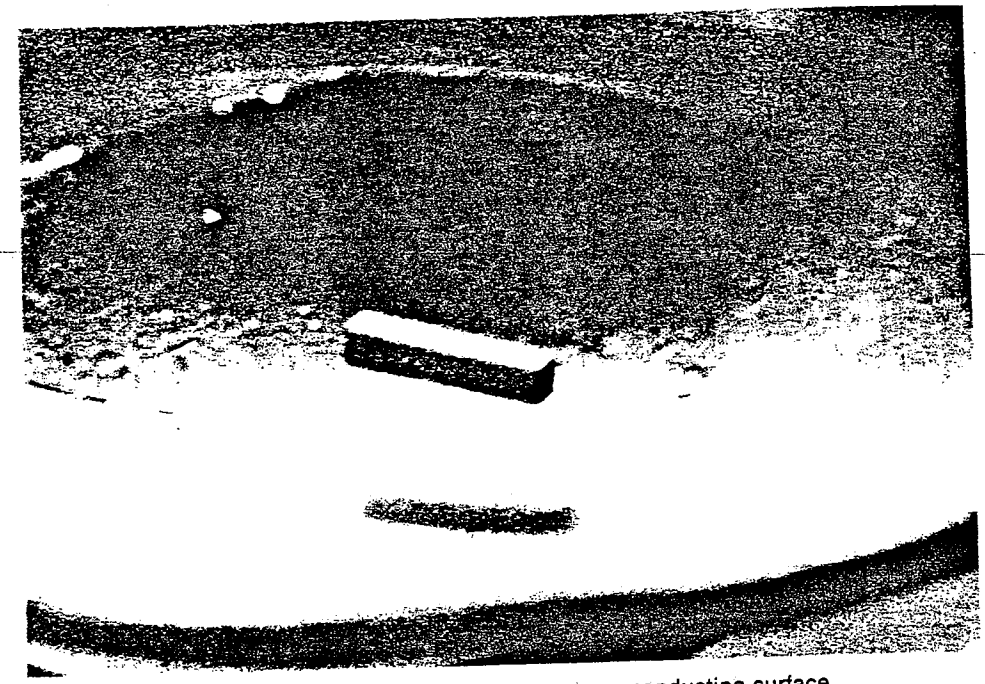

Figure 14-3 A permanent magnet floating over a superconducting surface.

Evidence that the lattice vibrations play an important role in the phenomenon of superconductivity came in 1950 when experiment revealed that the critical temperature of crystals made from different isotopes of the same element depends on the isotopic mass. The dependence, given by

$$M^{1/2}T_c = \text{const} \tag{14-1}$$

in which M is the average isotopic mass of the solid, is called the *isotope effect*. This relation shows that the critical temperature would go to zero (hence, no superconductivity) in the absence of lattice vibrations (when $M \to \infty$). The importance of lattice vibrations suggests that an electron-phonon interaction is responsible for superconductivity. We can no longer ignore those very interactions which were neglected in the independent particle model of a solid—the electron-phonon and also the electron-electron interactions—if we hope to get a theoretical explanation of

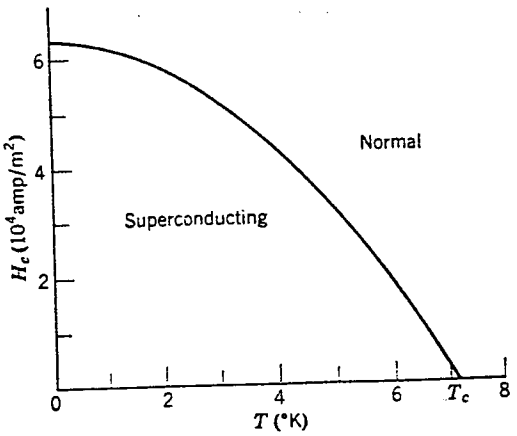

Figure 14-4 The variation with temperature of the critical field H_c for lead. Note that H_c is zero when the temperature T equals the critical temperature T_c.

superconductivity. In 1957, Bardeen, Cooper, and Schrieffer proposed a detailed microscopic theory, now known as the *BCS theory*, in which these interactions are included. The predictions of the BCS theory are in excellent agreement with experimental results. Let us now consider a qualitative picture of it.

An electron in a solid passing by adjacent ions in the lattice can act on these ions with a set of Coulomb attractions which gives each of them momentum that causes them to move slightly together. Because of the elastic properties of the lattice, this region of increased positive charge density will then propagate as a wave, which carries momentum, through the lattice. The electron has emitted a phonon! The momentum the phonon carries is supplied by the electron, whose momentum changed when the phonon was emitted. If a second electron subsequently passes by the moving region of increased positive charge density, it will experience an attractive Coulomb interaction, and thereby it can absorb all the momentum the moving region carries. That is, the second electron can absorb the phonon, thereby absorbing the momentum supplied by the first electron. The net effect is that the two electrons have exchanged some momentum with each other, and thus they have interacted with each other. Although the interaction was a two-step one, involving a phonon as an intermediary, it certainly was an interaction between the two electrons. Furthermore, it was an *attractive* interaction, since the electron involved in each of the steps participated in an attractive Coulomb interaction. The BCS theory shows that in certain conditions the attraction between two electrons due to a succession of phonon exchanges can exceed slightly the repulsion which they exert directly on each other because of the (shielded) Coulomb interaction of their like charges. Then the electrons will be weakly bound together, and form a so-called *Cooper pair*. We shall see that Cooper pairs are responsible for superconductivity.

The conditions for their formation, in numbers large enough to allow superconductivity, are (1) that the temperature be low enough to make the number of random thermal phonons present in the lattice small (they would inhibit the ordered processes involved in superconductivity); (2) that the interaction between an electron and a phonon be strong (so that a substance which has a relatively low resistance at room temperature, because its conduction electrons interact weakly with thermal lattice vibrations, will *not* be a possible superconductor at low temperature); (3) that the number of electrons in states lying just below the Fermi energy be large (these are the electrons which are energetically able to form Cooper pairs); (4) that the two electrons have "antiparallel" spins (then their space eigenfunction will be symmetric in a label exchange, which means that they will be close enough together to form a pair); and (5) that, in the absence of an externally applied electric field, the two electrons of a pair have linear momenta of equal magnitude but opposite direction (as will be explained next, this facilitates the participation of the maximum number of electrons in pair formation).

Because Cooper pairs are weakly bound, they are constantly breaking up and then reforming, usually with different partners. Also, because they are weakly bound they are large. (In Example 14-2 we shall estimate the typical separation of two electrons in a pair to be of the order of 10^4 Å.) Thus, within the region occupied by the electrons of a pair, there are very many other electrons that would also like to participate in the pairing process. The system will be most tightly bound, and therefore most stable, if they can do so. The system achieves this by having the total linear momentum of each pair equal to zero, in the absence of an applied electric field. The discussion of the formation of a pair shows that the total momentum of any pair is a constant, since the net result of exchanging a phonon between the two electrons is to preserve the total momentum of the pair. If all the pairs have the *same* constant total momentum, then there will be no inhibition to the unavoidable process of old pairs breaking up and new pairs reforming, because any pair can be converted to any other pair by

phonon exchange, and so the maximum number of pairs will be present. This conclusion is plausible from the qualitative argument we have given. It is put on a completely firm foundation by the quantitative calculations of the BCS theory, which show that the wave functions describing pair formation are in phase, and thus add constructively and lead to a large total probability for pair formation, when the pairs all have the same total momentum. In the absence of an applied electric field, symmetry considerations obviously demand that the common value of the pair total momentum be zero. So we see why the two electrons of each pair have linear momenta of equal magnitude, but opposite direction, in such circumstances. We also see that the ground state of the system is very highly ordered, in that all the pairs in the lattice are doing exactly the same thing as far as the motion of their centers of mass is concerned. This order extends through the lattice, and not just through the region occupied by a pair, because the pairs are relatively large and there are many of them so there is multiple overlapping. The order propagates through adjacent overlapping regions.

When an external electric field is applied, the pairs, which behave rather like particles with two electron charges, move through the lattice under the influence of the field. But they do it in such a way as to continue to maintain the order, because that will maintain their number at a maximum. Thus they carry current by moving through the lattice with all of their centers of mass having exactly the same momentum. The motion of each pair is locked into the motion of all the rest, and so none of them can be involved in the random scatterings from lattice imperfections that cause low-temperature electrical resistance. This is why the system is a superconductor.

It is tempting to think of a Cooper pair as acting like a boson, since it contains two fermions. If this could be done, superconductivity would be simply another example of Bose condensation, as in the superfluidity of liquid helium. That is, it would be the completely correlated motion of a set of bosons all in the same quantum state due to the effect of the $(1 + n)$ boson enhancement factor discussed in Chapter 11. Theories which preceded the BCS theory tried unsuccessfully to use this approach. The reason why it is not valid is that the individual electrons in each pair are weakly bound to the pair, which also means the pair is large. As a consequence, the eigenfunction for the system of overlapping pairs must take into account the exchange of labels of one electron from one pair and one electron from another pair, as well as the exchange of labels of one complete pair and another complete pair. In the latter exchange the system eigenfunction will not change sign because two fermion labels are being exchanged, but in the former the eigenfunction does change sign since only one fermion label is being exchanged. So Cooper pairs are neither purely bosonlike (no sign change), nor purely fermionlike (sign change) with respect to all eigenfunction label exchanges that must be considered. In a system of tightly bound helium atoms, the only type of label exchange that must be considered is an exchange of the label of one atom with the label of another. Such an exchange actually involves an even number of fermion label exchanges (each atom contains two electrons, two protons, and two neutrons), so the eigenfunction does not change sign and the atoms of the system act like bosons.

According to the BCS theory, the binding energy of a Cooper pair at absolute zero is about $3kT_c$. As the temperature rises, the binding energy is reduced, and goes to zero when the temperature equals the critical temperature T_c. Above T_c, a Cooper pair is not bound.

With a binding electron-electron interaction at absolute zero, it is energetically advantageous for two electrons, each in single-particle states just below the Fermi energy, $\mathscr{E}_F$, to promote themselves to vacant states just above $\mathscr{E}_F$ where they can interact in such a way as to form a Cooper pair. The energy required to put the electrons into the higher single-particle states is more than compensated for by the energy

made available by the binding of the Cooper pair they form. Thus the zero temperature Fermi distribution of a superconductor is unstable, in the sense that electrons in states within a range of the order of kT_c below the Fermi energy will leave those states and enter states within a similar range above the Fermi energy, where they will form pairs. The result is that the $T = 0$ distribution of occupied states of a superconductor looks something like a $T = T_c$ Fermi distribution for a normal conductor. The reason why the electrons must be above $\mathscr{E}_F$ to be able to freely form pairs is that a large number of unoccupied states are found only above $\mathscr{E}_F$, and unoccupied states must be available for the two electrons of a pair to enter after they change their momenta by one emitting and the other absorbing a phonon.

Although there is an almost continuous distribution of single particle states available to *each electron* in a superconductor at $T = 0$, the distribution of states available to the *system* is anything but continuous. As far as the system is concerned, there is its superconducting ground state, then an *energy gap* of width $\mathscr{E}_g$ in which there are no states at all, and above the gap a set of states which are nonsuperconducting. The gap width $\mathscr{E}_g$ equals the binding energy of a Cooper pair. The gap arises because if one electron of the system in a single particle state in the region of width $\sim kT_c$ surrounding $\mathscr{E}_F$ absorbs energy from some source, so that it makes a transition from that state to another single particle state only infinitesimally different in energy, then the pair of which it had been a member will be broken and the binding energy of the pair will be lost to the system. Thus the source must be able to supply an energy equal to a pair binding energy before an electron near $\mathscr{E}_F$ can make a transition to the energetically nearest state. (Even more energy must be supplied to excite an electron well below $\mathscr{E}_F$, despite the fact that it is not in a pair, since all the nearby states are already occupied.) Therefore the minimum energy that can be accepted by the ground state system, which is the width of its energy gap, is the binding energy of a Cooper pair. The states which begin at the top of the gap are not superconducting since in them the system has enough energy for pairs to be broken.

The width of the gap at $T = 0$ is $\mathscr{E}_g \simeq 3kT_c$. But it narrows as the temperature rises, and it becomes of zero width at $T = T_c$ where the pairs are no longer bound. At temperatures below T_c the superconducting ground state corresponds to a large scale quantum state in which the motions of all the electrons and ions are highly correlated. It takes the gap energy $\mathscr{E}_g$ to excite the system to the next higher state, which is not superconducting, and this is more energy than the thermal energy available to the system. For instance, at $T = 0.1T_c$ the value of the gap energy is still about $\mathscr{E}_g = 3kT_c$, while the thermal energy is about $kT = 0.1kT_c$.

For most superconductors near $T = 0$ the energy needed to bridge the gap corresponds to photons in the very far infared, or microwave, portion of the electromagnetic spectrum. The existence and width of the gap is established experimentally by the abrupt change in absorption of far infared or microwave radiation when the photon energy $h\nu$ drops below the gap energy.

Example 14-1. The critical temperature of mercury is 4.2°K.

(a) What is the energy gap in electron volts at $T = 0$?

►As stated earlier, the Cooper pair binding energy, or gap energy, is

$$\mathscr{E}_g \simeq 3kT_c$$

So

$$\mathscr{E}_g \simeq 3 \times 1.4 \times 10^{-23} \text{ joule/°K} \times 4.2\text{°K} = 1.8 \times 10^{-22} \text{ joule}$$
$$\simeq 1.1 \times 10^{-3} \text{ eV} \quad \blacktriangleleft$$

(b) Calculate the wavelength of a photon whose energy is just sufficient to break up Cooper pairs in mercury at $T = 0$. In what region of the electromagnetic spectrum are such photons found?

►The energy is

$$\mathscr{E}_g = h\nu = \frac{hc}{\lambda}$$

So the wavelength is

$$\lambda = \frac{hc}{\mathscr{E}_g} \simeq \frac{6.6 \times 10^{-34}\ \text{joule-sec} \times 3 \times 10^{8}\ \text{m/sec}}{1.8 \times 10^{-22}\ \text{joule}} = 1.1 \times 10^{-3}\ \text{m}$$

These photons are in the very short wavelength part of the microwave region. ◄

(c) Does the metal look like a superconductor to electromagnetic waves having wavelengths shorter than that found in part (b)? Explain.

►No, since the energy content of shorter wavelength photons is sufficiently high to break up the Cooper pairs, or excite the conduction electrons through the energy gap into the non-superconducting states above the gap. ◄

Example 14-2. (a) Estimate the size of a Cooper pair of binding energy $\mathscr{E}_g$.

►The wave function of a Cooper pair is made up of waves, describing its two component electrons, with wave numbers drawn from a range Δk corresponding to an energy range $\Delta\mathscr{E} \sim \mathscr{E}_g$. The energy range is centered on $\mathscr{E}_F$, and the wave number range is centered on the corresponding k_F. Since the energy of one of the electrons is

$$\mathscr{E} = \frac{p^2}{2m^*} = \frac{\hbar^2 k^2}{2m^*}$$

we have

$$\Delta\mathscr{E} = \frac{\hbar^2 2k\,\Delta k}{2m^*}$$

and

$$\frac{\Delta\mathscr{E}}{\mathscr{E}} = \frac{\hbar^2 k\,\Delta k 2m^*}{m^*\hbar^2 k^2} = \frac{2\Delta k}{k} \sim \frac{\Delta k}{k}$$

Setting $\mathscr{E} = \mathscr{E}_F$, $k = k_F$, and $\Delta\mathscr{E} = \mathscr{E}_g$, we have

$$\frac{\Delta k}{k_F} \sim \frac{\mathscr{E}_g}{\mathscr{E}_F}$$

As $\mathscr{E}_g/\mathscr{E}_F \sim 10^{-4}$ in a typical case, we obtain

$$\Delta k \sim 10^{-4} k_F$$

Since we saw in Chapter 13 that at the top of a band $k = \pi/a$, if the zeros of k and $\mathscr{E}$ are taken at the bottom of the band as we do here, we can set $k_F \sim 1/a$. We also know that the lattice spacing is $a \sim 1$ Å. Thus we find that

$$\Delta k \sim \frac{10^{-4}}{1\ \text{Å}}$$

is the range of wave numbers contained in the wave function for a Cooper pair. A very general property of waves ((3-14), which leads to the uncertainty principle) then immediately tells us that the extent in space of the wave function is

$$\Delta x \sim \frac{1}{\Delta k} \sim 10^4\ \text{Å}$$

This is the size of a typical Cooper pair. ◄

(b) Estimate the density of Cooper pairs in a superconductor.

►Example 13-1 shows that the density of conduction electrons in a metal is $n \sim 10^{22}/\text{cm}^3$. The fraction that will form Cooper pairs in a superconductor is of the order of $\Delta k/k_F \sim 10^{-4}$. So

$$n_{\text{Cooper pairs}} \sim 10^{18}/\text{cm}^3$$

Note that the volume of one pair is $\sim(10^4\ \text{Å})^3 = (10^{-4}\ \text{cm})^3 = 10^{-12}\ \text{cm}^3$. So each such volume contains $\sim 10^6$ overlapping pairs! ◄

The width of the forbidden gap, and the density of quantum states, in a superconductor can be determined from the current-voltage characteristic of a tunnel

junction. In such junctions a thin oxide layer ($\sim 10^{-9}$ m thick) separates a normal and a superconducting metal. Electrons tunnel through the barrier, which the nonconducting oxide layer represents, with the aid of an applied voltage. In 1962, Josephson predicted that if the metals on both sides of the junction are superconducting, a current can flow when no voltage is supplied. If a small voltage ($\sim$ a few millivolts) is applied, an alternating current of frequency in the microwave range results. These effects can be used to detect extremely small voltage differences and to measure with enormous precision the ratio e/h used in determination of the fundamental physical constants. Other superconducting effects predicted by Josephson permit a number of quantum properties to be seen in a very simple way, particularly the quantization of magnetic flux, discussed below.

There are many important applications of superconductivity. An obvious application is to superconducting electromagnets, whose fields arise from resistanceless currents flowing through the magnet windings, for use in electric motors and generators. A difficulty is that magnetic fields tend to be induced in the wires of the windings, which tends to destroy their superconductivity. But progress is being made in finding what are called *Type II superconductors*, which have Cooper pairs whose dimensions are small enough to allow a magnetic field to thread its way through the length of a wire in a set of localized channels. These channels lose their superconductivity, but the channels in between them do not. Several niobium-titanium alloys have been found which are Type II superconductors, and they also have the convenience of relatively high critical temperatures ($T_c \simeq 20°\text{K}$).

The absence of power dissipation in superconducting elements makes possible many electronic applications in which space requirements and transmission time requirements are limited, as in computers. Because superconductors are diamagnetic, they can be used to shield out unwanted magnetic flux. This can be put to use in shaping the magnetic lens system of an electron microscope, for example, to eliminate stray field lines and to greatly improve the practical resolving power of the instrument thereby.

Apart from such technological applications of superconductivity, of which a great many more can be cited, there is an increasing application of the theoretical ideas to other fields of physics. For example, these ideas have been applied to analyzing nuclear structure, with much success in accounting for otherwise unexplained experimental facts. In the next chapter we shall see similarities between the collective model of the nucleus and the BCS collective model of superconductivity. Some of the methods of superconductivity theory are being applied to the elementary particles of high-energy physics, as well, so that the theory suggests a unity underlying the various areas of quantum physics.

The Meissner effect can be stated in another way, namely, that it is possible to induce currents in a specimen in a time-invariant magnetic field simply by lowering the temperature. Such a statement contradicts Maxwell's equation $\oint \mathbf{E} \cdot d\mathbf{l} = -d\Phi_B/dt$ (or $\nabla \times \mathbf{E} = -\partial \mathbf{B}/\partial t$) and shows that the Meissner effect is not a classical effect but a quantum effect revealing itself on a macroscopic scale. This has been confirmed by experiments on a superconducting ring. If such a ring in a normal state is placed in a uniform magnetic field, and then cooled to the superconducting state, electric currents are established that flow in opposite directions on the inner and outer surfaces of the ring, as in the upper part of Figure 14-5. This excludes the field from the interior of the ring but does not affect the field inside the hole of the ring. When the external field is removed, the outside surface current disappears but the inside surface current persists. We say that the superconducting ring has trapped the original magnetic field in the hole, as in the lower part of Figure 14-5. When the magnetic flux trapped in the ring is measured as a function of the strength of the applied magnetic field, it is found that the flux is quantized, i.e., it increases in discrete steps. The system acts very much like a macroscopic Bohr atom in which one eigenfunction describes the correlated motion of the entire set of

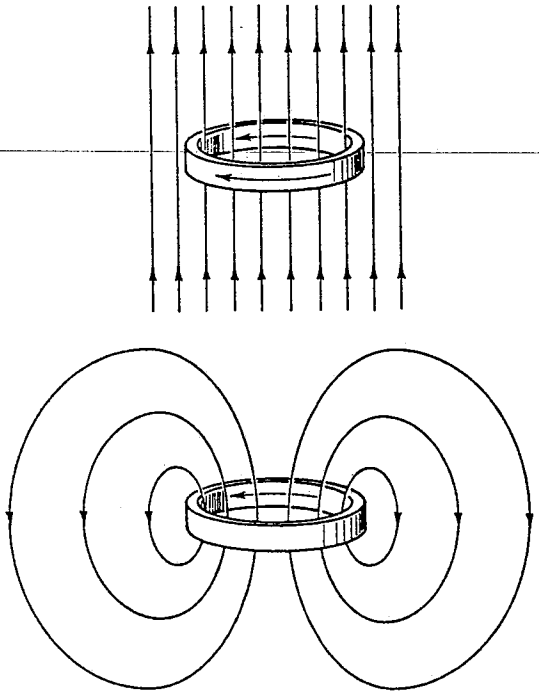

Figure 14-5 *Top:* A ring of superconducting material is cooled below the critical temperature in the presence of a uniform magnetic field. Currents are established as shown on the inner and outer surfaces of the ring, thereby excluding the field from the superconducting material comprising the ring. *Bottom:* The external field is removed. The outside surface current disappears, and the inside surface current persists. The result is that magnetic flux is trapped in the hole enclosed by the ring.

Cooper pairs traveling around the ring. Flux quantization arises because the eigenfunction must be single valued. The quantum of flux is $2\pi\hbar c/q$, where q is the charge carried by one pair. The measurements confirm the BCS prediction that $q = 2e$.

14-2 MAGNETIC PROPERTIES OF SOLIDS

Materials may have intrinsic magnetic dipole moments, or they may have magnetic dipole moments induced in them by an applied external magnetic field of induction. In the presence of a magnetic field of induction, the elementary magnetic dipoles, whether permanent or induced, will act to set up a field of induction of their own that will modify the original field. The student will recall that magnetic dipole moments, which can be regarded as microscopic currents (e.g., in atoms), are a source of *magnetic induction* **B** just as are macroscopic currents (e.g., in magnet windings). In fact, we can write

$$\mathbf{B} = \mu_0\mathbf{H} + \mu_0\mathbf{M} \tag{14-2}$$

in which **M**, called the *magnetization*, is the volume density of magnetic dipole moment, and **H**, called the *magnetic field strength*, is associated with macroscopic currents only. The magnetic vector **H**, which can be written as $\mathbf{H} = (\mathbf{B} - \mu_0\mathbf{M})/\mu_0$, plays a role in magnetism that is analogous to the role of **D** in electricity, since **D**, the electric displacement, originates only with free charges, not polarization charges. The magnetic vector **M**, which can be written as $\boldsymbol{\mu}/V$, the magnetic dipole moment per unit volume, has the same dimensions as **H**.

For certain magnetic materials, it is found empirically that the magnetization **M** is proportional to **H**. Hence, we can write

$$\mathbf{M} = \chi\mathbf{H} \tag{14-3}$$

Chapter 5 The Self-Consistent Field Method 137
5-1 The Bogolubov Equations 137
5-2 Theorems on the Pair Potential and the Excitation Spectrum 145
5-3 The Meissner Effect in Metals and Alloys 160

Chapter 6 Phenomenological Landau-Ginsburg Equations 171
6-1 Introduction 171
6-2 Construction of the Free Energy 172
6-3 Equilibrium Equations 176
6-4 The Two Characteristic Lengths 177
6-5 Situations where $|\psi|$ is Constant 182
6-6 Situations where $|\psi|$ Varies Spatially 195
6-7 Structure of the Vortex Phase in Strong Fields ($H \sim H_{C2}$) 201

Chapter 7 Microscopic Analysis of the Landau-Ginsburg Equations 210
7-1 Linearized Self-Consistency Equation 210
7-2 Landau-Ginsburg Equations 220
7-3 Surface Problems in the Landau-Ginsburg Region 227

Chapter 8 Effects of Strong Magnetic Fields and of Magnetic Impurities 247
8-1 Relation between Transition Temperature and Time-Reversal Properties 249
8-2 Ergodic versus Nonergodic Behavior—Gapless Superconductivity 255
8-3 Dirty Superconductors in High Magnetic Fields 267

Index 273

FROM SUPERCONDUCTIVITY OF METALS AND ALLOYS, GENNES P PINES (BENJAMIN, 1966)

1

FUNDAMENTAL PROPERTIES

1–1 A NEW CONDENSED STATE

We take a piece of tin and cool it down; at a temperature $T_0 = 3.7\,^\circ K$ we find a specific heat anomaly (Fig. 1-1a). Below T_0 the tin is in a new thermodynamical state. What has happened?

It is *not* a change in the crystallographic structure, as far as x rays can tell. It is *not* a ferromagnetic, or antiferromagnetic, transition. (It can be seen by magnetic scattering of neutrons, that tin carries no magnetic moment on an atomic scale.) The striking new property is that the tin has zero electrical resistance. (For instance, a current induced in a tin ring has been observed to persist over times > 1 year.) We say that tin, in this particular phase, is a superconductor, and we call the permanent current a supercurrent.

A large number of metals and alloys are superconductors, with critical temperatures T_0 ranging from less than $1\,^\circ K$ to $18\,^\circ K$. Even some heavily doped semiconductors have been found to be superconductors.

Historically, the first superconductor (mercury) was discovered by Kammerling Onnes in 1911.

The free energy F_S in the superconducting phase can be derived from the specific heat data and is represented on Fig. 1-1b (solid line). The dotted line gives the corresponding curve F_n for the normal metal. The difference $(F_S - F_n)_{T=0}$ is called the condensation energy. It is *not* of order $k_B T_0$ per electron; it is, in fact, much smaller, of order $(k_B T_0)^2/E_F$ (where E_F is the Fermi energy of the conduction electrons in the normal metal). Typically $E_F \sim 1$ eV and $k_B T_0 \sim 10^{-3}$ eV. Only a fraction $k_B T_0/E_F$ ($\sim 10^{-3}$) of the metallic electrons have their energy significantly modified by the condensation process.

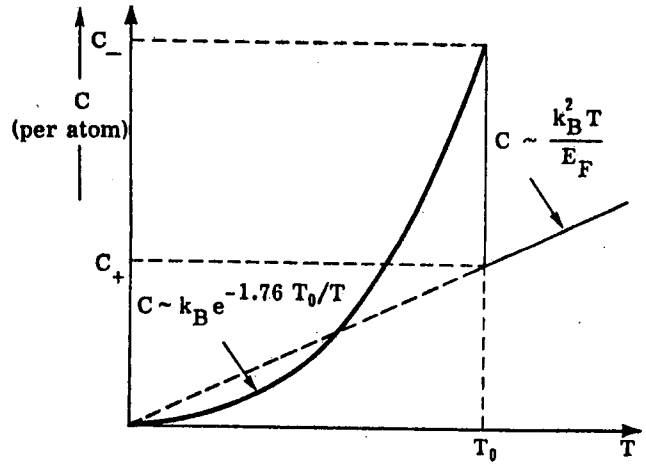

(a)

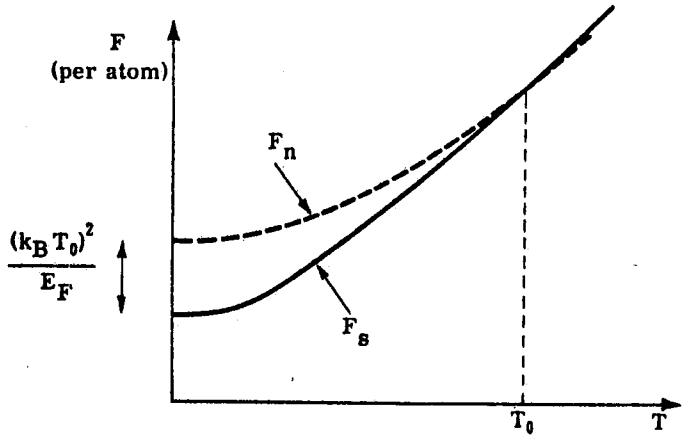

(b)

Figure 1-1

(a) The electronic specific heat C of a superconductor (in zero magnetic field) as a function of temperature (qualitative plot). Above T_0 (in the normal phase) $C_{(\text{per atom})} \sim k_B^2 T/E_F$ where E_F is the Fermi energy. At the transition point T_0, C has a discontinuity. At $T \ll T_0$, C is roughly exponential $C \sim \exp(-1.76\ T_0/T)$.

(b) Free energy of the superconducting phase (F_s) and of the normal phase (F_n) versus temperature. The two curves meet (with the same slope) at the transition point $T = T_0$. At $T = 0$ the difference $F_n - F_s$ is of order $(k_B T_0)^2/E_F$ per atom.

1–2 DIAMAGNETISM

The London Equation

We now extend our energy considerations to situations where there are supercurrents $\mathbf{j}_s(\mathbf{r})$ and associated magnetic fields $\mathbf{h}(\mathbf{r})$ in the sample.[1] We see that in the limit where all fields, currents, and so on, are weak and have a slow variation in space the condition of minimum free energy leads to a simple relation between fields and currents (F. and H. London, 1935).

We consider a pure metal with a parabolic conduction band; the electrons have an effective mass m. The free energy now has the following form:

$$\mathfrak{F} = \int F_s \, d\mathbf{r} + E_{kin} + E_{mag} \tag{1-1}$$

where F_s is the energy of the electrons in the condensed state at rest and E_{kin} is the kinetic energy associated with the permanent currents. Let us call $\mathbf{v}(\mathbf{r})$ the drift velocity of the electrons at point $\mathbf{r}$. It is related to the current density $\mathbf{j}_s$ by

$$n_s e\mathbf{v}(\mathbf{r}) = \mathbf{j}_s(\mathbf{r}) \tag{1-2}$$

(where e is the electron charge, and n_s the number of superconducting electrons per cm^3). Then we have simply

$$E_{kin} = \int d\mathbf{r}\ \tfrac{1}{2} m v^2 n_s \tag{1-3}$$

the integral being extended over the sample volume. Equation (1-3) would be exact for situations of uniform flow (v = const). It remains approximately correct for our present problem, provided that $\mathbf{v}(\mathbf{r})$ is a *slowly varying function of* $\mathbf{r}$. (We return to this limitation later.)

Finally, E_{mag} is the energy associated with the magnetic field $\mathbf{h}(\mathbf{r})$

$$E_{mag} = \int \frac{h^2}{8\pi}\, d\mathbf{r} \tag{1-4}$$

The field is related to $\mathbf{j}_s$ by Maxwell's equation

$$\text{curl } \mathbf{h} = \frac{4\pi}{c}\mathbf{j}_s \tag{1-5}$$

[1] We use **h** to denote a local field value. H will be reserved for the thermodynamic field.

Using (1-3), (1-4), and (1-5) we rewrite the energy E as

$$E = E_0 + \frac{1}{8\pi}\int [h^2 + \lambda_L^2 |\operatorname{curl} h|^2]\, dr$$

$$E_0 = \int F_s\, dr \qquad (1\text{-}6)$$

where the length λ_L is defined by

$$\lambda_L = \left[\frac{mc^2}{4\pi n_s e^2}\right]^{1/2} \qquad (1\text{-}7)$$

At $T = 0$, n_s is equal to n, the total number of conduction electrons per cubic centimeter. We can then compute λ_L explicitly. In simple metals such as Al, Sn, and so on, where m is close to the free electron mass, we find $\lambda_L \sim 500$ Å. For transition metals and compounds with narrow d bands, m is larger and λ_L is also larger (up to 2000Å).

We wish to minimize the free energy (1-6) with respect to the field distribution h(r). If h(r) changes by $\delta h(r)$, E changes by δE

$$\delta E = \frac{1}{4\pi}\int [h\cdot \delta h + \lambda_L^2 \operatorname{curl} h\cdot \operatorname{curl} \delta h]\, dr$$

$$= \frac{1}{4\pi}\int [h + \lambda_L^2 \operatorname{curl}\operatorname{curl} h]\cdot \delta h\, dr \qquad (1\text{-}8)$$

where we have integrated the second term by parts. The field configuration, in the interior of the specimen, which minimizes the free energy, must therefore satisfy the condition

$$h + \lambda_L^2 \operatorname{curl}\operatorname{curl} h = 0 \qquad (1\text{-}9)$$

Equation (1-9) was first proposed (with a slightly different notation) by F. and H. London. When combined with the Maxwell equation (1-5), it allows us to calculate the distribution of fields and currents.

Meissner Effect

We now apply the London equation and discuss the penetration of a magnetic field h into a superconductor. We choose the simplest geometry. The surface of the specimen is the xy plane, the region $z < 0$ being empty (Fig. 1-2). The field h and the current j_s depend only on z. In addition to the relation (1-9), h and j_s are always related by the Maxwell equations

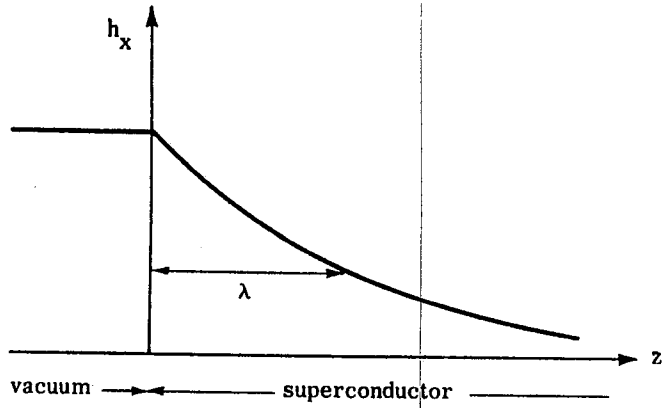

Figure 1-2
Field penetration in a superconductor. The field becomes negligibly small at distances larger than a few penetration depths λ. When the simple London equation (1-9) holds, the penetration is exponential $h = h_0 \exp(-z/\lambda_L)$.

$$\operatorname{curl} h = \frac{4\pi j_s}{c} \qquad (1\text{-}10)$$

$$\operatorname{div} h = 0 \qquad (1\text{-}11)$$

Two cases are possible:

(1) h is parallel to z. Then (1-11) reduces to $\partial h/\partial z = 0$ and h is spatially constant. Therefore curl h = 0 and $j_s = 0$ from Eq. (1-10). Inserting this into Eq. (1-11) we find $h = 0$. Therefore it is not possible to have a field normal to the surface of the specimen.

(2) h is tangential (and directed along the x axis). Then Eq. (1-11) is automatically satisfied. From Eq. (1-10) j_s is directed along the y axis:

$$\frac{dh}{dz} = \frac{4\pi j_s}{c} \qquad (1\text{-}12)$$

Finally, from Eq. (1-9),

$$\frac{dj_s}{dz} = \frac{ne^2}{mc} h \qquad (1\text{-}13)$$

$$\frac{d^2h}{dz^2} = \frac{h}{\lambda_L^2} \qquad \lambda_L^2 = \frac{mc^2}{4\pi ne^2} \qquad (1\text{-}14)$$

The solution that remains finite in the superconductor is exponentially decreasing,

$$h(z) = h(0)\, \exp(-z/\lambda_L) \qquad (1\text{-}15)$$

The field h penetrates only to a depth λ_L *inside the sample.* This result, established here for a semiinfinite slab, is easily generalized to a macroscopic specimen of arbitrary shape. As we have seen, the "penetration depth" λ_L is small. Therefore, in all cases, a *weak* magnetic field practically does not penetrate at all into a macroscopic specimen.[2] The lines of force are excluded as shown on Fig. 1-3.

The superconductor finds an equilibrium state where the sum of kinetic and magnetic energies is minimum, and this state, for macroscopic samples, corresponds to the expulsion of magnetic flux.

Experimentally, the expulsion of lines of force was shown by Meissner and Ochsenfeld in 1933. The Meissner result was particularly important in proving that a true equilibrium state was achieved.

Three remarks concerning the above derivation:

(1) Assuming the existence of permanent currents plus thermodynamic equilibrium, we are led to the diamagnetic properties. It is more usual to go the other way round: Taking the Meissner effect as a starting point, conclude that there exist permanent currents. I chose the first way because I wanted to show you the different contributions to the energy in a superconductor (Eq. 1-6). This list of energies will be useful later (Chapter 3).

(2) We obtained Eq. (1-9) from a minimum condition on the free energy $\mathcal{F}$. This is the correct thermodynamic potential when the external field sources are permanent magnets. When the source is a coil, with a fixed current I, the correct potential is not $\mathcal{F}$ but a different function $\mathcal{G}$ (the "Gibbs potential"). Fortunately, both potentials can be shown to lead to the same local equilibrium condition in the sample. (See Chapter 2 for a discussion of $\mathcal{F}$ and $\mathcal{G}$.)

(3) Note that the above calculation is valid only for weak applied fields. In higher fields it may become energetically more favorable

[2] In higher field different catastrophes may occur.

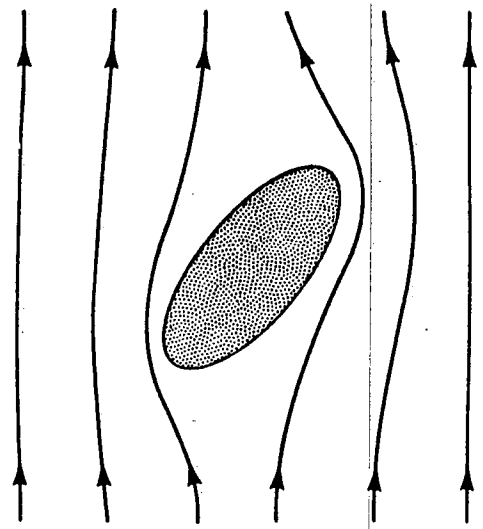

Figure 1-3
Distortion of the magnetic lines of force around a macroscopic superconductor ("macroscopic" means dimensions much larger than the penetration depth). If the fields are not too strong, the superconductor expels the lines completely (Meissner effect).

to destroy superconductivity in some parts of the sample and to allow the flux lines to penetrate. This will be considered in detail in Chapters 2 and 3.

1–3 ABSENCE OF LOW ENERGY EXCITATIONS

Let us begin by considering a free electron gas without interactions. The ground state is obtained by placing an electron into each individual momentum state **p**, of energy $p^2/2m$, until the Fermi energy $E_F = p_F^2/2m$ is reached. Above the Fermi energy E_F, all the levels are empty. (The condition $p = p_F$ defines the Fermi sphere, in momentum space.) In order to construct an excited state of the gas, it suffices to take an electron of momentum **p** from an initially occupied state ($p \le p_F$) and to place it into a state **p′** initially empty ($p' \ge p_F$) (Fig. 1-4). The excitation energy of this electron-hole pair is

$$E_{pp'} = \frac{p'^2 - p^2}{2m} \ge 0 \qquad (1\text{-}16)$$

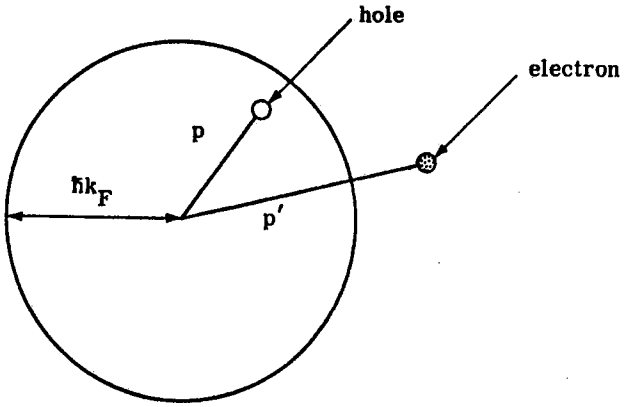

Figure 1-4
An excited state of the electron gas in a normal metal. One electron has been taken from a state of momentum $\mathbf{p}$ inside the Fermi sphere, to a state of momentum $\mathbf{p}'$ outside the Fermi sphere. The excitation energy $(p'^2 - p^2)/2m$ is very low if p and p′ are close to the Fermi momentum $p_F = \hbar k_F$.

f both p and p′ are close to the Fermi momentum, $E_{pp'}$ is very small; in a free electron gas there are numerous low energy excitations. In a normal metal, this free electron picture is not qualitatively modified. The low energy excitations are displayed by the following experiments:

a) The specific heat is relatively large and proportional to T (of order $k_B \cdot (k_B T/E_F)$ per electron).

b) Strong dissipative effects appear when the electrons are submitted to low frequency external perturbations (electromagnetic waves, ultrasonic waves, nuclear spin precession, and so on).

In most superconductors, the situation is completely different. The energy $E_{pp'}$, necessary to create a pair of excitations is no longer given by Eq. (1-16). It is necessary to at least furnish a certain "pairing energy" 2Δ:

$$E_{pp'} \geq 2\Delta \qquad (1\text{-}17)$$

Roughly speaking, this "gap" 2Δ is related to the transition temperature by $2\Delta = 3.5\, k_B T_0$. Thus typically 2Δ is of order 10°K (Table 1-1).

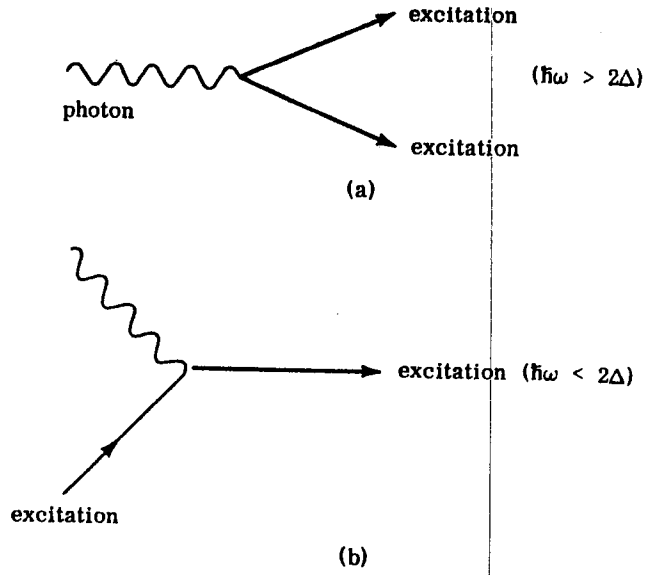

Figure 1-5
Typical dissipative processes in a superconductor. Fig. 1-5a shows the creation of a pair of excitations by one photon. This process can occur only if $\hbar\omega > 2\Delta$. Fig. 1-5b shows the absorption of the photon by a preexisting excitation. This process can occur even if $\hbar\omega < 2\Delta$, but it is weak at low temperatures, where there are very few thermal excitations. Similar processes are obtained by replacing "photon" by "phonon" in 1-5a and 1-5b.

Note that 2Δ is the energy needed to create two excitations. The energy per excitation is Δ.

Various experiments measure Δ. Here are some of them:

(a) The low temperature specific heat is now exponential and proportional to $\exp(-\Delta/k_B T)$.

(b) Absorption of electromagnetic energy. For $\hbar\omega \geq 2\Delta$ a photon of frequency ω can create an electron-hole pair. [This corresponds to photons in the far infrared; typical wavelengths are in the 1mm range (Fig. 1-5a).]

(c) Ultrasonic attenuation. Here the phonon is of low frequency and cannot decay by creation of a pair of excitations. But it can be absorbed by collision with a preexisting excitation (Fig. 1-5b). This

Table 1-1
Values of the energy gap 2Δ (at 0°K) in °K[a]

	P	A	T
Zn		3.17	
Cd	1.8		
Hg	18.4		18.0
Al	6.01	4.4	4.2
In	13.6	11.9	11.9
Ga		4.03	
Sn	13.0		12.9
Pb	28.7		30.9
V	18.0	18.5	18.0
Nb	27.4	37.4	35.0
Ta		15.7	16.1
La			

[a]For a bibliography on energy gas measurements see D. H. Douglas, Jr., and L. M. Falicov, *Low Temperature Physics*, Vol. IV, edited by C. G. Gorter (Amsterdam: North Holland Publishing Co., 1964). The experiments are classified as follows: P photon absorption (microwave or far infrared photons); A ultrasonic attenuation; T tunneling. The ultrasonic experiments are often performed in single crystals, in which case, 2Δ depends slightly on the direction of the sound wave.

process is proportional to the number of preexisting excitations, thus to $\exp(-\Delta/k_B T)$.

(d) Tunnel effect. A superconductor S and a normal metal N are separated by a thin insulating barrier (typical thickness 25 Å) (Fig. 1-6a). The quantum mechanical tunnel effect allows individual electrons to pass through the barrier. The electron must have been excited from the condensed phase, and this requires an energy Δ. There is no current at low temperatures unless we apply a voltage V across the junction such that the energy gain eV is larger than Δ. The current voltage characteristic has the form shown in Fig. 1-6b.

Question: Is the existence of an energy gap a necessary condition for the existence of permanent current (superfluidity)? The answer is no. A number of situations have been found where superfluidity occurs with no gap in the one particle excitation spectrum. The simplest example is "surface superconductivity"—certain metals or alloys, in a suitable range of field, are superconducting only in a thin sheath (typically 1000Å) near the sample surface. Excitations from the inner (normal) regions can leak up to the surface—there is no gap in the energy spectrum. (This has been checked recently by tunneling experiments.) However the sheath is superconducting! There are other examples, some of which we shall discuss later.

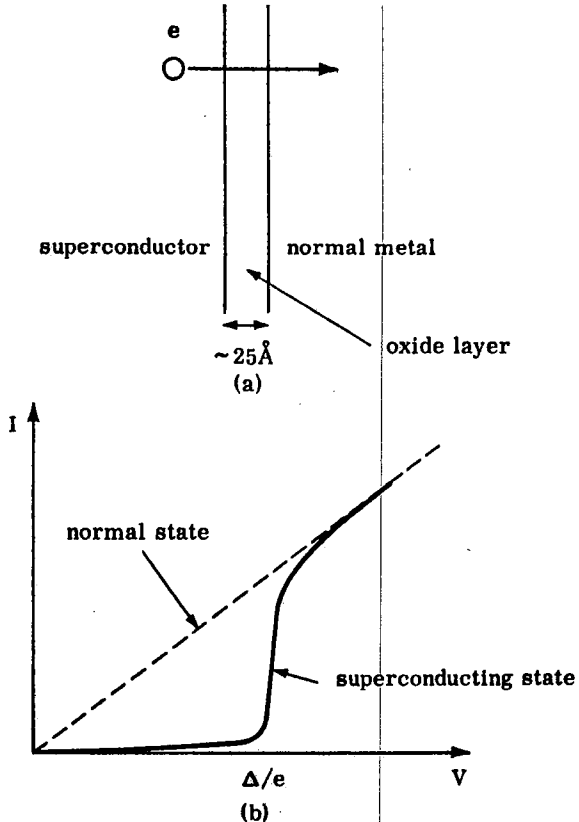

Figure 1-6

A tunneling junction between a normal metal and a superconductor. (a) Shows the geometry. (b) Shows the current-voltage characteristic when s is superconducting ($T \ll T_0$) and also when s is normal ($T > T_0$). Typically for a junction 1 mm × 1 mm the resistance V/I when both metals are normal may range from 10^{-2} to 10^4 ohms. When $T \ll T_0$, to extract one electron from the superconducting condensate requires a minimum energy Δ. Essentially no current flows until $eV = \Delta$.

-4 TWO KINDS OF SUPERCONDUCTORS

Our derivation of the London equation (1-9) assumes a slow varia-
on in space of $\mathbf{v}(\mathbf{r})$ or of the supercurrent $\mathbf{j}_s(\mathbf{r})$. What do we mean
the word "slow"? In the condensed state, the velocities of two elec-
ons (1) and (2) are correlated if the distance between them R_{12} is
naller than a certain range. For pure metals, the correlation length
called ξ_0. Our derivation applies when $\mathbf{v}(\mathbf{r})$ has a negligible vari-
ion over distances $\sim \xi_0$. To estimate ξ_0 we notice that the important
main in momentum space is defined by

$$E_F - \Delta < \frac{p^2}{2m} < E_F + \Delta \tag{1-18}$$

ere E_F is the Fermi level. The thickness of the shell in p space
fined by Eq. (1-18) is $\delta p \cong (2\Delta/v_F)$ (where $v_F = p_F/m$ is the ve-
city at the Fermi level; we have made use of the fact that $\Delta \ll E_F$
all cases). A wave packet formed of plane waves whose momentum
s an uncertainty δp has a minimum spatial extent $\delta x \sim (\hbar/\delta p)$. This
ds us to take

$$\xi_0 = \frac{\hbar v_F}{\pi \Delta} \tag{1-19}$$

he factor $1/\pi$ is arbitrary but will become convenient later.) The
gth ξ_0 defined by Eq. (1-19) is called the *coherence length* of the
perconductor.

Equations (1-15) and (1-13) show that h, $\mathbf{j}_s$, or v vary on a scale
. Thus our derivation of the London equation holds only if $\lambda_L \gg \xi_0$.
(1) In simple (nontransition) metals as we have seen, λ_L is small
300Å). The Fermi velocity v_F is large ($v_F \lesssim 10^8$ cm/sec) and ac-
ding to Eq. (1-19) ξ_0 is also large ($\xi_0 \cong 10^4$ Å for aluminum). Thus
these metals the London equation does not apply. In fact, they do
ibit the Meissner effect, but in order to calculate the penetration
th it is necessary to replace Eq. (1-9) by a somewhat more com-
cated relation, the form of which has been suggested by Pippard.
call these first kind (Type I) or Pippard superconductors and dis-
s them in Chapter 2.

(2) For transition metals and intermetallic compounds of the type
Sn, V_3Ga, the effective mass is very large, λ_L is large ($\sim$2000 Å)
the Fermi velocity is small ($\sim 10^6$ cm/sec). Also, in these
compounds the transition temperature T_0 above which superconductivity disappears is found to be high (18°K in Nb_3Sn). As we will see later, Δ is roughly proportional to T_0 and is therefore larger. For all these reasons ξ_0 is very small (~50Å). Therefore for this class of materials Eq. (1-9) is well applicable in weak fields. We call these second kind (Type II) or London superconductors.

In order to complete this discussion, it is necessary to mention the case of superconducting alloys, for which the coherence length and penetration depth are modified by mean free path effects, which we will discuss later. Qualitatively, if the mean free path due to disorder in the structure is short, the coherence length becomes smaller than $\hbar v_{\mathcal{F}}/\pi\Delta$ and λ_L is increased with respect to Eq. (1-7). Therefore it frequently occurs that the addition of impurities into a Pippard superconductor transforms it into a London superconductor.

The distinction here between the two classes is crucial for all experiments made in the presence of external fields. Historically, during a period of 20 years after the discovery of the Meissner effect, experiments were mainly carried out in first kind superconductors. The detailed study of second kind superconductors is much more recent. Paradoxically, the theory has followed the inverse order. Equation (1-9) was introduced by the London brothers in 1935, but the necessary modifications for first type superconductors was only proposed by Pippard in 1953. We now study in detail the magnetic properties of the two types.

REFERENCES

On superfluidity:

F. London, *Superfluids*, Vol. I, 2nd ed. New York: Dover, 1961.

General discussion of experimental data on superconductors:

E. A. Lynton, *Superconductivity*, 2nd ed. London: Methuen and Co., 1965.

More recent advances on the superfluidity concept:

J. Bardeen and R. Schrieffer, *Progress in Low Temperature Physics*, Vol. III, edited by C. G. Gorter. Amsterdam: North Holland, 1961.

J. M. Blatt, *Theory of Superconductivity*. New York: Academic Press, 1964.

Proceedings of the Brighton Symposium on Quantum Fluids (Brighton, 1965) to be published in *Reviews of Modern Physics* 1966.

3

MAGNETIC PROPERTIES OF SECOND KIND SUPERCONDUCTORS

3-1 MAGNETIZATION CURVES OF A LONG CYLINDER

Type II superconductors are characterized by the following macroscopic properties:

(1) A cylinder placed in a longitudinal field H does not exhibit a "perfect" total flux expulsion (Meissner effect), except for weak field $H < H_{C_1}$.[1]

If one calculates the critical field H_C defined by the difference in free energies between the normal and superconducting states in zero field:

$$F_n - F_s = \frac{H_C^2}{8\pi} \tag{3-1}$$

one finds that H_{C_1} is clearly smaller than H_C. For example, for the compound V_3Ga, caloric measurements in zero field (giving $F_n - F_s$) indicate $(H_C)_{T=0} \simeq 6000$ G, and magnetic measurements give $(H_{C_1})_{T=0} \simeq 200$ G.

(2) For $H > H_{C_1}$, lines of force penetrate the cylinder, but even

[1]The notation H_{C_1} for the first penetration field has been recommended by the participants of the Colgate Conference on Superconductivity (1963).

at thermal equilibrium this penetration is not complete. The flux ϕ passing through the cylinder remains less than its value when the sample is in the normal state. This implies the existence of permanent currents in the specimen, which is thus still superconducting. This situation exists for fields $H_{C_1} \leq H \leq H_{C_2}$. H_{C_2} is larger than H_C and is sometimes very large—for V_3Ga $(H_{C_2})_{T=0} \sim 300{,}000$ G.

(3) For $H > H_{C_2}$ a macroscopic sample does not show any expulsion of flux $B \equiv H$. However superconductivity is not completely destroyed. In an interval $H_{C_2} < H < H_{C_3}$ there remains on the surface of the cylinder a superconducting sheath (of typical thickness 10^3 Å). (In most cases $H_{C_3} \sim 1.69 H_{C_2}$.) The existence of this sheath can be shown, for instance, by measuring the resistance between two probes on the sample surface. It is found that for low measuring currents the resistance vanishes. Physically the sheath has the following origin: It is easier to nucleate a small superconducting region near the sample surface—just as it is easier to grow bubbles on the bottom of a glass of beer than to grow them from an arbitrary point in the beer. (A somewhat more sophisticated version of this argument will be discussed in Chapter 5.)

The variation with temperature of the fields H_{C_1}, H_{C_2}, H_{C_3} is represented in Fig. 3-1. We now focus our attention on the region $H_{C_1} < H < H_{C_2}$ where partial flux penetration occurs. The existence of this region of the (H,T) plane was clearly shown for the first time in early experiments on alloys by Schubnikov (1937). We call it the Schubnikov phase, or sometimes the vortex state. (The latter name comes from the microscopic picture to be derived in Section 3-2.)

The partial flux penetration in the Schubnikov phase can be described in terms of a diagram B(H); the aspect of this diagram is shown in Fig. 3-2. Sometimes, instead of the induction B, the experimentalists prefer to plot the "magnetization" M defined by

$$M = \frac{B - H}{4\pi} \tag{3-2}$$

The M(H) curve is shown in Fig. 3-3.

(In practice the observation of these curves is often complicated by difficulties in attaining equilibrium; for example, structural defects oppose the displacement of the lines of force.)

In Fig. 3-3 the dashed line represents the magnetization curve found for a first kind superconductor with the same H_C. These two curves are related by a remarkable property—the areas they subtend are equal.

and we conclude that the area subtended by the curve of Fig. 3-3 depends only on H_c. From the equilibrium magnetization curves, one can therefore determine H_c and the condensation energy.

We now discuss the transition occurring when the applied field H becomes equal to one of the limiting values H_{c_1} or H_{c_2}. Consider first the transition at H_{c_2}. Experimentally this is a *second-order* transition in all cases studied up to now.

(1) Magnetization measurements show that the B(H) curve is continuous at $H = H_{c_2}$.

(2) In the few cases (V_3Ga) where thermal measurements have been performed, it appears that there is no latent heat for the transformation, but only a discontinuity in the specific heat.

It is possible to relate this discontinuity to the magnetization curves by a purely thermodynamic analysis (Goodman, 1962). Let i and j be the two phases of interest (for the case at hand i would represent the Schubnikov phase and j the phase with $B \equiv H$, where the bulk of the sample is normal)

$$G_i = F_i(T, B_i) - \frac{B_i H}{4\pi} \tag{3-11}$$

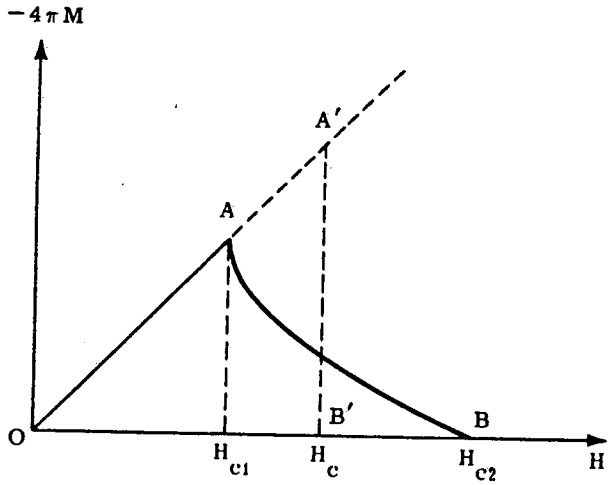

Figure 3-3
The reversible magnetization curve of a long cylinder of Type I (dotted line) or Type II (solid line) superconductor. If the two materials have the same thermodynamic field H_c, the areas OAB and OA′B′ are equal.

is the Gibbs function per cm^3 of the ith phase. The relation between the field H and the induction B in this phase is obtained by minimizing G for fixed H and T

$$\frac{\partial}{\partial B_i} F_i(T, B_i) = \frac{H}{4\pi} \tag{3-12}$$

the entropy S_i is deduced from the relations

$$S_i = -\left(\frac{\partial G_i}{\partial T}\right)_H = -\frac{\partial F_i}{\partial T} \tag{3-13}$$

When the field satisfies a certain condition $H = H^*(T)$, there is an equilibrium between the phases i and j (i.e., for the present case $H^* = H_{c_2}$). On this curve, one has

$$G_i = G_j \tag{3-14}$$

Suppose that there is no latent heat associated with the transformation. Then, along the curve $H = H^*(T)$, the two phases have the same entropy

$$S_i = S_j \tag{3-15}$$

We first show that this excludes any discontinuity in B at the transition. To show this, we calculate the variation of F_i when one moves along the equilibrium curve [$dH = (dH^*/dT)\, dT$]

$$\frac{dF_i}{dT} = \frac{\partial F_i}{\partial T} + \frac{\partial F_i}{\partial B_i}\frac{dB_i}{dT} \tag{3-16}$$

From this equation and using (3-12) and (3-13), we obtain the variation of G along the equilibrium curve

$$\frac{dG_i}{dT} = -S_i - \frac{B_i}{4\pi}\frac{dH^*}{dT} \tag{3-17}$$

Along the equilibrium curve we have constantly $G_i = G_j$, therefore $dG_i/dT = dG_j/dT$; if also $S_i = S_j$ we necessarily have $B_i = B_j$; B is continuous at the transition.

We now calculate the specific heat in constant field

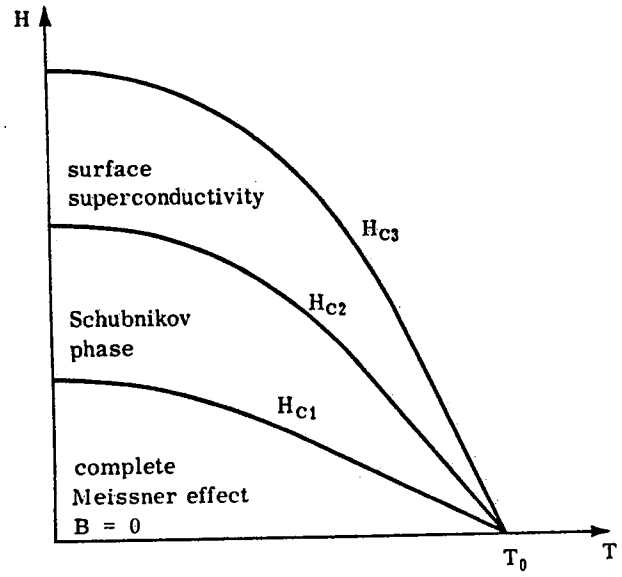

Figure 3-1
Phase diagram for a long cylinder of a Type II superconductor.

Proof: Let G_S be the Gibbs function per unit volume for the superconducting state

$$G_S = F_S(B) - \frac{BH}{4\pi} \tag{3-3}$$

G_S is a minimum for fixed H, that is, at equilibrium

$$\left(\frac{\partial G_S}{\partial B}\right)_H = 0 \tag{3-4}$$

Let G_n be the Gibbs function for the normal state

$$G_n = F_n + \frac{B^2}{8\pi} - \frac{BH}{4\pi} \tag{3-5}$$

At thermodynamic equilibrium in the normal phase $(\partial G_n/\partial B)_H = 0$; therefore, B = H and

$$G_n = F_n - \frac{H^2}{8\pi} \tag{3-6}$$

Let the field vary from H to H + δH. From (3-3) and (3-4)

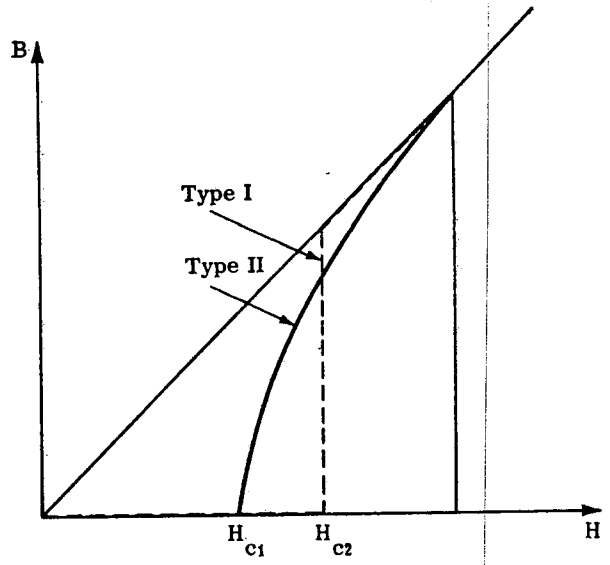

Figure 3-2
The induction (or flux/cm^2) in the cylinder as a function of the applied field H. The full curve applies for a Type II superconductor, the dotted curve for a Type I.

$$\frac{\partial G_S}{\partial H} = -\frac{B}{4\pi} \tag{3-7}$$

and from (3-6)

$$\frac{\partial G_n}{\partial H} = -\frac{H}{4\pi} \tag{3-8}$$

$$\frac{\partial}{\partial H}(G_n - G_S) = \frac{B - H}{4\pi} = M \tag{3-9}$$

We now integrate this relation between H = 0 and $H = H_{c2}$. At $H = H_{c2}$, the two phases are in equilibrium and $G_n = G_S$. For H = 0, B = 0 we have $G_n = F_n$, $G_S = F_S$, and by definition

$$(F_n - F_S)_{B=0} = \frac{H_c^2}{8\pi}$$

The result is therefore

$$\int_0^{H_{c2}} M dH = \frac{-H_c^2}{8\pi} \tag{3-10}$$

$$C_i = T\left(\frac{\partial S_i}{\partial T}\right)_H \tag{3-18}$$

e can transform the second factor by calculating the total derivative the entropy along the equilibrium curve

$$\frac{dS_i}{dT} = \left(\frac{\partial S_i}{\partial T}\right)_H + \left(\frac{\partial S_i}{\partial H}\right)_T \frac{dH^*}{dT} \tag{3-19}$$

rom (3-15), $dS_i/dT = dS_j/dT$ along the equilibrium curve and

$$C_j - C_i = T\frac{dH^*}{dT}\left[\left(\frac{\partial S_i}{\partial H}\right)_T - \left(\frac{\partial S_j}{\partial H}\right)_T\right] \tag{3-20}$$

/e transform $(\partial S_i/\partial H)_T$ by using (3-13) and (3-12)

$$\left(\frac{\partial S_i}{\partial H}\right)_T = \left(\frac{\partial S_i}{\partial B_i}\right)_T \left(\frac{\partial B_i}{\partial H}\right)_T = -\frac{\partial^2 F_i}{\partial B_i \partial T}\left(\frac{\partial B_i}{\partial H}\right)_T$$

$$= -\frac{1}{4\pi}\frac{\partial H(B_i\,T)}{\partial T}\left(\frac{\partial B_i}{\partial H}\right)_T \tag{3-21}$$

inally, we write the variation of H* with respect to T in the form

$$\frac{dH^*}{dT} = \left(\frac{\partial H}{\partial T}\right)_{B_i} + \left(\frac{\partial H}{\partial B_i}\right)_T \frac{dB}{dT} \tag{3-22}$$

/here $dB/dT = dB_i/dT = dB_j/dT$ represents the variation of B along he equilibrium curve. On inserting $(\partial H/\partial T)_B$ from (3-22) into (3-21) ve find

$$\left(\frac{\partial S_i}{\partial H}\right)_T = -\frac{1}{4\pi}\frac{dH^*}{dT}\left(\frac{\partial B_i}{\partial H}\right)_T + \frac{1}{4\pi}\frac{dB}{dT} \tag{3-23}$$

$$C_j - C_i = \frac{T}{4\pi}\left(\frac{dH^*}{dT}\right)^2\left[\left(\frac{\partial B_j}{\partial H}\right)_T - \left(\frac{\partial B_i}{\partial H}\right)_T\right] \tag{3-24}$$

Therefore, if one knows H*(T) and the permeabilities $(\partial B_i/\partial H)_T$ for each of the phases, one can predict the discontinuity in the specific heat. For the transition (i → j) we have a finite permeability (> 1) in the vortex state (i) from Fig. 3-2 and a permeability equal to 1 in the normal state (j). Therefore $C_i > C_j$. At this time all the necessary information is not available to compare (3-24) to experiment. However, for V_3Ga, $C_i - C_j$ and dH_{c_2}/dT are known and if one makes a reasonable extrapolation for $\partial B/\partial H$ in order to predict its value at H_{c_2} one finds an agreement to within about 10% from magnetic and calorimetric measurements. A similar analysis can be carried out in principle for the transition at $H = H_{c_1}$. Here, however, the permeability $(\partial B/\partial H)_{H=H_{c_1}}$ in the Schubnikov phase is probably infinite, as shown by the theoretical calculations of Section 3-2. From (3-24) this leads to an infinite peak in the specific heat at the transition. The singularity is, in fact, weak and easily masked by hysteresis effects. It has been observed recently (on Niobium) by the Rutgers group.

3–2 VORTEX STATE: MICROSCOPIC DESCRIPTION

Negative Surface Energy

We have previously seen that in a London ($\xi < \lambda$) superconductor the surface tension of a wall separating normal and superconducting regions becomes negative. Under these conditions, we guess that in the presence of a field a state is created where the N and S regions are finely divided and where the wall energy gives an important contribution to the thermodynamic potential. This situation is very different from that encountered for a Pippard superconductor where the walls are less numerous and where their energy can be neglected in a macroscopic treatment.

Consider, for example, the limit where B is small (that is, few lines of force penetrate the specimen and only a small fraction of the sample is normal). There are essentially two possibilities to maximize the surface to volume ratio for the N regions:

We can form lamina of very small thickness ($\geq \xi$) or filaments of small diameter ($\sim \xi$). In the case of $\lambda \gg \xi$, theoretical calculations show that the second solution is lowest in energy.[2] We therefore find filaments. They are represented in Fig. 3-4a.

Each filament has a hard core of radius ξ where the superconducting electron density n_s falls as is shown in Fig. 3-4c. The lines of force are not confined to the hard core; the field is maximum at the center of the filament but extends a distance λ (Fig. 3-4b). Annular

[2]See problem, page 71.

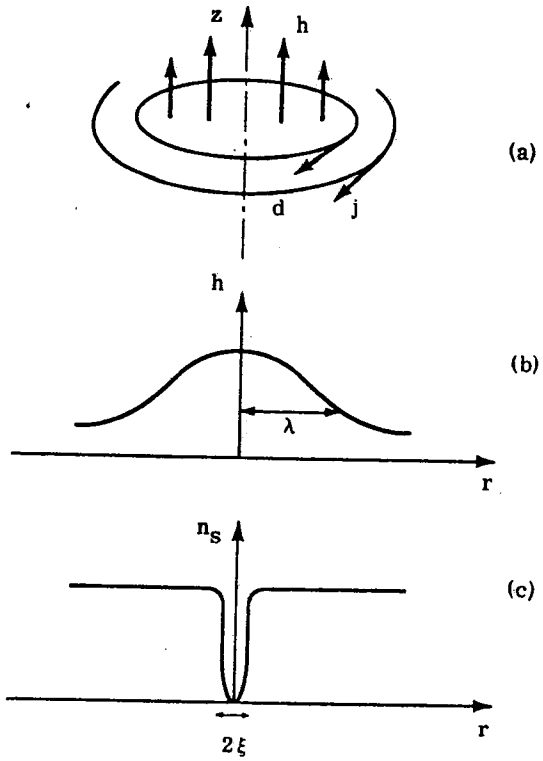

Figure 3-4

Structure of one vortex line in a Type II superconductor. The magnetic field is maximum near the center of the line. Going outwards, h decreases because of the screening in an "electromagnetic region" of radius ~λ (the penetration depth) (Fig. 3-4b). On the other hand, the number of superconducting electrons per cm^3 n_s is reduced only in a small "core region" of radius ξ (Fig. 3-4c).

currents j encircle the filament and screen out the field for $r \gtrsim \lambda$. For $r > \xi$, that is, in most of the region of interest, the currents and fields can be simply calculated by London's equations. It will be shown that the radius and exact form of the hard core only appear in the argument of a logarithm; therefore it will not be necessary to know them accurately. In the limit $\xi \ll \lambda$ we shall, in fact, see that the properties of a filament are very easy to calculate.

What is the flux $\phi = \int h d\sigma$ carried by a filament?

Experiment and theory show us that if a bulk superconducting annulus surrounds some lines of force the enclosed flux can only take on discrete values

$$\phi = k\phi_0 \qquad (k \text{ is an integer}) \tag{3-25}$$

$$\phi_0 = \frac{ch}{2e} = 2 \times 10^{-7}\ \text{G cm}^2$$

The explanation of this effect will be given at the end of Chapter 4. The same result applies here. In order to attain the state of maximum subdivision, each filament carries one quantum of flux ϕ_0. This condition fixes the field scale in Fig. 3-4b, and the structure of the filament is completely defined.

Such a quantized filament, formed of a very thin hard core surrounded by currents rotating about the axis, is very analagous to the vortex lines found in superfluid He^4 when the helium container is rotated. The only important difference is that the helium atoms are not charged, making e = 0 in Eq. (1-13). We see that the penetration depth λ in He^4 is infinite and the particle currents j, instead of decreasing exponentially for $r > \lambda$, decrease very slowly (as in 1/r) far from the filament. Historically, vortex lines were first discussed for the He^4 problem by Onsager and Feynman; the generalization to superconductivity is due to Abrikosov (1956). When the superconducting metal contains a finite density of these lines, we say that it is in the vortex state.

Properties of One Isolated Vortex Line

We now study in detail the structure of one vortex line in the limit $\lambda \gg \xi$. The "hard core" of radius ξ is very small and we shall, for the moment, neglect completely its contribution to the energy.

Then the line energy is given by the formula

$$\mathcal{J} = \int_{(r > \xi)} d\mathbf{r}\ \frac{1}{8\pi}\left[h^2 + \lambda^2 (\text{curl } h)^2\right] \tag{3-26}$$

Equation (3-26) has been derived in Chapter 1 (assuming $\lambda \gg \xi$). For a pure superconductor, the penetration depth λ has the London value

$$\lambda_L = \left[\frac{mc^2}{4\pi n_s e^2}\right]^{1/2} \tag{3-27}$$

'or a superconducting alloy, with $\lambda \gg \xi$, Eq. (3-26) still applies, ut with a modified (larger) value of λ, as explained in Chapter 2 (see ie discussion after Eq. 2-20). In Eq. (3-26) the integration is carried out in all space outside of the "hard core" ($r > \xi$). We also hoose to compute the energy per unit length of line; the resulting energy per cm $\mathfrak{J}$ is called the line tension. Demanding that $\mathfrak{J}$ be a minimum leads as usual to the London equation

$$\mathbf{h} + \lambda^2 \operatorname{curl}\operatorname{curl}\mathbf{h} = 0 \qquad |r| > \xi \tag{3-28}$$

n the interior of the hard core Eq. (3-28) must be replaced by something more complicated. But, since the hard core has a very small adius, we can try to replace the corresponding singularity, simply y a two-dimensional delta function $\delta_2(r)$, and write

$$\mathbf{h} + \lambda^2 \operatorname{curl}\operatorname{curl}\mathbf{h} = \phi_0 \delta_2(r) \tag{3-29}$$

/here ϕ_0 is a vector along the line direction. We now show that the trength ϕ_0 in (3-29) represents the total flux carried by the line.

Integrate (3-29) over the interior surface of a circle C of radius r ncircling the axis of the cylinder and use the curl formula:

$$\int \mathbf{h}\cdot d\sigma + \lambda^2 \oint \operatorname{curl}\mathbf{h}\cdot d\boldsymbol{\ell} = \phi_0 \tag{3-30}$$

f the circle has a radius $r \gg \lambda$, the currents $j(r) = c/4\pi \operatorname{curl}\mathbf{h}$ are egligible and the line integral along the perimeter of the circle vanshes. Thus the total flux carried by the filament has the value ϕ_0.

We now pass on to the explicit solution of (3-30) to which is added he Maxwell equation

$$\operatorname{div}\mathbf{h} = 0 \tag{3-31}$$

The field h is directed along the z axis; the current lines are circles n the xy plane. It is easy to predict the value of curl h, that is, the current, in the region $\xi \ll r \ll \lambda$. In fact, if we reconsider (3-30) vith a circle C whose radius is in this domain, the term $\int \mathbf{h}\cdot d\mathbf{r}$ is negligible (only a fraction r^2/λ^2 of the flux ϕ_0 passes through the circle C) and we have

$$\lambda^2\, 2\pi r\, |\operatorname{curl}\mathbf{h}| = \phi_0 \tag{3-32}$$

and

$$|\operatorname{curl}\mathbf{h}| = \frac{\phi_0}{2\pi\lambda^2}\frac{1}{r} \qquad (\xi < r \ll \lambda) \tag{3-33}$$

Since h is directed along the z axis, we have $|\operatorname{curl}\mathbf{h}| = -dh/dr$ and upon integrating this relation

$$h = \frac{\phi_0}{2\pi\lambda^2}\left[\ln\left(\frac{\lambda}{r}\right) + \text{const}\right] \qquad (\xi < r \ll \lambda) \tag{3-34}$$

In order to derive the constant of integration in (3-34), it is necessary to write the complete solution to (3-30) and (3-32), which is

$$h = \frac{\phi_0}{2\pi\lambda^2} K_0\left(\frac{r}{\lambda}\right) \tag{3-35}$$

where K_0 is the zero-order Bessel function of an imaginary argument defined as in Morse and Feshbach.[3] The important properties of this solution are the asymptotic form (3-34) for $r \ll \lambda$ (it is found that the constant vanishes) and the asymptotic form for large distances

$$h = \frac{\phi_0}{2\pi\lambda^2}\sqrt{\frac{\pi\lambda}{2r}}\, e^{-r/\lambda} \qquad (r \gg \lambda) \tag{3-36}$$

Once the fields are determined, it is easy to calculate the energy $\mathfrak{J}$. On integrating the second term in (3-28) by parts,

$$\mathfrak{J} = \frac{\lambda^2}{8\pi}\int d\sigma\cdot \mathbf{h}\times\operatorname{curl}\mathbf{h} \tag{3-37}$$

where the integral $\int d\sigma$ is to be taken over the surface of the hard core (cylinder of radius $\sim\xi$). It is convenient to calculate $\mathfrak{J}$ per cm of length along the filament. Then

$$\mathfrak{J} = \frac{\lambda^2}{8\pi}\, 2\pi\xi h(\xi)\,|\operatorname{curl}\mathbf{h}(\xi)| \tag{3-38}$$

which is, from (3-34) and (3-33),

$$\mathfrak{J} = \left(\frac{\phi_0}{4\pi\lambda}\right)^2 \ln\left(\frac{\lambda}{\xi}\right) \tag{3-39}$$

DISCUSSION OF THIS FORMULA

(1) $\mathfrak{J}$ only depends upon ξ logarithmically.

(2) $\mathfrak{J}$ is a quadratic function of the flux. Upon going to a situation where the flux is $2\phi_0$, it is preferable to have two filaments of flux ϕ_0 (total energy $2\mathfrak{J}$) than a filament of double flux (energy $4\mathfrak{J}$). This

[3] *Methods of Theoretical Physics*, (New York: McGraw-Hill, 1953), Chap. 10, p. 1321.

justifies the choice for ϕ_0 of the minimum flux value, that is, the quantum of flux.

(3) It is possible to rewrite $\mathcal{J}$ at $T = 0$ in a rather different form by using the relations

$$\phi_0 = \frac{ch}{2e}, \quad \xi = \xi_0 = \frac{\hbar v_F}{\pi \Delta(0)} \tag{3-40}$$

and a relation (which will be proven by the microscopic theory) between the condensation energy and the energy gap $\Delta(0)$:

$$\frac{H_c^2}{8\pi} = \tfrac{1}{2} N(0)\Delta^2(0) \tag{3-41}$$

where $N(0) = m^2 v/2\pi^2\hbar^3$ is the density of states (for one direction of spin) at the Fermi energy in the normal state per unit energy and per cm^3. Upon regrouping these formulas, we obtain

$$\mathcal{J} = \frac{\pi^3}{3} \frac{H_c^2}{8\pi} \xi^2 \ln \frac{\lambda}{\xi} \qquad (T = 0) \tag{3-42}$$

This formula is interesting for the following reason:

Until now we have neglected the contribution of the hard core to the line energy. In fact, superconductivity is more or less destroyed in the hard core section and this takes an extra energy $\mathcal{J}_{\text{int}} \sim (H_c^2/8\pi)\xi^2$.

Dimensionally from (3-42) this energy is comparable to $\mathcal{J}$. Numerically, however, it is much smaller. A more detailed calculation gives for the total energy

$$\mathcal{J} = \left(\frac{\phi_0}{4\pi\lambda}\right)^2 \left(\ln \frac{\lambda}{\xi} + \epsilon\right) \qquad (\lambda \gg \xi) \tag{3-43}$$

The numerical constant ϵ includes the effect of the hard core and is of the order of 0.1.

Problem. Discuss the structure of vortices in a thin film, the applied magnetic field being normal to the film surface (J. Pearl, 1964).

Solution. Again there is a "hard core" of radius ξ (which we assume to be small) surrounded by current rings. But since the currents are restricted to the thickness d of the film, their screening capacity is weak and the "electromagnetic region" is more spread out than in a long vortex line.

Inside the film, we apply Eq. (3-29)

$$\mathbf{h} + \frac{4\pi\lambda^2}{c} \operatorname{curl} \mathbf{j} = \phi_0 \delta_2(\mathbf{r}) \mathbf{n}_z$$

where $\mathbf{j}$ is the current density and $\mathbf{n}_z$ is a unit vector normal to the film. It is convenient to use the vector potential $\mathbf{A}$ rather than the field $\mathbf{h} = \operatorname{curl} \mathbf{A}$. In the London gauge, we find

$$\mathbf{A} + \frac{4\pi\lambda^2}{c} \mathbf{j} = \Phi$$

where $\Phi_r = \Phi_z = 0$ and $\Phi_\theta = \phi_0/2\pi r$.

Now average over the thickness d of the film. If $d \ll \lambda$, $\mathbf{A}$ and $\mathbf{j}$ are nearly constant in the thickness. Call $\mathbf{J}$ the total current $\mathbf{J} = \mathbf{j}d$. Then

$$\mathbf{J} = \frac{c}{4\pi} \frac{1}{\lambda_{\text{eff}}} (\Phi - \mathbf{A})$$

$$\lambda_{\text{eff}} = \frac{\lambda^2}{d}$$

Now replace the film by a infinitesimally small current carrying sheet in the plane $z = 0$, the current density being $J\delta(z)$. This will be valid when d is much smaller than the range of the electromagnetic region.

In terms of the current sheet the equation valid for all space is

$$\operatorname{curl} \operatorname{curl} \mathbf{A} = \operatorname{curl} \mathbf{h} = \frac{4\pi}{c} \mathbf{j} = \frac{1}{\lambda_{\text{eff}}} \delta(z)(\Phi - \mathbf{A})$$

or (since $\operatorname{curl} \operatorname{curl} \mathbf{A} = -\nabla^2 \mathbf{A}$ in the London gauge)

$$-\nabla^2 \mathbf{A} + \mathbf{A} \frac{1}{\lambda_{\text{eff}}} \delta(z) = \Phi \frac{1}{\lambda_{\text{eff}}} \delta(z)$$

This result was derived here from the London Eq. (3-29). In actual thin films, such a simple equation does not usually hold. But it is still correct to assume a linear current response of the form $\mathbf{J} = (c/4\pi\lambda_{\text{eff}})(\Phi - \mathbf{A})$, where λ_{eff} is some unknown constant, which can be obtained from another experiment (λ_{eff} is, in fact, the effective penetration depth in parallel fields, which could be measured on a hollow cylinder made with the same film).

To solve the equation for $\mathbf{A}$, introduce the three-dimensional Fourier transform

$$\mathbf{A}_{qk} = \int \mathbf{A}(xyz) \exp i(q_x x + q_y y + kz)\, dx\, dy\, dz$$

and the two-dimensional transforms

$$\mathbf{A}_q = \frac{1}{2\pi} \int dk\, \mathbf{A}_k = \int \mathbf{A}\delta(z)\, \exp i(q_x x + q_y y)\, dx\, dy\, dz$$

$$\mathbf{A}_q = \int \mathbf{A}(xy)\, \exp i(q_x x + q_y y)\, dx\, dy = i\frac{\phi_0}{q^2}\, \mathbf{n}_z \times \mathbf{q}$$

Then

$$-(q^2 + k^2)\mathbf{A}_{qk} + \frac{1}{\lambda_{eff}}\mathbf{A}_q = \frac{1}{\lambda_{eff}}\Phi_q$$

Solve for $\mathbf{A}_{qk}$ and integrate over k:

$$\mathbf{A}_q = \frac{1}{2\pi} \int dk\, \frac{1}{q^2 + k^2}(\mathbf{A}_q - \Phi_q)\frac{1}{\lambda_{eff}} = \frac{1}{2q\lambda_{eff}}(\mathbf{A}_q - \Phi_q)$$

$$\mathbf{A}_q = \Phi_q \frac{1}{1 + 2q\lambda_{eff}}$$

From this, all required information can be extracted:

(a) The current has components

$$\mathbf{J}_q = \frac{c}{4\pi\lambda_{eff}}(\Phi_q - \mathbf{A}_q) = \frac{c}{4\pi\lambda_{eff}}\Phi_q \frac{2q\lambda_{eff}}{1 + 2q\lambda_{eff}}$$

When $q \gg \lambda_{eff}^{-1}$, $\mathbf{J}_q$ is proportional to Φ_q. Thus at small distances r from the center of the vortex

$$\mathbf{J}(r) = \frac{c}{4\pi\lambda_{eff}}\Phi(r)$$

$$J = \frac{c\phi_0}{8\pi^2\lambda_{eff} r} \qquad (\xi \ll r \ll \lambda_{eff})$$

When $q \ll \lambda_{eff}^{-1}$

$$\mathbf{J}_q = \frac{c}{4\pi\lambda_{eff}} 2q\lambda_{eff}\Phi_q = \frac{c\phi_0}{2\pi}\frac{i\mathbf{n}_z \times \mathbf{q}}{q}$$

$$J = \frac{c\phi_0}{4\pi^2 r^2} \qquad (r \gg \lambda_{eff})$$

The size of the screening region is λ_{eff}. But even beyond λ_{eff}, J decreases only slowly with distance.

(b) The normal field component h_z in the film is derived from

$$h_{zq} = iq \times A_q = \frac{\phi_0}{1 + 2q\lambda_{eff}}$$

When $q \gg \lambda_{eff}^{-1}$

$$h_{zq} \sim \frac{\phi_0}{2q\lambda_{eff}}$$

$$h_z(r) \sim \frac{\phi_0}{4\pi\lambda_{eff} r} \qquad (\xi < r \ll \lambda_{eff})$$

At large r we derive h_z most easily from the current J

$$h_z = -\frac{4\pi\lambda_{eff}}{c}\frac{1}{r}\frac{d}{dr}(Jr)$$

$$\cong \frac{2}{\pi}\frac{\phi_0\lambda_{eff}}{r^3}$$

(c) The self-energy of the vortex is derived from Eq. (3-26); the required components of $\mathbf{h}$ and curl $\mathbf{h}$ at the core surface ($\xi \ll \lambda_{eff}$) are quoted above. The result is

$$E = \left(\frac{\phi_0}{4\pi}\right)^2 \frac{1}{\lambda_{eff}} \log\frac{\lambda_{eff}}{\xi} = \frac{137}{16}\frac{\hbar c}{\lambda_{eff}} \log\frac{\lambda_{eff}}{\xi}$$

Typically $\lambda_{eff} \sim 1000$Å and $E \sim 30$eV.

(d) The force between two vortices is

$$\mathbf{F}_{12} = \frac{\phi_0}{c}\, \mathbf{n}_z \times \mathbf{J}(R_{12})$$

Note that at long distances $J \sim 1/R^2$ and the repulsion energy decreases only like 1/R. This long range is due to the fact that most of the interaction takes place not through the superconductor, but through the empty space above and below.

Interactions between Vortex Lines

TWO VORTEX LINES

Consider two parallel lines directed along the z axis with positions $\mathbf{r}_1 = (x_1, y_1)$, $\mathbf{r}_2 = (x_2 y_2)$. The magnetic field distribution is determined by the equations

$$\mathbf{h} + \lambda^2\, \text{curl curl}\, \mathbf{h} = \phi_0[\delta(\mathbf{r} - \mathbf{r}_1) + \delta(\mathbf{r} - \mathbf{r}_2)] \qquad (3\text{-}44)$$

which is the generalization of (3-29). The solution $\mathbf{h}$ is the superposition of the fields $\mathbf{h}_1$ and $\mathbf{h}_2$ due to the filaments (1) and (2).

$$h(r) = h_1(r) + h_2(r)$$
$$h_1(r) = \frac{\phi_0}{2\pi\lambda^2} K_0\left(\frac{r - r_1}{\lambda}\right) \tag{3-45}$$

The energy of the system is still written

$$F = \int \frac{h^2 + \lambda^2 (\text{curl } h)^2}{8\pi} dr = \frac{\lambda^2}{8\pi} \int h \times \text{curl } h \cdot d\sigma \tag{3-46}$$

Here the integral $\int d\sigma$ is to be taken over the surfaces of the two hard cores ($|r - r_i| = \xi$); writing explicitly the two contributions to h we obtain

$$F = \frac{\lambda^2}{8\pi} \int (d\sigma_1 + d\sigma_2) \cdot (h_1 + h_2) \times (\text{curl } h_1 + \text{curl } h_2) \tag{3-47}$$

There are 8 terms that we regroup as follows: First the individual energy of each filament

$$\frac{\lambda^2}{8\pi} \left[\int d\sigma_1 \cdot h_1 \times \text{curl } h_1 + \int d\sigma_2 \cdot h_2 \times \text{curl } h_2 \right] = 2\mathfrak{I}$$

then the terms

$$\int (h_1 + h_2) \cdot (\text{curl } h_1 \times d\sigma_2 + \text{curl } h_2 \times d\sigma_1)$$

which tend toward 0 in the limit where $\xi \ll \lambda$ because $h_1 + h_2$ and curl h_1 are finite in the domain of integration $\int d\sigma_2$. There remains an important contribution

$$U_{12} = \frac{\lambda^2}{8\pi} \int (h_1 \times \text{curl } h_2 \cdot d\sigma_2 + h_2 \times \text{curl } h_1 \cdot d\sigma_1) \tag{3-48}$$

In effect, curl h_2 is proportional to $1/|r - r_2|$ for $|r - r_2| \ll \lambda$ from (3-33) and after integration one obtains a finite result as $\xi \to 0$. If we set

$$h_{12} = h_1(r_2) = h_2(r_1) = \frac{\phi_0}{2\pi\lambda^2} K_0\left(\frac{r_1 - r_2}{\lambda}\right) \tag{3-49}$$

then using (3-33) we obtain

$$U_{12} = \frac{\phi_0 h_{12}}{4\pi} \tag{3-50}$$

F_{12} represents the interaction energy (per cm) of two filaments. This is a *repulsive* energy which decreases as $(1/\sqrt{r_{12}})\, e^{-r_{12}/\lambda}$ at large distances, and which diverges as $\ln(|\lambda/r_{12}|)$ at short distances.

A remark about forces. Let us compute the force f_2 experienced by line 2, as due to the interaction U_{12}

$$f_{2x} = -\frac{\partial U_{12}}{\partial x_2} = -\frac{\phi_0}{4\pi} \frac{\partial h_{12}}{\partial x_2} \tag{3-51}$$

Introduce now the current $j = n_s ev$, which would exist, in the presence of line 1 alone, at the point $x_2 y_2$. Then $j_y = -(c/4\pi)(\partial h_{12}/\partial x_2)$ by Maxwell's equation and we have

$$f_{2x} = \frac{\phi_0}{c} j_y = \tfrac{1}{2} h n v_y \tag{3-52}$$

When more than one line is acting on line 2, Eq. (3-52) remains valid provided we interpret v as the total superfluid velocity at point $(x_2 y_2)$.

Conclusion. A line is in static equilibrium when the superfluid velocity at any point on the line is 0.

MAGNETIZATION CURVES

We now form the Gibbs function, minimize it, and deduce the density of vortices existing in the sample in thermal equilibrium.

$$G = n_L \mathfrak{I} + \sum_{ij} U_{ij} - \frac{BH}{4\pi} \tag{3-53}$$

The first term represents the individual energies of the lines, n_L is the number of lines per cm², related to the induction B by

$$B = n_L \phi_0 \tag{3-54}$$

(This expresses the fact that each vortex carries a flux ϕ_0.) The second term in (3-53) describes the repulsive interactions between vortices; the explicit form of U_{ij} is given by (3-49) and (3-50). Finally, the last term gives the effect of the field H and favors large values of B. It plays the role of a pressure that tends to increase the density of vortices.

In order to numerically evaluate the interaction term, it is useful to distinguish several regions:

(1) In the small induction region ($n_L \lambda^2 \ll 1$), only the interaction

etween nearest neighbor vortices is important and the sum ΣU_{ij} converges rapidly.

(2) When B is larger ($n_L \lambda^2 \gg 1$), the range λ of the interaction ecomes large compared to the spacing of the filament lattice, and ther methods are preferable to evaluate ΣU_{ij}.

(3) Finally, when n_L becomes comparable to $1/\xi^2$, the hard cores egin to overlap and the elementary methods used in this section are o longer valid. But, qualitatively, we may guess that when the hard ores do overlap, superconductivity is destroyed in the bulk. This coresponds to inductions $B \sim \phi_0/\xi^2$.

HE FIRST PENETRATION FIELD H_{c_1}

At very low line densities (low B), the interaction term in Eq. (3-52) s small and we shall first neglect it completely. Then, using Eq. (3-53) e get

$$G \cong B\left(\frac{\mathfrak{J}}{\phi_0} - \frac{H}{4\pi}\right) \tag{3-55}$$

When $H < 4\pi\mathfrak{J}/\phi_0$, G is an increasing function of B. The lowest G s obtained for B = 0 (complete Meissner effect).

When $H > 4\pi\mathfrak{J}/\phi_0$, we can lower G by choosing $B \neq 0$. There is ome flux penetration.

We conclude that the first penetration field is given by

$$H_{c_1} = \frac{4\pi\mathfrak{J}}{\phi_0} = \frac{\phi_0}{4\pi\lambda^2} \log \frac{\lambda}{\xi} \tag{3-56}$$

H_{c_1} is often much smaller than the "thermodynamic" field H_c defined y (3-1). For T = 0, for example, on using (3-40) and (3-41), we find

$$\frac{H_{c_1}}{H_c} = \frac{\pi}{\sqrt{24}} \frac{\xi}{\lambda} \ln\left(\frac{\lambda}{\xi}\right) \tag{3-57}$$

he result is therefore $H_{c_1}/H_c \sim \xi/\lambda$ and this may be much smaller han 1. A measurement of H_{c_1} and H_c, in principle, allows a determination of ξ and λ. For example, for V_3Ga, if at T = 0, $H_c \sim 6000$ G nd $H_{c_1} \sim 200$ G, one finds from (3-56) that $\lambda \cdot \xi \sim 80$ and then, from 3-56), $\lambda \sim 2000$Å and $\xi \sim 25$Å. These orders of magnitude are still ather inaccurate because of current uncertainties in H_c and H_{c_1}, but t is hoped that the situation will improve in the near future.

FIELDS SLIGHTLY LARGER THAN H_{c_1}

For finite line densities (finite B's) we must take into account the interaction term in Eq. (3-53). To minimize this repulsive energy, the lines will take a regular arrangement. Detailed calculations based on (3-53) show that, at all B's, the most favorable arrangement is triangular, as shown on Fig. 3-5 (J. Matricon, 1964).

If H is only slightly larger than H_{c_1}, we can guess that the equilibrium density of lines n will be small, and thus the distance between neighboring lines d will be large. If $d > \lambda$, we may keep only the nearest neighbor contributions to the interaction term in (3-53) and write

$$G \cong \frac{B}{4\pi}\left[H_{c_1} - H + \tfrac{1}{2} z \frac{\phi_0}{2\pi\lambda^2} K_0\left(\frac{d}{\lambda}\right)\right] \tag{3-58}$$

where z is the number of nearest neighbors of one line (z = 6 for the triangular lattice), d is related to the induction B through the relation

$$B \equiv \phi_0 n_L = \frac{2}{\sqrt{3}} \frac{\phi_0}{d^2} \quad \text{(triangular lattice)} \tag{3-59}$$

Equation (3-59) can be easily verified on Fig. 3-5. The function G(B) is represented in Fig. 3-6. Since $H > H_{c_1}$, the initial slope $(\partial G/\partial B)_{B=0}$

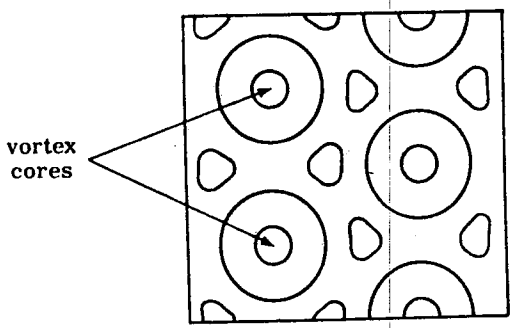

Figure 3-5
A triangular lattice of vortex lines (after Kleiner, Roth, and Autler, *Phys. Rev.*, 133A, 1226 (1964). The plane of the figure is normal to the field direction. The contours give the lines of constant n_s. This figure describes the situation at high fields (nearly overlapping cores).

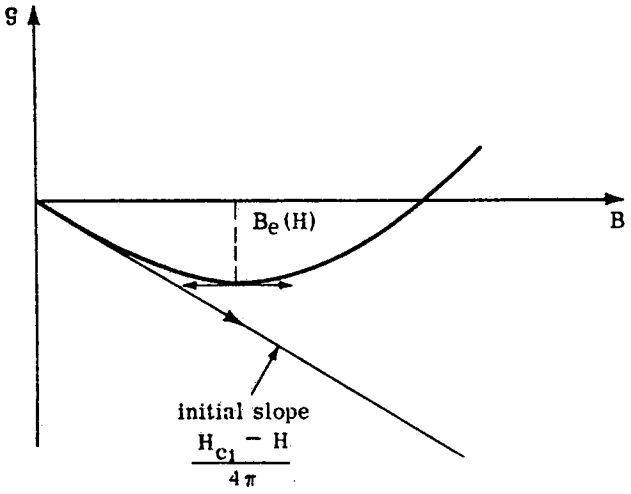

Figure 3-6

The thermodynamic potential $\mathcal{G}$ as a function of the induction B ($B = n_L \phi_0$ measures the number of vortices per cm^2 n_L). The equilibrium value of B [$B_e(H)$] corresponds to the minimum of $\mathcal{G}$.

is negative. As B increases, the interaction term begins to contribute but rather slowly, since it is proportional to $K_0(d/\lambda)$. When $d > \lambda$ we may write, according to (3-36)

$$K_0\left(\frac{d}{\lambda}\right) \sim \exp\left(-\frac{d}{\lambda}\right) = \exp\left[-1.07\sqrt{\frac{\Phi_0}{B\lambda^2}}\right] \qquad (3\text{-}60)$$

Thus the interaction term is exponentially small at small B's. At larger B's however, it dominates the over-all behavior and G(B) increases. There is a minimum of G for some value B = B(H). B(H) is the induction found at equilibrium in the field H. The theoretical B(H) or M(H) has been computed along these lines by Goodman and is shown on Fig. 3-7, together with experimental results on a particularly good MoRe alloy.

The following points must be noticed:

The theoretical curve has an infinite slope $(\partial M/\partial H)_{H=H_{c_1}} = \infty$ at the first penetration field. Physically, this reflects the fact that the lines repel each other like $e^{-d/\lambda}$, that is, we may think of their interaction as having a finite range λ. At field slightly larger than H_{c_1} it is thus possible to form many lines in the sample without competing against the interaction energy. The experimental curve does not show

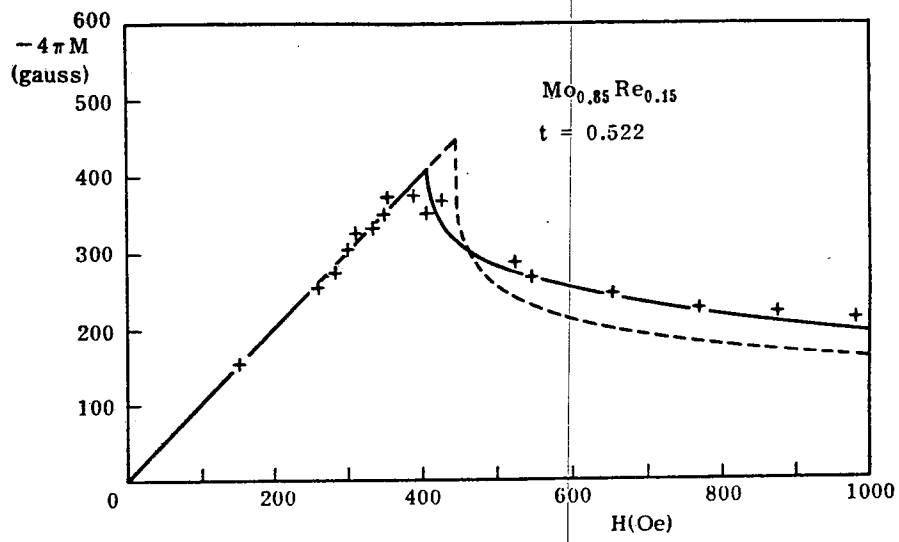

Figure 3-7

Experimental magnetization of a molybdenum-rhenium alloy at $T = 0.52T_0$ (after Joiner and Blaugher, *Rev. Mod. Phys.*, 36, 67 (1964). Also shown are two theoretical magnetization curves (after B. B. Goodman). The broken curve is for a laminar model, the continuous one for vortex lines.

a very large slope $(\partial M/\partial H)_{H=H_{c_1}}$; this is not very surprising since in the region of interest the interactions between lines are very weak and the lines can easily be pinned by structural defects. However, as we depart from H_{c_1} by more than 10%, we get good agreement between theory and experiment.

A similar theoretical curve can be drawn for another model where the flux-carrying units are not vortex lines, but laminas (see problem, p. 71). If the distance between laminas is d, we again find a repulsion between units proportional to $e^{-d/\lambda}$. However, in this case, the induction B is proportional to d^{-1}, while in the line case it is proportional to d^{-2} as shown by Eq. (3-59). Thus the fall of M(H) for $H > H_{c_1}$ is more rapid in the laminar model than in the vortex line model. The two theoretical curves are compared on Fig. 3-7; it is apparent that the vortex line gives a better fit, as emphasized by Goodman.

DOMAIN $\frac{1}{\lambda^2} \ll n_L \ll \frac{1}{\xi^2}$

In this region the vortices form a rather dense lattice and the interactions extend to distant neighbors. The interaction energy can then be calculated by the following method: The field h(r) directed along the z axis is the solution of

$$\mathbf{h} + \lambda^2 \operatorname{curl}\operatorname{curl}\mathbf{h} = \phi_0 \sum_i \delta_2(\mathbf{r} - \mathbf{r}_i)$$

$$\operatorname{div}\mathbf{h} = 0 \tag{3-61}$$

where $\mathbf{r}_i = (x_i, y_i)$ denotes the position of the ith vortex. The points $\mathbf{r}_i$ form a two-dimensional periodic lattice. We define the Fourier transform h_J by

$$h_J = n_L \int_{\text{cell}} h(x_i, y_i) \exp[i(J_x x + J_y y)]\, dx\, dy$$

Since $h(x_i, y_i)$ is periodic, h_J is nonvanishing only when $\mathbf{J}$ is a reciprocal lattice vector. From (3-61),

$$h_J = \frac{n_L \varphi_0}{1 + \lambda^2 J^2} \tag{3-62}$$

Finally the free energy becomes

$$\mathcal{F} = \frac{1}{8\pi} \int (h^2 + \lambda^2 \operatorname{curl}^2 h)\, d\mathbf{r}$$

$$= \frac{1}{8\pi} \sum_J h_J^2 (1 + \lambda^2 J^2) = \frac{B^2}{8\pi} \sum_J \frac{1}{1 + \lambda^2 J^2}$$

$$= \frac{B^2}{8\pi} + \frac{B^2}{8\pi} \sum_{J \neq 0} \frac{1}{1 + \lambda^2 J^2} \tag{3-63}$$

In the sum $\Sigma_{J \neq 0}$, the minimum magnitude of the vectors $\mathbf{J}$ is of the order $1/d \sim \sqrt{n_L}$ and $\lambda^2 J^2 \sim n_L \lambda^2 \gg 1$ in the domain of interest. Therefore $1/(1 + \lambda^2 J^2)$ can be replaced by $1/\lambda^2 J^2$. Finally we must perform the sum $\Sigma_{J \neq 0}\, 1/J^2$, which depends on the particular lattice considered. Here, we will simplify the calculation by replacing the sum by an integral

$$\sum \frac{1}{J^2} \to \frac{1}{(2\pi)^2} \frac{1}{n_L} \int \frac{dJ_x\, dJ_y}{J^2} \to \frac{1}{2\pi n} \int_{J\,\min}^{J\,\max} \frac{J\, dJ}{J^2}$$

$$= \frac{1}{2\pi n_L} \ln \left| \frac{J\,\max}{J\,\min} \right|$$

with $J\,\min \sim 1/d$ and $J\,\max \sim 1/\xi$ (the Fourier components relative to the interior of the hard core must be excluded). We finally find

$$F = \frac{B^2}{8\pi} + \frac{B}{4\pi} H_{c_1} \frac{\ln \beta d/\xi}{\ln \lambda/\xi}$$

$$G = F - \frac{BH}{4\pi} \tag{3-64}$$

In (3-64) β is a numerical constant of the order unity (for the triangular lattice, Matricon has calculated $\beta = 0.381$). The B(H) relation is obtained as usual by imposing $\partial G/\partial B = 0$. This gives

$$H = B + H_{c_1} \frac{\ln\left(\beta' \frac{d}{\xi}\right)}{\ln \frac{\lambda}{\xi}} \tag{3-65}$$

where $\beta' = \beta\, e^{-1/2}$ and where d is always related to B by Eq. (3-59). The logarithmic dependences predicted by (3-65) are in rather good agreement with the experimental data on reversible magnetization curves in materials with $\lambda \gg \xi$.

DOMAIN $n_L \sim \xi^{-2}$

Here, as already pointed out, our simple model breaks down, and we shall need a more elaborate approach based on the Landau-Ginsburg equations (Chapter 5). The upper critical field H_{c_2} is of order Φ_0/ξ^2. This, physically, corresponds to the onset of overlap between the hard cores.

Problem. Compare the Gibbs function in the filamentary structure described above with that of a possible laminar structure.

Solution. As before, we shall limit our considerations to the case $\lambda \gg \xi$. The laminar structure will be formed of planes, for example, perpendicular to the x axis, and equidistant (spacing d)(Fig. 3-8). In the neighborhood of each of these planes, over a thickness $\sim 2\xi$, the superconductivity is strongly perturbed (N regions). In the remainder (S regions), the density of superconducting electrons has the value n_s. Such a model has been discussed in detail by Goodman (1961). The fields h(x) (parallel to the z axis) are determined by the London equation

$$h = \lambda^2 \frac{d^2 h}{dx^2}$$

except in the thin (N) regions. The solution is of the form

$$h = H_m \cosh(x/\lambda)/\cosh P$$

where $P = d/2\lambda$ and H_m is the field in the N regions. The free energy of the (S) regions becomes, from (3-26),

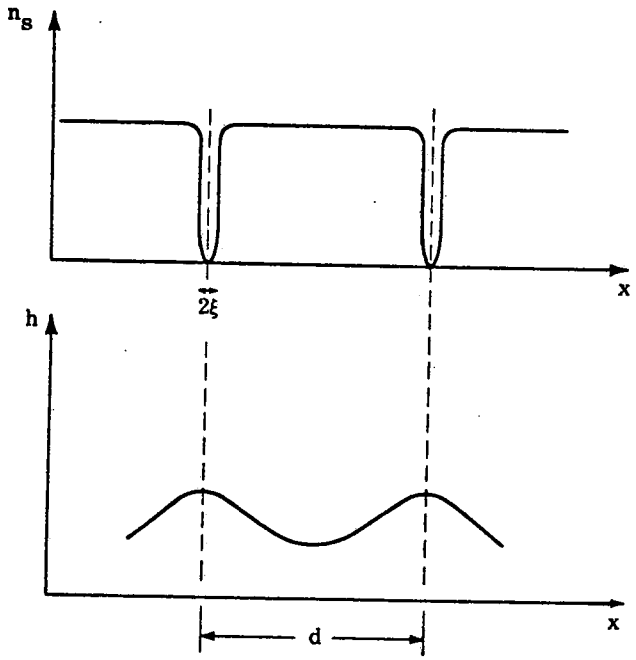

Figure 3-8
The laminar model for the Schubnikov phase. Thin normal sheets N of thickness $\sim 2\xi$ alternate with superconducting sheets S. The N sheets repel each other. The range of the repulsive forces is the penetration depth λ.

$$F_1 = \frac{2}{d}\int_0^{d/2} dx\, \frac{h^2 + \lambda^2\left(\frac{dh}{dx}\right)^2}{8\pi} = \frac{H_m^2}{8\pi}\frac{\tanh P}{P}$$

t is necessary to add the formation energy of the N regions

$$F_2 \cong \frac{H_c^2}{8\pi}\frac{2\xi}{d} = \frac{H_c^2}{8\pi}\frac{1}{P\kappa}$$

where $\kappa = \lambda/\xi$. Finally, to obtain the Gibbs function, we must add a term

$$-\frac{BH}{4\pi} = -H\frac{H_m}{4\pi}\frac{\tanh P}{P}$$

$$G_{laminar} = \frac{\lambda}{8\pi}\left[H_m^2\frac{\tanh P}{P\kappa} + \frac{H_c^2}{P} - 2HH_m\frac{\tanh P}{P}\right]$$

On minimizing G with respect to H_m we obtain $H = H_m$.

$$G_{laminar} = \frac{1}{8\pi P}\left[-H^2\tanh^2 P + \frac{H_c^2}{\kappa}\right]$$

For $H < H_c/\sqrt{\kappa}$ the minimum G is obtained for infinite P, which corresponds to a complete Meissner effect. For $H > H_c/\sqrt{\kappa}$ the minimum occurs for finite P. The initial field for penetration is therefore $H_c/\sqrt{\kappa}$ for the laminar model. This is to be compared with the result for the vortex line model, Eq. (3-56).

$$H_{c1} = \frac{\pi}{\sqrt{24}}\frac{H_c}{\kappa}\ln\kappa \quad (\kappa \gg 1)$$

for $\kappa \gg 1$, $H_{c1} < H_c/\kappa$. For $H_{c1} < H < H_c/\kappa^{1/2}$, we have

$$G_{vortex} < G_{Meissner}$$

$$G_{laminar} = G_{Meissner}$$

therefore, $G_{vortex} < G_{laminar}$; that is, the vortex state is more favorable in the weak induction domain.

It is also possible to make the comparison in the region where H is larger ($H \sim H_c$, for example). We are then in the region $P \ll 1$ for the laminar model By expanding $\tanh P \cong P - P^3/3$ and minimizing G, we obtain

$$G_{laminar} = -\frac{H^2}{8\pi} + \left(\frac{3}{2\kappa}\right)^{2/3}\frac{H_c^{4/3}\,H^{2/3}}{8\pi}$$

In the vortex line model, the potential is determined from (3-64) and (3-65)

$$G_{vortex} = -\frac{1}{8\pi}(H - H')^2$$

$$H' = H_{c1}\frac{\ln \lambda/d}{\ln\kappa} = \nu\frac{H_c}{\kappa}$$

where ν is a constant of order unity. For $T = 0$

$$\nu = \frac{\pi}{24}\ln\frac{\lambda}{d}$$

In the region of interest $H' \ll H$ and

$$G_{vortex} = -\frac{H^2}{8\pi} + \nu\frac{HH_c}{4\pi\kappa}$$

$$\frac{G_{\text{laminar}} + \frac{H^2}{8\pi}}{G_{\text{vortex}} + \frac{H^2}{8\pi}} = \text{const}\left(\frac{\kappa H_c}{H}\right)^{1/3}$$

when $H < \kappa H_c$ (which roughly corresponds to the upper critical field H_{c2}), $G_{\text{laminar}} > G_{\text{vortex}}$. Thus the vortex state is still most stable in the intermediate and high field regions.[4]

Problem. Discuss the equilibrium magnetization curves for a second kind superconductor in the form of an ellipsoid of revolution, the field being applied along the ellipsoidal axis.

Solution. The equations div $\mathbf{B} = 0$, curl $\mathbf{H} = 0$, and $\mathbf{B} = (\mathbf{H}/|\mathbf{H}|)B_e(H)$, where $B_e(H)$ is the equilibrium induction in the presence of a field H measured for a long cylinder, allow a solution where B and H are constant in the ellipsoid with $H = H_0 - NM = H_0 - N(B - H)/4\pi$ where N is the demagnetizing coefficient of the ellipsoid. The relation between B and the applied field is therefore given by the implicit formula

$$G = B_e\left(\frac{H_0 - \frac{NB}{4\pi}}{1 - \frac{N}{4\pi}}\right)$$

B is nonzero for $H_0 > H_{c1}(1 - N/4\pi)$. The slope $(dB/dH_0)_{B=0}$ is finite and equal to $4\pi/N$. The upper critical field remains equal to H_{c2} since $B(H_{c2}) = H_{c2}$ when the transition is second order.

Problem. Discuss the scattering of slow neutrons by a regular lattice of vortex lines in a superconductor.

Solution. The interaction between neutron and lines is $\mu_n h(\mathbf{r})$ where $\mu_n = 1.91\, e\hbar/Mc$ is the neutron moment and M the neutron mass. Consider a scattering event where the neutron momentum changes from $\hbar\mathbf{k}_0$ to $\hbar(\mathbf{k}_0 + \mathbf{q})$. The corresponding scattering amplitude is given by the Born approximation formula

$$a = \frac{M}{2\pi\hbar^2}\int \mu_n h(\mathbf{r})\, e^{i\mathbf{q}\cdot\mathbf{r}}\, d\mathbf{r}$$

This is nonzero only if $\mathbf{q} = \mathbf{J}$, where $\mathbf{J}$ is a reciprocal lattice vector associated with the two-dimensional "line lattice." From (3-62) we find

[4]These elementary calculations of G are not sufficient in the neighborhood of H_{c2}. We return later to a study of the region using the Landau–Ginsburg equations.

$$\int h(\mathbf{r})\, e^{i\mathbf{J}\cdot\mathbf{r}}\, d\mathbf{r} = \frac{BV}{1 + \lambda^2 J^2} = \frac{n_L \phi_0 V}{1 + \lambda^2 J^2}$$

where V is the sample volume and n_L the number of lines per cm^2. Thus

$$a_J = \tfrac{1}{2}\, 1.91\, \frac{n_L V}{1 + \lambda^2 J^2}$$

For a triangular lattice of lines with nearest neighbor distance d, we have $n_L = (2/\sqrt{3})(1/d^2)$ and, for the first reflection, $J = (4\pi/\sqrt{3})\, d^{-1}$. Taking B = 2000 G ($n_L = 10^{10}$), we get $d \sim 10^3$ Å and $J \sim 6.7\ 10^5\ cm^{-1}$. For $\lambda = 1000$Å this gives $(\lambda J)^2 \cong 45 >> 1$. We compute the amplitude a per atom (since this is the quantity familiar to experimentalists). Inserting for V an atomic volume of 30Å^3 we get $a \cong 0.7\ 10^{-13}$ cm. The corresponding "coherent scattering cross section" is $4\pi a^2 \sim 5 \times 10^{-28}\ cm^2 = 0.5$ millibarns—a small, but measurable value.

The scattering angle θ for this first reflection is very small $\theta \cong (J/k_0) = (2/\sqrt{3})(\lambda_n/d)$ where we have introduced the neutron wavelength $\lambda_n = 2\pi/k_0$. At best, with subthermal neutrons we can make λ_n as large as ~5Å. For the above example this leads to angles $\theta \sim 6.10^{-3}$ rad (or 20' of arc). The experiment has been performed on Nb metal (Cribier, Jacrot, et al., 1964). Due to the $1/(1 + \lambda^2 J^2)$ dependence of a, it has been possible only to observe the first reflection (with the smallest J). (See Fig 3-9.)

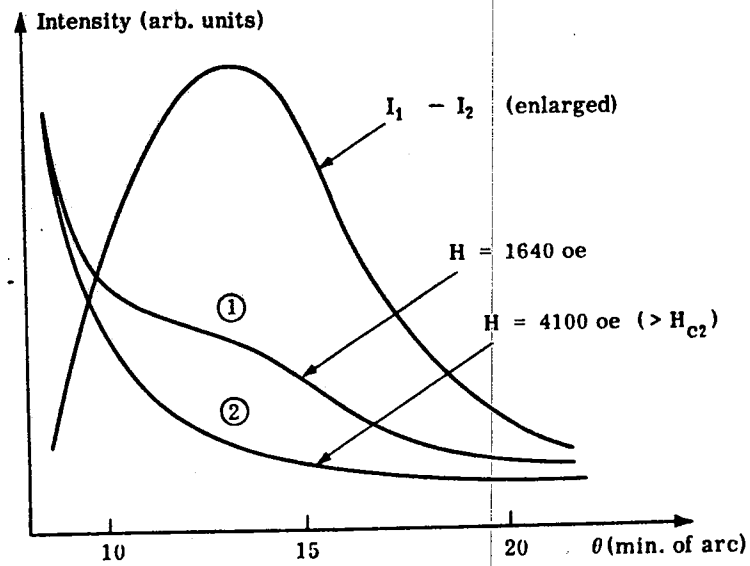

Figure 3-9
Neutron scattering by an array of vortex lines in niobium metal at T = 4.2° K. (Courtesy of D. Cribier.)

Problem. Calculate the broadening of a nuclear magnetic resonance line arising from the field inhomogeneities associated with the vortex state (P. Pincus, 1964).

Solution. In intermediate fields $H_{c1} \ll H \ll H_{c2}$ where the vortices form a dense lattice, the field distribution is given by the Fourier transform of Eq. (3-62). A knowledge of all the moments of the field distribution would completely determine the nuclear magnetic resonance line shape (if this were the only source of broadening). However if the line does not have anomalous wings, as is often the case (Jaccarino and Gossard, 1964), the second moment is a good measure of the line width (see A. Abragam, *Principles of Nuclear Magnetism*, Clarendon Press, 1961). Thus the line width is given by

$$\Delta H = [\langle h^2 \rangle - \langle h \rangle^2]^{1/2}$$

where $\langle\rangle$ denotes a spatial average. The term $\langle h \rangle$ is just $n_L \phi_0 = B$. $\langle h^2 \rangle$ can easily be calculated from Eq. (3-62):

$$\langle h^2 \rangle = S^{-1} \int h^2(\mathbf{r})\, d\sigma = \sum_J h_J h_{-J} = n_L^2 \phi_0^2 \sum_J [1 + (\lambda J)^2]^{-2}$$

where S is the surface area of the sample perpendicular to the field. On replacing the sum over reciprocal lattice vectors by an integral in a similar manner as is done in the text after Eq. (3-63), we obtain

$$\Delta H = \frac{B}{\sqrt{4\pi}} \frac{d}{\lambda} \left[1 + \left(\frac{2\pi\lambda}{d}\right)^2\right]^{-1/2}$$

where for simplicity we have assumed a square lattice. This result is valid in the domain $d \gg \xi$. In the intermediate field region $d \ll \lambda$, this leads to

$$\Delta H \cong \frac{1}{\sqrt{2}} \times \frac{\phi_0}{(2\pi)^{3/2} \lambda^2}$$

Notice that this width is of the order of H_{c1} (for V_3Ga, $\lambda \sim 2000$Å, $\Delta H \approx 20$ Oe) and remains nearly field independent on to fields of the order of H_{c2} where the inhomogeneous broadening vanishes. For fields near H_{c1} ($d \gtrsim \lambda$), the broadening is more severe. More detailed calculations of the line shape using Eq. (3-62) have been performed by Matricon.

Problem. Compute the energy of a vortex line near the surface of the specimen, the line being parallel to the surface.

Solution. Let the line, and the fields, be parallel to the z axis, the limiting surface being the y0z plane, the sample occupying the half-space $x > 0$. The field $\mathbf{h}(\mathbf{r})$ is governed by the equation

$$\mathbf{h} + \lambda^2 \operatorname{curl}\operatorname{curl} \mathbf{h} = \phi_0 \delta_2(\mathbf{r} - \mathbf{r}_L)$$

where $\mathbf{r}_L$ represents the two-dimensional coordinate of the line [we shall take

$\mathbf{r}_L = (x_L, 0)$] and ϕ_0 is a vector, of length ϕ_0, along z. The boundary conditions on the surface are

$$\mathbf{h} = \mathbf{H} \qquad (\operatorname{curl} \mathbf{h})_x = 0 \qquad \text{(0 normal current)}$$

where H is the applied field. The solution $\mathbf{h}(\mathbf{r})$ will be written as

$$\mathbf{h} = \mathbf{h}_1 + \mathbf{h}_2$$

where $\mathbf{h}_1 = \mathbf{H} \exp(-x/\lambda_L)$ represents the field penetration in the absence of any line, while $\mathbf{h}_2$ is due to the line, and can be obtained by a method of images. To the line $(x_L, 0)$ we add an image of opposite sign located at $(-x_L, 0)$ and take for $\mathbf{h}_2$ the algebraic sum of the field due to the line and image. Thus $\mathbf{h}_2$ automatically vanishes on the limiting surface $x = 0$ and the boundary condition is satisfied.

Having constructed $\mathbf{h}(\mathbf{r})$, we now compute the thermodynamic potential

$$\mathcal{G} = \int d\mathbf{r} \left\{ \frac{\mathbf{h} + \lambda^2 (\operatorname{curl} \mathbf{h})^2}{8\pi} - \frac{\mathbf{H} \cdot \mathbf{h}}{4\pi} \right\}$$

The integral is taken in the sample volume ($x > 0$) except for the core region of the line, which is excluded. The last term is the microscopic analog of the standard $\mathbf{B} \cdot \mathbf{H}/4\pi$ term for macroscopic systems. We transform $\mathcal{G}$ into a surface integral, using the London equation for $\mathbf{h}$, and we obtain

$$\mathcal{G} = \frac{\lambda^2}{4\pi} \int_{\text{(core and plane)}} d\boldsymbol{\sigma} \cdot (\tfrac{1}{2}\mathbf{h} - \mathbf{H}) \times \operatorname{curl} \mathbf{h}$$

The surface integral $\int d\sigma$ includes the surface of the hard core (giving a contribution $\mathcal{G}'$) and the surface of the specimen (giving a contribution $\mathcal{G}''$). As usual the only important term in $\int_{\text{core}} d\sigma$ (in the limit $\xi \to 0$) comes from the singular term in curl h, and the result is

$$\mathcal{G}' = \frac{\phi_0}{4\pi} (\tfrac{1}{2}\mathbf{h}(\mathbf{r}_L) - \mathbf{H})$$

The second term $\mathcal{G}''$ may be written as

$$\mathcal{G}'' = \frac{\lambda^2}{8\pi} \int_{\text{plane}} d\boldsymbol{\sigma} \cdot \mathbf{h}_1 \times \operatorname{curl} \mathbf{h}$$

since on the sample surface $\mathbf{h} = \mathbf{h}_1 = \mathbf{H}$. Writing curl h = curl $\mathbf{h}_1$ + curl $\mathbf{h}_2$ we can separate in $\mathcal{G}''$ a term involving $\mathbf{h}_1 \times$ curl $\mathbf{h}_1$, which is the energy in the absence of the line, an additive constant we drop from now on. We are left with

$$\mathcal{G}'' = -\frac{\lambda^2}{8\pi} \int_{\text{plane}} d\boldsymbol{\sigma} \cdot \mathbf{h}_1 \times \text{curl } \mathbf{h}_2$$

We rewrite this integral as

$$\int_{\text{plane}} = \int_{\text{core+plane}} - \int_{\text{core}}$$

By making use of London's equation for $\mathbf{h}$, in the region outside the core, we have

$$\int_{\text{core+plane}} d\boldsymbol{\sigma} \cdot \mathbf{h}_1 \times \text{curl } \mathbf{h}_2 = \int_{\text{core+plane}} d\boldsymbol{\sigma} \cdot \mathbf{h}_2 \times \text{curl } \mathbf{h}_1$$

$\mathbf{h}_1$ is not singular near the line axis; thus the core contribution to the right-hand side vanishes when $\xi \to 0$. The integral on the plane also vanishes since $(h_2)_{x=0} = 0$. Finally

$$\mathcal{G}'' = \frac{\lambda^2}{8\pi} \int_{\text{core}} d\boldsymbol{\sigma} \cdot \mathbf{h}_1 \times \text{curl } \mathbf{h}_2 = \frac{\phi_0 h_1(r_L)}{8\pi}$$

$$\mathcal{G} = \frac{\phi_0}{4\pi} [H \exp(-x_L/\lambda) + \tfrac{1}{2} h_2(r_L) - H]$$

[Note incidentally that $\mathcal{G} = 0$ when $x_L = 0$, that is, when the line is just on the surface, since $h_2(x = 0) = 0$.] If we analyze $h_2(r_L)$ into a direct term and an image term, the direct term gives as a contribution to $\mathcal{G}$ the line self-energy $\mathcal{E} = \phi_0 H_{c1}/4\pi$. The image term describes an attraction between line and image, of value $-(\phi_0/8\pi)\, h(2x_L)$ where $h(r)$ is the function giving the field at distance r of a single line (Eq. 3-35). Finally

$$\mathcal{G} = \frac{\phi_0}{4\pi} [H \exp(-x_L/\lambda) - \tfrac{1}{2} h(2x_L) + H_{c1} - H]$$

Discussion

(1) The term $(\phi_0 H/4\pi) \exp(-x_L/\lambda)$ describes the interaction of the line with the external field and the associated screening currents. It has the same form as Eq. (3-50). It is a repulsive term.

(2) The term $-\phi_0 h(2x_L)/8\pi$ represents the attraction between the line and its image. The magnitude of this energy differs from Eq. (3-62) by a factor $\frac{1}{2}$. But the force derived from it has the conventional magnitude $\phi_0 j/c$ [when differentiating $h(2x_L)$ with respect to x_L, we get a factor 2].

(3) The aspect of $\mathcal{G}(x_L)$ for various values of the applied field H is shown on Fig. 3-10. When $H \sim H_{c1}$ there is a strong barrier opposing the entry of a line. We can understand this barrier as follows: When $H = H_{c1}$, $\mathcal{G}(x_L = 0) = \mathcal{G}(x_L = \infty) = 0$. If we start from x_L large and bring the line closer to the surface, the repulsive term ($\sim \exp(-x_L/\lambda)$ dominates the image term ($\sim \exp(-2x_L/\lambda)$. Thus $\mathcal{G}$ becomes positive and we have a barrier. The barrier disappears, however, in high fields as is clear in Fig. 3-13. When $H > H_S = \phi_0/4\pi\lambda\xi$, it can be seen from the equation for $\mathcal{G}$ that the slope $(\partial\mathcal{G}/\partial X_L)_{x_L=\xi}$ becomes negative.[5]

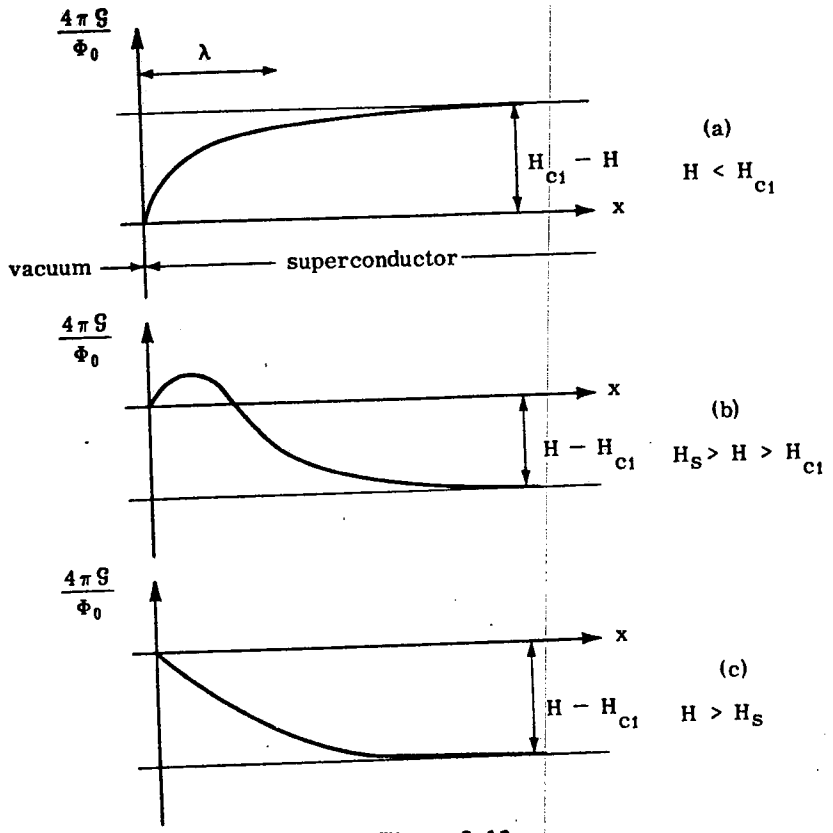

Figure 3-10

Surface barrier impeding the entry of the first flux line is a Type II superconductor. (a) When $H < H_{c1}$, the force on the line always points towards the surface: no lines can exist (in an ideal specimen). (b) When $H_S > H > H_{c1}$ the line gains an energy $(\phi_0/4\pi)(H - H_{c1})$ as it reaches the deep inside of the sample. But there is a barrier near the surface, and the line will not enter if the surface is clean. (c) When $H > H_S$, the barrier disappears.

[5] We shall see later from the microscopic analysis that the field H_S thus defined is of the order of the thermodynamic critical field H_c.

The conclusion is that, at field $H < H_S$, the lines cannot enter in an ideal pecimen (although their entry is thermodynamically allowed as soon as $H > H_{c1}$). These surface barrier effects have been predicted independently by Bean nd Livingston and by the Orsay group. They have been observed experimen- ally on lead thallium alloys (Tomash and Joseph) and on niobium metal (de Blois and de Sorbo). (The sample surface must have very few irregularities n the scale of λ.)

Vortex Line Motions

Consider the two antiparallel vortices of Fig. 3-11. According to Eq. (3-50) they attract each other. Will they move under the action of his force, or will they stand still? This question is very much de- ated at the present time. My personal belief is that in a *pure metal* ach line will drift in the other's velocity field. They will thus both nove at right angle from their common plane, with a velocity

$$v_{drift} = v_{12} \tag{3-66}$$

where v_{12} is the superfluid velocity at point 2 due to the presence of line 1.

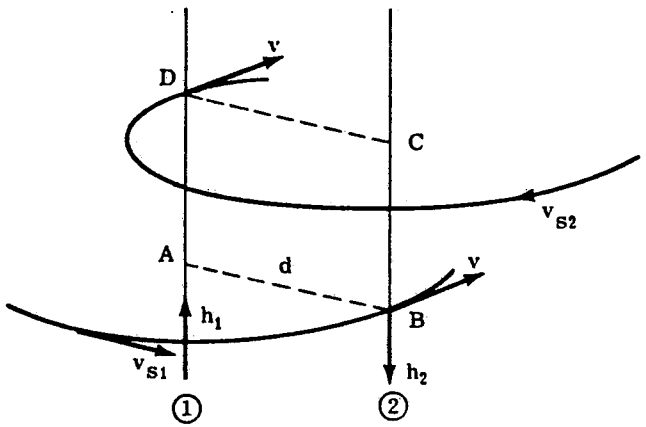

Figure 3-11
Two antiparallel vortex lines in a pure superconductor of Type II. v_{S1} (v_{S2}) is the superfluid velocity induced by line 1 (2). Each line drifts with the local superfluid velocity **v**. For that particular geometry both lines go with the same velocity. Note that **v** is normal to the plane ABCD of the lines.

Such drift motions should lead to amusing collective modes for an assembly of vortex lines in a very pure metal of Type II. (P. G. de Gennes, J. Matricon, 1962.)

In *dirty* superconductors, on the other hand, friction between the lines and the lattice will dominate the motion. The two antiparallel vortex lines AD and CB will then move toward one another, as shown on Fig. 3-12, with a velocity

$$v_{drift}(2) = -v_{drift}(1) = \frac{f}{\eta} \tag{3-67}$$

where f is the attractive force between the lines, as given by Eq. (3-52) and η is a viscosity coefficient. We can estimate η with the following assumptions: suppose that the currents due to line 1 are not distorted near the core of line 2. This core then carries a current density $j = nev_{12}$. But this core is essentially normal. Thus we expect a loss (per unit length of line 2)

$$W = \frac{j^2}{\sigma\pi\xi^2}$$

where $\sigma = ne^2\tau/m$ is the normal state conductivity and ξ the core radius. This power dissipation must also be equal to $fv_{drift}(2) = 1/\eta f^2$. Recalling from Eq. (3-52) that $f = \frac{1}{2}nhv_{12}$, we obtain

$$\eta = \frac{n\tau h^2}{4\pi m\xi^2} \tag{3-68}$$

Viscous motions which are reasonably well described by this type of damping have been observed in dirty materials by Kim and co-workers.

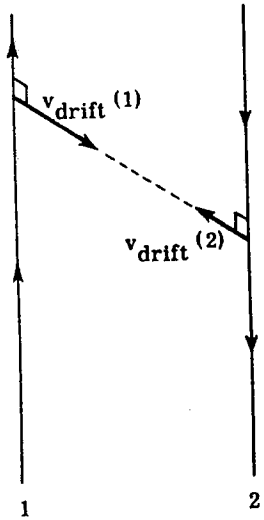

Figure 3-12
Two antiparallel vortex lines in a *dirty* superconductor of Type II: the lines move toward each other with a drift velocity controlled by friction with the lattice.

3–3 NONEQUILIBRIUM PROPERTIES

Up to now, we have restricted our attention to the *reversible* behavior of second type superconductors. We have seen that when the coherence length ξ is small, they can remain superconducting up to very high fields, of order $H_{c_2} \sim \phi_0/\xi^2$.

From a technical point of view, however, what is most interesting is to obtain superconducting wires that can carry high currents. But this condition cannot be realized at thermal equilibrium, as shown by the following argument: Consider a cylindrical wire of radius a carrying a total current I. (When I is weak, this current is, in fact, entirely carried by a surface sheet, of thickness λ, around the cylinder.) The field at the surface of the wire is

$$H = \frac{2I}{ca} \tag{3-69}$$

The situation is stable when $H < H_{c_1}$. When $H > H_{c_1}$, vortex lines begin to appear. They are bent in circles (following the lines of force). Once created at the surface, with radius a, they tend to shrink (to decrease their line energy) and finally annihilate near the axis of the wire. This process dissipates energy. Thus in an ideal specimen we have 0 resistance only if $H < H_{c_1}$ or $I < (ca/2)\, H_{c_1}$. If we want to carry higher currents with our wire, we need to *pin* the vortex lines, that is, to quench their motion by suitably chosen lattice defects, and achieve a nonequilibrium situation. While the field H_{c_2} is an intrinsic property of the metal (or alloy), the critical current measured on a wire is extremely sensitive to the metallurgical state of the sample. This distinction between the factors ruling H_{c_2} and I was stressed first by Gorter.

In practice, a favorable defect structure is obtained by the following procedures:

(1) imperfect sintering (e.g., Nb_3Sn)
(2) cold work (e.g., MoRe alloys)
(3) precipitation processes (e.g., lead alloys)

The resulting materials, with high critical currents, are called *hard superconductors*.

The coupling mechanisms between the lines and the defects are only vaguely known at the present time. A rather simple case is met when we have large cavities, due to imperfect sintering, in the superconducting material. A vortex tends to remain pinned to the cavity, since this corresponds to a smaller length of line in the superconducting material, and thus to a smaller line energy. The mechanical stresses realized by cold work impose slight modifications to the condensation

energy and to the local density of superconducting electrons n_s. This results in local modifications of λ, ξ, and thus of the line energies J and interactions U. These interactions are rather complex, and in the following we only present a phenomenological description of their effects.

Critical State at Zero Temperature

Consider a hard superconductor in an applied magnetic field H (along Oz). In equilibrium the line density would have the value $B(H)/\phi_0$ and be the same at all points. We now consider a metastable situation where the induction B is not equal to B(H) but varies from point to point—say in the x direction. Thus (1) the line density is not constant, (2) there is a macroscopic current $J = (c/4\pi)(\partial B/\partial x)$ flowing in the y direction. The forces acting on the line system can be decomposed in the following way: First, because of the repulsive interactions between lines, the regions of high line density (high B) tend to expand towards the regions of low density. This may be described in terms of the pressure p in our two-dimensional line system.[6] The force (per cm^3) is $-\partial p/\partial x$. This has to be balanced by a pinning force due to the structural defects. This pinning force, however, cannot become arbitrarily large. It must stay below a certain threshold value α_m

$$\left|\frac{\partial p}{\partial x}\right| < \alpha_m \tag{3-70}$$

If at some point $|\partial p/\partial x|$ is larger than α, then the lines start moving and dissipation occurs until condition (3-70) is again satisfied. In practice the line density $(1/\phi_0)B(x)$ will thus adjust itself so that the threshold condition is just realized at all points [equality in (3-70)]. The state thus realized is called the *critical state*, and was first described by Bean. We can get some physical feeling for this critical state by thinking of a sand hill. If the slope of the sand hill exceeds some critical value, the sand starts flowing downwards (avalanche). The analogy is, in fact, rather good, since it has been shown (by careful experiment with pickup coils) that, when the system becomes overcritical, the lines do not move by single units, but rather in the form of avalanches including typically 50 lines or more.

We now proceed to compute explicitly the pressure p of the line system, to be inserted in (3-70). We consider a group of N lines intersecting a surface S in the xy plane. Their energy (per cm along Oz) is

[6] We make an isotropic approximation and neglect the tensor properties of p.

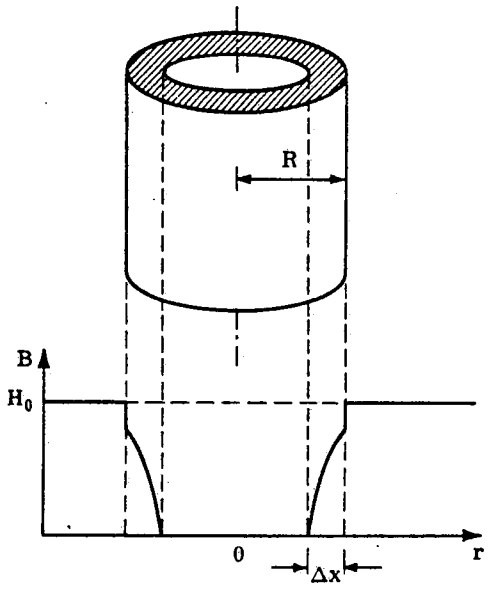

Figure 3-14
Magnetization measurements on a cylinder (external field increasing). The flux lines penetrate only in the hatched area.

(1) If R is much smaller than Δx, the induction is nearly uniform in the sample, $B = B(H)$, $\phi = \pi R^2 B(H)$.[7]

(2) If $R \gg \Delta x$ we have essentially a one-dimensional situation. If x denotes the radial distance, we may write

$$\phi = 2\pi R \int_{R-\Delta x}^{R} dx\, B(x) \qquad (3\text{-}74)$$

At the edge of the flux ($x = R - \Delta x$), we have $B = 0$, $H(B) = H_{c_1}$. At the surface of the cylinder ($x = R$), again assuming no surface barriers, we have the equilibrium value of B corresponding to the external field H. $B = B(H)$. Transforming dx by (3-72) and (3-70), we get

$$\phi = 2\pi R \int_{H_{c_1}}^{H} dH\, \frac{B^2(H)}{4\pi \alpha_{mH}}$$

[7]We assume that there is no surface barrier impeding the entrance of vortex lines in the cylinder. Surface barriers do occur sometimes, but their effects can easily be separated.

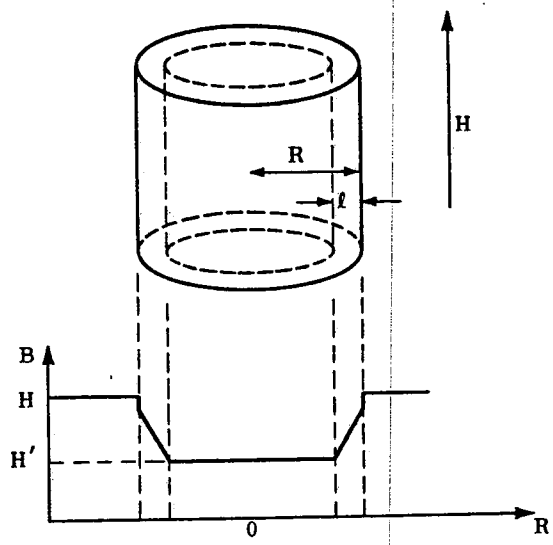

Figure 3-15
Principle of the Kim experiments on hollow cylinders of hard superconductors. An external field H is applied. The field H′ inside the cylinder is measured.

where α_{mH} stands for $\alpha_m[B(H)]$. Of particular interest is the derivative of ϕ

$$\frac{d\phi}{dH} = \frac{R}{2} \frac{B^2(H)}{\alpha_{mH}} \qquad (3\text{-}75)$$

Thus from magnetization measurements in increasing fields, we may derive α_{mH} and $\alpha_m(B)$. Another method, devised by Kim and coworkers, makes use of *hollow* cylinders as shown in Fig. 3-15. A field H is applied on the outside of the cylinder and the field H′ in the cylinder is measured. When H is increased from 0, H′ first stays strictly equal to 0. Then, when the flux front reaches the inner surface of the cylinder, H′ starts to increase (ideally H′ would first jump abruptly to H_{c_1}, and then grow steadily). The interest of the method is to give a direct determination of Δx, for that particular value of H where H′ starts to increase.

More complicated situations are met if the field H is alternatively increased and decreased, as shown in Fig. 3-16. Then we meet regions

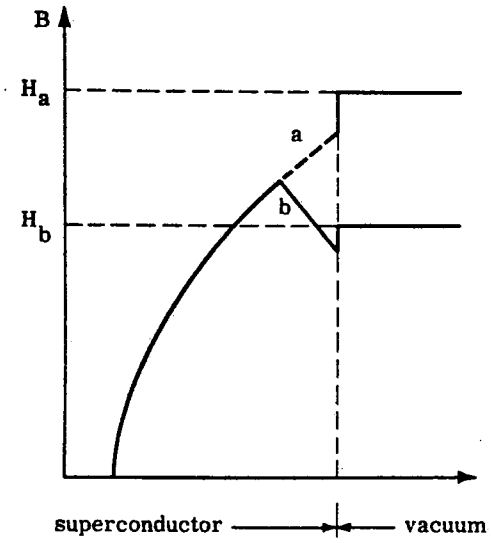

Figure 3-16
Flux distribution in a hard superconductor when the applied field is first raised to H_a (broken curve) and decreases to H_b (full curve).

with $dB/dx > 0$ and regions with $\partial p/\partial x < 0$, but the absolute value $|\partial p/\partial x|$ stays equal to α_m. This permits a detailed calculation of all hysteresis cycles when $\alpha_m(B)$ is known.

Flux Creep at Finite Temperatures

At finite temperatures, if $\partial p/\partial x \neq 0$, the vortex lines will tend to move (from the regions of high B towards the regions of low B) by activated jumps across the pinning barriers. We call the average flow velocity of the lines (in the x direction) v_x. Various methods can be used to detect this flow, or "creep":

(1) Magnetic measurements, with thick cylinders or hollow cylinders. In the latter case, for instance, if H has been raised from 0 to some value and then kept constant, we observe that H' increases slowly in time.

(2) Electrical measurements. If the lines of force are moving, they create electromotive forces that can be measured directly. The most simple situation is represented in Fig. 3-17. A wire (in the y direction) carries a current of density J, and is submitted to an external

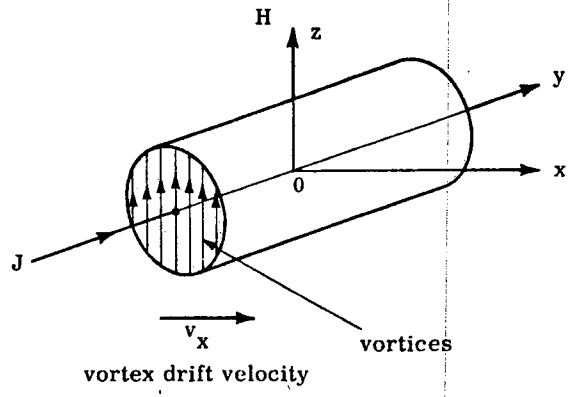

Figure 3-17
Electrical measurements on a hard superconductor wire. There is a current $J = -(c/4\pi)(\partial B/\partial x)$ in the y direction, thus $\partial B/\partial x < 0$. The lines are more closely packed on the left side of the wire: they drift with a velocity v_x towards the positive x axis.

field H in the z direction. Thus we have a nonzero $\partial B/\partial x = 4\pi J/c$ and the lines (pointing along Oz) tend to drift in the x direction. The resulting electric field E_y is along the wire axis (Oy) and in the limit $H \gg H_{c_1}$, it is given by

$$E_y = \frac{Bv_x}{c} \tag{3-76}$$

To prove (3-76) we compute the power dissipation per unit volume: this is the work done by the presence gradient on the lines, that is, $(\partial p/\partial x)v_x$. By setting this equal to $E_y J$ and making use of (3-72'), we get (3-76). Thus we need an electric field E_y to maintain the current J. As pointed out by Anderson and Kim, this dissipative effect in the superconducting state explains many features of the resistive behavior of hard superconductors.

The main difference between (1) the magnetic measurements and (2) the electric ones lies in the order of magnitude of the velocities involved. In case (1) the creep typically is measured over intervals of hours or days, and the velocities are of order 1 mm/day or 10^{-6} cm/sec. In case (2) taking $B = 10^4$ $E_y = 1$ μV/cm, we get $v_x \sim 10^{-2}$ cm/sec. The main difficulty of (2) is related to possible inhomogeneities in the wire; experimentally it is found that different portions of the same wire have different E_y's.

The results show unambiguously that
(a) the creep velocity has an *activation energy* behavior

$$v_x = v_0 \exp(-E/k_B T) \tag{3-77}$$

v_0 is not very accurately known, but may be in the range of 10^3 cm/sec in typical cases. The energy E may be as high as 100°K.
(b) the energy E depends on the pressure gradient $\partial p/\partial x$

$$E = E_0 - \left|\frac{\partial p}{\partial x}\right| \rho^4 \tag{3-78}$$

where ρ has the dimensions of a length, and is typically of order 500Å. We can relate E_0 and ρ to the critical pressure gradient α_m, if we notice that for $T \to 0$ the velocity v_x will depart from 0 only when $E = 0$

$$\alpha_m = \frac{E_0}{\rho^4} \tag{3-79}$$

These results (mainly obtained by Anderson, Kim, and co-workers) have various important consequences. First, since v_x varies rapidly with E according to (3-77), it is possible to extend the crictical state concept to finite temperatures. Define a limiting velocity v_{min} below which the line motion cannot be detected. Then, if

$$\frac{E}{k_B T} > \log \frac{v_0}{v_{min}}$$

the line structure is frozen. Thus the critical state at temperature T corresponds to

$$E_0 - \rho^4 \left|\frac{dp}{dx}\right| = k_B T \log \frac{v_0}{v_{min}} \tag{3-80}$$

$$\left|\frac{dp}{dx}\right| = \alpha_m \left(1 - \frac{k_B T}{E_0} \log \frac{v_0}{v_{min}}\right)$$

In general α_m will depend on T (since α_m involves λ, ξ, and the condensation energy, which are all temperature dependent). But if T is much smaller than the transition point T_0 this dependence may be neglected and all the temperature variation in (3-80) comes from the factor $k_B T$. A linear dependence of $|dp/dx|$ on T has indeed been observed experimentally by Kim on various alloys and compounds—the critical currents of hard superconductors are strongly temperature dependent even when $T \ll T_0$.

Another important consequence of (3-77), pointed out by Anderson, is the possibility of severe thermal instabilities. If in a small region of the sample the pinning energy E_0 is slightly smaller than elsewhere, the vortex lines in this region will dissipate a large power, $[(\partial p/\partial x)\, v_x]$ per cm^3, and this will tend to raise the local temperature, if the thermal conductivity of the material is low. This temperature rise will, in turn, increase the line velocity v_x according to (3-77) and may finally result in an instability. These thermal processes have to be taken into account in the design of superconducting coils.

CONCLUDING REMARKS

Our description of pinning and creep has been strictly phenomenological. Of course, we would like to interpret E_0, ρ, and v_0 in terms of microscopic processes. There are two difficulties:

(1) What is the coupling between defects and lines? As pointed out earlier an important term is related to local modifications of the penetration depth λ by strain or by impurity gradients. Another, more obvious, contribution stems from local modifications of the superconducting condensation energy. There may be other contributions.

(2) How can we describe the metastable equilibrium and the irreversible motions of strongly coupled vortex lines in the presence of random perturbations? Coming back to the sand-hill analogy, we need a theory for the equilibrium slope of the sand hill and a theory for the avalanches—both are complicated. For the vortex line system there is an interesting suggestion, due to Frank—creep may take place by a motion of dislocations in the two-dimensional line lattice.

REFERENCES

Vortex line structure:
A. Abrikosov, *Zh. Eksperim. i Teor. Fix.*, **32**, 1442 (1957), translated by *Soviet Phys.—JETP*, **5**, 1174 (1957).
B. B. Goodman, *Rev. Mod. Phys.*, **36**, 12 (1964).

Reversible magnetization curves:
J. D. Livingston, *Phys. Rev.*, **129**, 1943 (1963).
T. Kinsel, E. A. Lynton, and B. Serin, *Phys. Letters*, **3**, 30 (1962).

Neutron diffraction by lines:
D. Cribier, B. Jacrot, L. M. Rao, and B. Farnoux, *Phys. Letters*, **9**, 106 (1964).

Superconductor Research Pace Quickens

GREG FISHER*
ACerS Director of Technical Services
MICA SCHOBER*
ACerS Technical Services Manager

Another chapter is unfolding in the contributions to modern technology by advanced ceramics, with the advancements surprising the researchers involved, as well as the general scientific community. Specifically, ceramics as superconductors seems a contradictory concept since the more common ceramics for utilitarian and technical uses are insulators intrinsically.

Thus, the announcement by Bednorz and Mueller in *Z. Phys. B.* of the discovery of superconductor properties in La_2CuO_4 brought nothing but skepticism from both the physics and ceramic communities. This was heightened by the lack of convincing proof in their experiments and the fact that previous superconductor testing of $La_{1+x}Ti_{2-x}O_4$ and $BaPb_{1-x}Bi_xO_3$ ceramics revealed no improvements over metal alloy materials such as $Nb_{12}Al_3Ge$ and Nb_3Ge, i.e., a superconductor transition temperature beginning at 13 K vs 21–23 K for the metal alloy.

However, certain ceramics are proving to be the best thing for superconductivity since the theory was first developed. Before explaining how ceramics based on rare- and alkaline-earth copper oxides are advancing superconductivity, a brief explanation of the phenomenon and its historical development is in order.

Superconductor Principles

The most basic phenomenon of superconductivity is the complete disappearance of electrical resistivity as a material is cooled below some critical temperature. This is the phenomenon associated with the discovery of superconductivity, and it has long been linked to properties of materials, particularly metals and metal alloys, at temperatures approaching absolute zero (0 K). Disruption of the zero resistivity property of the materials at temperatures below the critical temperature is found when either a current exceeding a specific value, the critical current density, is passed through the material or a magnetic field of strength greater than a critical field strength is applied to the material.

A second phenomenon associated with superconductors below the critical temperature is diamagnetism or the expulsion of magnetic fields that would otherwise permeate magnetizable materials and create a magnetization within them. This phenomenon is termed the Meissner effect and may be determined by evaluating the magnetic susceptibility of a material, i.e., the magnetic susceptibility of a superconductor drops to zero as it is cooled below the critical temperature.

Superconductivity results from atomic and crystallographic ordering such that the lattice vibrations of the atoms in the crystal structure of the materials (phonons) have little interaction with the conducting electrons, and the conducting electrons are ordered into Cooper pairs. The theory, termed BCS for John Bardeen, Leon N. Cooper, and John Robert Schrieffer, indicates that conducting electrons of opposite spin act in unison.

The specific heat associated with changes in kinetic energy of the electrons in superconductors undergoes a sharp transition at the critical temperature. (The specific heat of the electrons is the difference in specific heat for the lattice—the same for normal state and superconducting materials of equal atomic and X-ray density—and the total thermal energy applied to the material.) The relation of the specific heat of the electrons (C_e) in a superconductor to temperature has two discrete ranges. Well below the critical temperature, log C_e is proportional to $1/T$. Nearer the critical temperature, the relation is more closely approximated by $C_e \propto T^3$. This means an energy gap exists for electrons in a superconductor between the superconducting condition of Cooper pairs to normal conducting or insulating unordered electronic structures. The value for this energy gap, according to the BCS theory, is $2\Delta_0 = 3.53T_c$.

So, for materials with higher transition temperatures, the bonding energy between the Cooper pair electrons is greater. Values for the energy gap are determined from tunneling experiments, where the voltage required to create a sharp rise in the current flowing from a superconductor through an insulator into a normal state, negative biased conductor without supplying thermal excitation to the electrons determines the energy gap, i.e., $V = \Delta/e$.

When two superconductors are separated by an insulating film which has low resistivity, a Josephson junction is formed. This configuration of materials is currently being explored for use in electronic devices for its unique capability of passing current in the form of Cooper pairs via tunneling from one superconductor to the other through the insulating film without applied voltage. The current flow is controlled by magnetic fields in the junction and decreases with higher field strength.

Oscillating currents result in Josephson junction configurations when voltages are applied across the junction. The frequency of the Cooper pairs passing through the junction increases by 4.84×10^{14} Hz for each volt applied. The current carrying capacity, J_c or critical current density, is directly associated with the thermal energy gap of the Cooper pair electrons. At higher current values, large densities of current carriers are present in the superconductor and the interactions with phonons (lattice vibrations), dislocations in crystal structure, and grain boundaries increase significantly. The critical current density is both a function of the current carrier density (number of Cooper pairs per unit volume) and materials processing.

The transition of superconductors to a normal (conductor or insulator) state can be effected by an external magnetic field as well as temperature increase. As already noted, the field strength at which this occurs is appropriately termed the critical field (H_c). These field strength values are measured on long, thin cylindrical or ellipsoidal samples where the field is oriented parallel to the long axis of the sample for a sharp transition to a normal state. In other orientations, slower transitions occur involving increased portions of the sample as the field strength increases. Sharp transitions in the appropriate orientation are indicative of what are termed Type-I superconductors. Even for fields oriented parallel to the long axis of a superconducting sample, some superconductors undergo a more gradual transition to normal magnetic susceptibility. These are referred to as Type-II superconductors.

The Meissner effect, or the complete expulsion of an applied magnetic flux as a material cools below its transition temperature, is found only for Type-I superconductors with the geometry and orientation in the field already described. Other materials, and other orientations of samples, have only a partial Meissner effect, trapping some of the magnetic flux. Just which intrinsic material properties cause magnetic flux trapping or pinning for alloys, semiconductors, and other Type-II superconductors depends on bulk materials properties, as is the case for the critical current density. In fact, the two are related through magnetic flux quantization or the discrete magnetic flux values (fluxoids) that can enter the Type-II superconductors. Currents passing through the superconductor tend to move these fluxoids from different pinning locations

*Member, the American Ceramic Society.

and thus heat the materials, causing them to transform to a normal state.

A skin effect also pertains to the Meissner phenomenon. For even Type-I superconductors the magnetic flux due to an applied field is not expelled completely. Instead, an electromagnetic penetration depth exists where the magnetic flux is pinned in the sample, ranging from 39 to 130 nm for different materials.

Superconductivity occurs in many materials including 27 of the metallic elements in their usual crystallographic form at atmospheric pressure. For 11 chemical elements that are metal, semimetal, or semiconductor, superconductivity occurs at low temperature in conjunction with high pressure. Some materials that are not superconducting in their usual crystallographic form can be made so by producing a highly disordered crystal structure. By the same considerations, some compounds of materials, e.g., Ag_2F, can be superconducting even though the constituents are not. The best superconducting materials produced until recently were V_3Ga, Nb_3Sn, $Nb_{12}Al_3Ge$ (T_c=21 K), and Nb_3Ge (T_c=23 K).

The progress in production of these commercially employed superconductor alloys has been slow in comparison to the events of the past year. Most of the delay in employing the materials, despite the distinct advantages of superconductive materials at superconducting conditions, has been the limitations of engineering refrigeration systems to maintain the materials below their critical temperatures. Ceramic superconductors have begun to alleviate needs for complex engineering of liquid He (boiling point at 4.2 K) refrigeration systems capable of maintaining temperatures below T_c for these metal alloys. But before examining that advancement, a chronology of the developments in superconductivity is needed to place the engineering aspects in proper perspective.

Discovering High T_c

Dutch physicist Heike Kamerlingh Onnes discovered superconductivity in 1911. While working with metals at low temperatures he observed that the electrical resistivity of mercury practically disappears when the material is cooled to near 4 K. Onnes was awarded the Nobel Prize for his research in low temperature physics in 1913. There was no theory to explain such phenomena, so it was assumed that superconductors were similar to other materials, with the only difference being their electrical resistance was zero at low temperatures.

In 1933, more advances were brought to the attention of the scientific community. Previous superconductivity theories were shattered, as it was discovered that such materials were diamagnetic. Experimental evidence soon enabled scientists to formulate a theory of electromagnetic properties of superconductors. As technology progressed in the 1950's, more daring researchers not only defined separate interrelationships in superconducting materials, but also promulgated a theory of superconductive mechanisms.

The efforts of Bardeen, Cooper, and Schrieffer, who were involved in defining those mechanisms, were rewarded in 1972 when they received the Nobel Prize for physics. The BCS theory of superconductivity was thus born. Recently, John Bardeen, one of the original authors of the BCS theory, qualified the mechanism as being adequate for near-absolute zero temperatures, up to ≈40 K. He suggested the necessity for another mechanism at ≥90 K.

The experiments conducted until the 1950's involved metals or metal alloys as the best materials for demonstrating superconductivity. Yet, progress in obtaining a higher T_c was still lacking. In 1973, J. R. Gavaler obtained the alloy Nb_3Ge, with a T_c of a modest 23 K. In practical terms, this simply meant that superconductors were still at a premium, not only from a manufacturing standpoint, but also from a maintenance perspective. Liquid helium had to be used to maintain the very low temperatures required for their adequate functioning. Uses for superconducting metals or alloys were found in giant particle accelerators, medicine, and fast transportation. But the costs involved were still prohibitive, primarily due to helium cooling requirements. Recent discoveries in this field involve the attainment of a much higher—in fact, previously unimaginable—T_c.

Superconductors had been known as metallic compounds. In fact, oxidizing these materials was thought to inhibit superconductivity. Yet, two researchers at IBM Zurich Research Labs, Karl Alex Mueller and Johannes Georg Bednorz, took a different approach in studying superconductivity. In 1983, they began researching metal oxides. In December 1985, Mueller and Bednorz finally obtained a very promising mixed oxide of barium, lanthanum, and copper (BaLaCuO) whose critical superconducting temperature reached 35 K. This discovery drastically improved previous results by 12 K. The research work had been thoroughly documented and published by April 1986. In February 1986, two Japanese scientists, Tetsuya Ogushi and Yoshihisa Osono, reported superconductivity at 44 K in niobium-germanium-aluminum-oxygen thin films.

Obviously, the scientific community quickly questioned the validity of these results. In fact, due to the lack of sensitive equipment at IBM Zurich, Mueller and Bednorz could not test the diamagnetic properties (Meissner effect) of their newly discovered oxide. The structure of the thin film reported by the Japanese researchers was also questioned. Reproducible superconducting properties were soon confirmed by researchers in China, the U.S., and other countries. AT&T Bell Labs undertook a special project on these compounds, accompanied by other major industrial and academic organizations. Soon, AT&T Bell Labs scientists Bertram Bartlogg and R. J. Cava superseded the T_c of 35 K reached by Mueller and Bednorz, attaining 38 K.

During late-1986 and early-1987, discoveries of superconducting materials with ever higher T_c made news almost daily. This sudden enthusiasm was spurred largely by a team of scientists at the University of Houston led by Paul C. W. Chu. They began varying the pressure applied to the so-called BaLaCuO compound. The results were startling. Chu and coworkers attained the highest temperature ever known to allow superconductivity, 52.5 K. The reported discovery made headlines in January 1987. Encouraged by the results, Chu varied the composition of the oxide, by replacing barium with strontium and then calcium, and by replacing the lanthanum with yttrium, reasoning that pressure and smaller cation size might induce a different superconducting mechanism.

Since Chu's first announcement, many other teams have successfully obtained higher T_c's. In March 1987 Marvin Cohen and coworkers at Lawrence Berkeley Lab announced a new yttrium-barium-copper-oxygen compound becoming superconductive at 100 K. In April 1987, Chu again reported superconducting transitions at 97 K in materials whose composition is similar to the original oxide, but otherwise undisclosed.

Given the overwhelming amount of data recently reported and the pace of scientific discoveries in this field, one can only begin to understand to what extent our daily existence might be affected by a new superconductor era. Implications on the engineering aspects of large scale production of superconductors are still largely to be determined.

Materials Processing Factors

The key to developing the superconducting materials based on $YBa_2Cu_3O_7$ or other rare-earth–alkaline-earth copper oxides is the processing parameters used to establish the superconducting phase and produce materials which are free of the so-called "green" phase, or Y_2BaCuO_5, which is not superconducting. At least this is consistent with the findings of those researchers working in materials preparation and finding sharper T_c transitions for purer materials. While it is possible to produce the superconducting compound, or 123 as it is known, through traditional powder processing methodology such as milling Y_2O_3, $BaCO_3$, and CuO powders, chemical precipitation methods are preferred for the production of pure materials and control of impurities. W. F. Hammetter and others from Sandia National Labs indicate they have coprecipitated all of the cations for the Y-Ba-Cu-O compounds through metal salt solution precursors in a mixing cell reactor when the pH of the system was held at 13.5.

Regardless of the source of the raw powders, all researchers reporting to date indicate that a calcining process after milling is essential. Generally, this is best accomplished by pressing the powder to 240 MPa and surrounding it with additional powder to isolate it from the calcining crucible (alumina is preferred). However, some researchers report only calcining the dried, milled powder without prior compaction. In either case, there is still some discrepancy on the best calcining temperature to use. For instance,

P.E.D. Morgan of Rockwell Int'l reports using 500°C calcining temperatures for chemically precipitated powders; most other researchers indicate calcining at 900° to 950°C. However, precautions on the upper end of this calcining temperature have been issued by K. G. Frase, E. G. Liniger, and D. R. Clarke of IBM and R. S. Roth of NBS from work being conducted on the phase diagram of the Y_2O_3-BaO-CuO system. They indicate that for compositions which might be deficient in Y_2O_3 a liquid phase begins to form at ≈930°C.

A second milling of the material has been reported as standard processing procedure for homogenizing the prereacted powder. In some cases the reground material has been sieved, with the finer materials being used to produce research materials and the coarser grades being used as crucible packing for either calcining or sintering stages. The initial calcining has been reported to last from 0.5 to 8 h. One precaution on the reacting phases and starting materials chosen was brought out at the special program on High T_c Superconductor Oxides conducted at the American Ceramic Society's 89th Annual Meeting in Pittsburgh, PA, on April 29: the 1400°C decomposition temperature of $BaCO_3$, i.e., materials calcined at the reported temperatures and times are not fully free of carbonaceous materials if $BaCO_3$ is used as a starting material. Alternative materials such as $Ba(OH)_2$ were suggested during the meeting. For most reports dealing with materials processing to date, air atmosphere is satisfactory for calcining these materials, although some may prefer oxygen atmosphere.

Sintering formed ceramic superconductor material is generally being reported at 950°C, possibly taking advantage of some liquid phase formation in cases where materials are Y_2O_3 deficient. Tarascon has reported firing as high as 1120°C over a 12-h period and held there for 36 h in phase analysis studies, and Hammetter has reported firing at 1100°C for 2 h for the sintering of tape cast specimens.

Because this material, in fact the whole group of copper oxides being examined as superconductors, can be considered to be oxygen sponges, the atmosphere during sintering is critical to the superconductivity of the final product. In fact, the role of oxygen in the structure of the materials is critical to the formation of either an insulator or a superconductor. All researchers report using at least flowing air during sintering to try to preserve the oxygen content of the material. Most are using flowing O_2.

Oxygen-Structure Interactions

Cooling of these materials has been reported at 100°C/min, 200°C/min, furnace cooled, and air quench, depending on the type of study. The cooling rate along with the firing temperature, atmosphere, and soak at temperature all affect the oxygen content of the material and thus its structure. It is the basic structure of the materials that seems to be controlling the

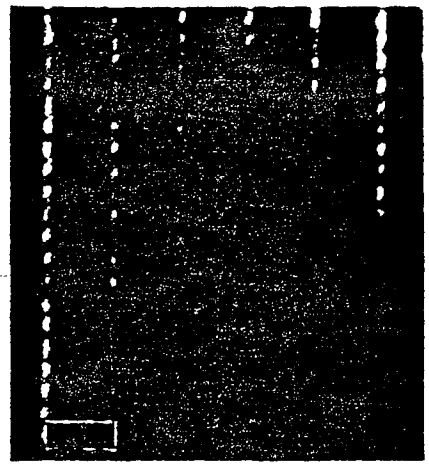

Fig. 1. Shown here magnified ≈20 million times is the first picture, taken by IBM scientists, of the atomic structure of the new high temperature superconductors. The vertical columns of lighter spots consist of copper and oxygen atoms; they are flanked by dark vertical columns of barium atoms. Inside the columns of barium atoms are atoms of yttrium, a rare earth element. The box encloses three atoms that form the basic unit cell which is repeated throughout the material. The box is 1.2 nm long.

superconductivity. Oxygen content alters that structure, as does temperature.

All researchers report that both the La_2CuO_4 and $YBa_2Cu_3O_7$ materials are of the K_2NiF_4 perovskite structure. This structure has a basal plane consisting of copper and oxygen atoms and is layered such that Ba and Y atoms are stacked in the c direction of the unit cell (Fig. 1). The greatest controversy in the physics of these superconductors lies in the function of each atom within the unit cell and its effect on the formation of Cooper pairs. In studies of the effects of Sr doping on the superconducting properties of La_2CuO_4, the optimum concentration of Sr was found to occur where the material was on the verge of a transition from tetragonal to orthorhombic symmetry.

In studies of the $YBa_2Cu_3O_7$ material, effects of rare earth substitution were found by Chu to be insignificant, even when magnetic ions—previously believed to destroy superconductivity—were introduced. When Chu substituted smaller ions for Ba, changes in the T_c were not strictly related to the ion size and the shifts from tetragonal to orthorhombic structure because of possible substitutions of Ca occurring in the Cu lattice sites. Some researchers, among them Bednorz and Mueller, believe that the alkaline earth ions may substitute for rare earths in the structure, yielding a mixed valence state of Cu^{2+} and Cu^{3+} and, thus, an enhanced phonon-electron interaction between oxygen p electrons and copper d electrons in the basal plane of the La_2CuO_{4-y} crystal structure. They also find that those materials that are doped to sufficiently distort their structure to just short of the transition to orthorhombic at room temperature have the highest T_c for onset of superconductivity, i.e., they are the easiest to force into a transition to orthorhombic symmetry upon cooling below room temperature.

Most related to the firing stages of producing these superconducting materials are the transitions in the materials structure with oxygen content. For instance, the $YBa_2Cu_3O_x$ materials will have a tetragonal structure if $x=6.5$ and an orthorhombic structure when $x=6.9$. P. K. Gallagher of IBM and others report that these materials will go from insulating to superconducting to insulating again as oxygen is added to the structure. Those materials with $x=6.38$ are insulating, and when $x>7.1$ they also are insulating. The best superconductors are found with $x=6.98$.

Controlling the oxygen content of the material requires greater control in processing than just supplying flowing O_2 during firing. Observations of weight loss in these materials during firing at >900°C even in oxygen atmospheres indicates that annealing is necessary. Most research has shown that low temperature (500°C) annealing proves better at restoring the oxygen content of the material to values close to $YBa_2Cu_3O_7$.

Annealing times at 450°–500°C are being set anywhere from 2–3 d to 16 h for the best restoration of oxygen into the structure. However, some researchers report annealing at 900°C with favorable result in T_c, while others are using slow cooling to maintain oxygen stoichiometry. Gallagher reports that to keep the oxygen content from going beyond the optimum of 6.98 it would be necessary to reduce the P_{O_2} in the furnace atmosphere as the sample cools to near room temperature and, therefore, annealing at temperatures where oxygen pickup occurs may not be necessary to achieve stoichiometry, provided cooling through the oxygen pickup regime (900°–430°C) is done slowly enough to reach chemical equilibrium with the flowing O_2 atmosphere of the furnace. However, Chu reports (*Science*, vol. 235, p. 567) that the best superconductivity results on $(La_{0.9}Ba_{0.12})CuO_{4-y}$ he produced were for samples that were fired in air for 26 h at 925°C, after calcining at 900°C for 4 h and again for 8 h, when heat treatments at 900°C in a reduced O_2 atmosphere were used.

Early reports of the discovery of these superconducting materials indicated an oxygen defect structure might be playing a key role in the higher temperature onset of superconductivity. There is still some controversy over this position. In the basic structure of the material, the Y atoms require 8-fold coordination, and the Ba require 10- or 12-fold coordination. This gives the appearance of oxygen vacancies in the layered structure. As oxygen content of the material is lowered to <7 the effect is more pronounced but is not critical to the superconducting properties of the material as long as the oxygen content remains within the limits around stoichiometry already defined. For $La_2Cu_2O_x$, according to P.E.D. Morgan, an oxygen vacancy structure in an orthorhombic

Fig. 2. IBM scientists Robert B. Laibowitz and Roger H. Koch shown measuring a superconducting thin film. The graph on the upper PC monitor shows the sudden drop in electrical resistance of the film as its temperature drops below the superconductivity transition temperature after immersion in liquid nitrogen.

material does exist with one-half O vacancy per unit cell. However, Morgan has been able to achieve superconducting properties for this material at 4 K.

Almost all researchers find that as these materials cool past their T_c values a shift in the structure accompanies the superconductivity phenomenon. As this shift in structure occurs, it is believed that the Cu-O bonds in the basal plane of the structure become compressed. This compression yields greater overlap of the Cu *d* and O *p* orbitals and formation of Cooper pairs between these electrons. Testing to determine the lattice vibration interaction has so far yielded negative results, possibly requiring new theoretical treatments for these materials.

Transition Temperature Dependence

The push to obtain materials with high T_c has revealed several key criteria to materials processing for these materials, and how materials processing and compositions influence the transition temperature. The most readily reported influence on T_c for these materials, coming as a result of the advances produced by Chu, is the material purity influence. When more than one phase is present in the ceramic, both the value of T_c (as measured for resistivity) and its sharpness in transition are affected. Purer materials generally have high T_c values and sharp transitions in resistivity dropoff (Fig. 2) on the order of <2 K. However, this does not mean that chemically doped materials may not have sharper transitions and larger T_c values. Some researchers have identified that Sr doping of La_2CuO_4 at 0.15% produces higher T_c values and sharper transitions in resistivity with temperature. Rather, it is the single phase ceramic as compared to multiphase materials that generally have better transitions.

For instance, Wayne State University researchers have observed an anomaly at 240 K for a material which has an onset of temperature vs resistivity drop at 100 K that does not become superconducting until 60 K. Chu has confirmed that this material is multiphase, accounting for the gradual transition in resistivity with temperature.

Other chemical influences on T_c values have been speculated and tested. The first of these was the influence of the lanthanide ion being used. This was, in fact, how Chu made the initial discovery of the $YBa_2Cu_3O_7$ material, by substituting Y for La in the materials examined by Bednorz and Mueller. Extensive tests conducted by Chu indicate that the rare earth ion has no influence on the onset of superconductivity in these materials; even allowing magnetic ions to exist at the lanthanide site did not destroy superconductivity and had little influence on T_c.

Substitution for Ba in these materials does change the T_c value. When smaller Sr ions are used, the structure of the material collapses and the transition temperature is significantly reduced to 77 K from 97 K. However, when Ca ions are substituted, T_c also drops, possibly due to some Ca ions locating in the basal plane, according to Chu. A combination of both Sr and Ca substitutions has been indicated as also producing superconductivity. The size of the magnetic field that will cause restoration of normal (nonsuperconducting) properties of these materials also is somewhat dependent on the transition temperature, at least on how close to the transition temperature the material is when subjected to the magnetic field. For instance, Chu has investigated the upper critical field for $YBa_2Cu_3O_7$, reporting 200–500 T, or $2–5\times10^6$ G. This is compared to a value of 0.5 G for the Earth's magnetic field. Close to the transition temperature, the value for the critical field will drop to zero, as will the critical current density. The high critical field value means that these materials could potentially be used to generate very large magnetic fields when used as the conductor of an electromagnet, provided sufficient current can be passed through it and large enough ferromagnets can be produced. This is the major subject of discussion for Supercollider debates.

Initial investigation by R. J. Cava and others on the $YBa_2Cu_3O_7$ materials showed that critical current densities of 1100 A/cm² could be achieved. Even though this is roughly equivalent to the current densities of copper wire at room temperature, the expectations of much higher current densities for superconductor materials initially seemed to be a road block for these materials.

At the beginning of May 1987, IBM researchers overcame this problem by producing bulk single crystals of the materials of the order of several millimeters wide by 200 μm thick and measuring the critical current in them at 77 K. They discovered that the J_c exceeded 100 000 A/cm² and that a bias in current flow occurs in thicker films. The research team also produced thin film single crystals 1 μm thick by 2.54 cm in diameter. While these single crystals cannot be equated to the current-carrying needs of coils for electromagnets, this research shows that the critical current values obtained by Cava were not indicative of an intrinsic property of the ceramics but were an anomaly of the processing or polycrystalline nature of the materials.

Fig. 3. By adapting a technique called plasma spraying, IBM scientists Richard Guarnieri and Jerome Cuomo and their research team were able to coat a variety of large and smaller objects with high temperature superconducting material. The variety of shapes shown here, including spirals, a large copper panel, and spherical vessels, demonstrate the potential of the IBM technique for making superconducting objects and coatings for advanced scientific research and industrial applications.

Other advances have continued since the discovery of 94–100 K superconductivity onset in the $YBa_2Cu_3O_7$ materials by Chu and others. The first (if any came before others in this fast-breaking field) of these was the discovery of 105 K superconductivity onset identified by the research team at Alfred University headed by Robert Snyder. This material shows sharp reduction in resistivity with drop in temperature. Ongoing investigations at the Nuclear Research Center at Karlsruhe, Fed. Rep. of Germany, under the direction of Constatin Politis, show T_c onset of 120 K for a slight variant of the $YBa_2Cu_3O_7$ material. They have been trying to increase the polaron effect in the material by substituting F for O, producing $YBa_2Cu_3O_8F$. For some time researchers at Wayne State University have insisted that they see the beginning of superconductivity in Y-Ba-Cu-O materials at 240 K. However, the materials they are using are relatively impure and multiphase. They have only seen sharp drops in resistivity beginning at 100 K and full superconductivity at 60 K.

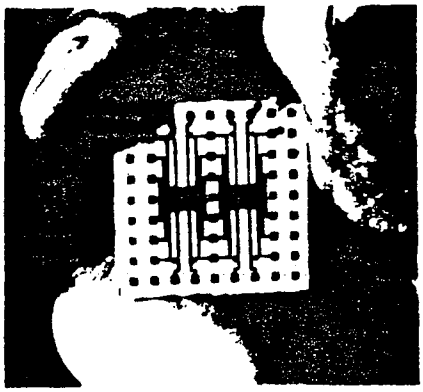

Fig. 4. Closeup of a ceramic substrate patterned with high temperature superconducting wires made with a new IBM plasma spray technique. Such wires might be used to connect logic and memory chips in computers. The superconducting wires were applied by IBM scientists in a pattern similar to those used to connect today's computer chips. The ability to make such wiring patterns from high temperature superconducting material is an important step toward adapting the material for possible future use in computers.

Almost all other research teams working with the Y-Ba-Cu-O system say they can duplicate some anomaly in the resistivity vs temperature curve at 240 K, but few think it represents superconductivity. Some researchers have even speculated that the anomaly could be the onset of semiconductor properties in the material. The researchers at Wayne State believe that they have superconductivity at 240 K for at least a portion of the material due to the generation of an ac current in the material while it is subjected to microwaves, something predicted by the BCS theory for Josephson junctions. They therefore speculate that their material contains phases of superconducting material separated by nonconductors on a microscopic scale in their samples. Because of these anomalous results, most research teams are relying more heavily on magnetic susceptibility measurements rather than bulk resistivity measurements to determine superconductivity.

The most recent announcements of high transition temperatures came from separate sources. Energy Conversion Devices Inc. claimed it produced a superconducting material with zero resistivity at 155 K on May 7, 1987. This was only two weeks after it had found 125 K materials. The firm is holding the composition confidential until it can publicize its findings. Chu has also made major new announcements of increased T_c for this group of ceramic materials. He identified local surface superconductivity in multiphase ceramics with a temperature of 225 K or −47.7°C. Soviet researchers claim superconductors with T_c values of −37°C. However, most of the scientific community remains skeptical of these claims until further reports are available.

Products at Ready

One outstanding aspect of the superconductivity research is the strong rush for commercially feasible products within a few months of initial discovery of the materials and an as yet unexplained physical phenomena. Typically, 20 yr may go by before commercial realization of a materials science development. Perhaps IBM, AT&T, GTE, and many other companies involved sense the great potential for these developments (akin to the development of the transistor or integrated circuit) and are juggling for patent positions. Whatever the reason, not only are researchers working with pressed pellets and disks produced by hot pressing at 349 MPa, but D. W. Johnson of AT&T has shown that ceramic tape with limited flexibility (50–200 μm thick) can be produced with critical current densities at 200 A/cm^2. Presently, he has not disclosed why tape casting has been one of the preferred means of product production.

Others, including the group at AT&T, have been approaching the problem of producing flexible wires with reasonable critical current densities. The AT&T group uses the scheme of placing the ceramic superconductor into an Ag tube and cold-drawing the tube to fine wire thickness. After drawing and coiling to conform to a magnet shape, the wire is fired to convert the ceramic to the fired superconductor material. They indicate that T_c values for these wires are >90 K. There is some discrepancy as to whether Argonne National Lab researchers or those at Toshiba Corp. produced the first wires solely using the ceramic material, but in either case the products are far from the practical materials needed for superconducting electromagnets. Argonne extrudes their wire in 0.2 mm diameter. Initial testing of the critical current density of this wire showed values of only 5 A/cm^2. However, later reports indicate that 191 A/cm^2 is now being achieved.

Techniques of spraying the ceramic material onto the surface of other materials after drawing the substrate into wire form are the focus of current investigations at Alfred University, according to Robert Snyder. This line of production investigation was brought to the attention of most research groups by IBM, which suggested plasma spraying as means to coat the ceramic superconductor material onto large substrates of complex shape, and fabricating conductor lines onto ceramic substrates (Figs. 3 and 4). Most of the research teams see these materials being commercially employed within 2–5 yr.

While superconducting magnets, with the Supercollider as an ideal testing ground since it is government funded, are the principal driving force for many of the investigators, IBM is focusing strongly on the electronic applications of these materials. Josephson junctions are one form of electronics technology in which these materials could be employed, even though IBM at one time abandoned Josephson junction technology as too costly, with little commercial application in their current product line. Other firms, such as

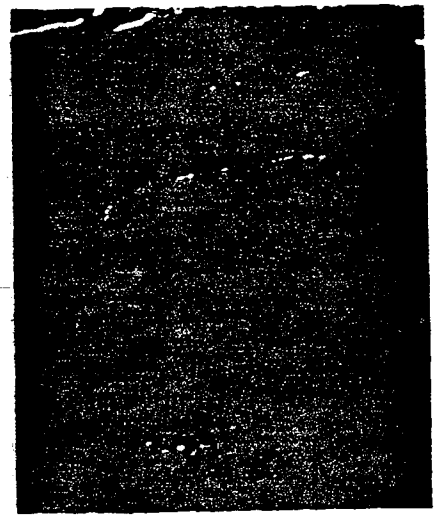

Fig. 5. Seen here magnified >500 times, a high temperature superconducting thin-film electronic device—a "SQUID" (Superconducting Quantum Interference Device)—can be used for extremely sensitive magnetic measurements, even of the tiny magnetic fields caused by electrical currents in the human brain. Made from a class of new superconducting materials discovered by IBM scientists, the new SQUID is only 1/100 the thickness of a human hair. Surface irregularities are in a layer of gold deposited on top of the superconductor.

HYBRES, Elmsford, NY, have developed Josephson junction technology IC chips with rise times of 5 ps, 70 GHz bandwidth, and sensitivities of 50 μV using Nb superconductors, and should be anxious to employ these ceramics in film form. IBM has developed superconducting quantum interference devices (SQUIDS) (Fig. 5) from these ceramics which work as extremely sensitive magnetic detectors (on the order of the field strength generated by electrochemical-neurological impulses produced by synapses in the human brain).

While there is still a great deal of skepticism, especially among those involved in the production of metal alloy superconductors, the developments in ceramic superconductors will lead to a wide range transformation in technology. Already envisioned as benefiting from these ceramic superconductors because of their ability to superconduct when cooled to liquid nitrogen temperatures (let alone the possibilities from the outside chance of superconductors operating at freon coolant refrigeration system temperatures) are: (1) power generation through superconducting magnets, generators, and electromotors in both the conventional fuel and nuclear fusion industries; (2) transportation through electromagnetically elevated trains and battery-powered automobiles with highly efficient superconductor electromotors; (3) microelectronics and computers through increased use of Josephson junctions, zero resistivity interconnects, and high power integrated devices; (4)

medical diagnostics through lower cost nuclear magnetic resonance imaging and neurological research; (5) agriculture and defense through remote sensing in satellite uses; and (6) mining and mineral resources through improved magnetic separators for ore purification.

The fast pace of discovery in this field is generated both by a sense of greatness in the achievements by the individual research teams, some talk of Nobel Prize possibilities arising from the discoveries, the potential impact on society, and the large potential gains that can be achieved in commercial applications. In efforts to support the pace of research, both the Dept. of Energy (DoE) and National Science Foundation (NSF) have directed some of their materials research funding to superconductor research. The DoE has $10 million dedicated to superconductor research at the present time, while NSF doubled its budget to $5 million as the high T_c announcements were being made. Uncharacteristically, NSF also earmarked $1 million for three of its materials research labs—University of Illinois, Northwestern University, and Stanford University—for basic research and $600 000 for research into processing of these materials into usable forms. While this will do a great deal to sustain the effort, panelists at a recent Conference held by the House Republican Task Force on High Technology and Competitiveness encouraged Congress to release $100 million for superconductor research and development, 75% earmarked for manufacturing implementation to prevent the U.S. from losing the technology transfer race in superconductors to Japan, as has happened in other instances.

Suggested Further Reading

Encyclopedia Britannica, pp. 715–19, 1986.

M. D. Lemonick, "Superconductors!," *Time*, May 11, 1987, pp. 64–70, 75.

T. Ogushi and Y. Osono, "Superconductivity in Nb-Ge-Al-O Films above 44 K," *Appl. Phys. Lett.*, 48 [17] 1167–68 (1986).

C. W. Chu, P. H. Hor, R. L. Meng, L. Gao, and Z. J. Huang, "Superconductivity at 52.5 K in the Lanthanum-Barium-Copper-Oxide System," *Science*, January 30, 1987, pp. 567–69.

J. M. Tarascon, L. H. Greene, W. R. McKinnon, G. W. Hull, and T. H. Geballe, "Superconductivity at 40 K in the Oxygen-Defect Perovskites $La_2Sr_xCuO_{4-y}$," *Science*, March 13, 1987, pp. 1373–76.

J. G. Bednorz, K. A. Mueller, and M. Takashige, "Superconductivity in Alkaline Earth-Substituted La_2CuO_{4-y}," *Science*, April 3, 1987, pp. 73–75.

Von B. Grande, Hk. Mueller-Buschbaum, and M. Schweizer, "About Oxocuprates: XV, The Crystal Structure of Rare-Earth Oxocuprates, La_2CuO_4, Gd_2CuO_4," *Z. Anorg. Allg. Chem.*, 428, 120–24 (1977).

R. Dagani, "Superconductivity Seen at Record High Temperatures in Metal Oxides," *Chem. Eng. News*, February 2, 1987, pp. 29–30.

M. Vogel, "Electrifying Breakthrough at Alfred Galvanizes Race Toward 'Superconductor'," *The Buffalo News*, May 10, 1987, H7, H12.

K. G. Frase, E. G. Lininger, and D. R. Clarke, "Phase Compatibilities in the System Y_2O_3-BaO-CuO at 950°C," *Adv. Ceram. Mater.*, in press.

P. W. Anderson, "The Resonating Valence Bond State in La_2CuO_4 and Superconductivity," *Science*, March 6, 1987, pp. 1196–98.

Materials and Processing Report, 2 (1) pp. 1–2.

R. Dagani, "Superconductivity: A Revolution in Electricity Is Taking Shape," *Chem. Eng. News*, May 11, 1987, pp. 7–16.

W. J. Cook, R. Z. Cheanoff, M. Lord, P. Dworkin, J. A. Seamonds, and M. Bosc, "Seeking the Perfect Wire," *U.S. News & World Report*, May 11, 1987, pp. 66–71. ■

THE FOUR POINT ELECTRICAL PROBE

The four point electrical probe is a very versatile device used widely in physics for the investigation of electrical phenomena. Colorado Superconductor Inc. has especially designed two four point superconducting devices from the $YBa_2Cu_3O_7$ and the $Bi_2CaSr_2Cu_2O_9$ materials for such investigations. The **Complete Exploration Kit** an the **Super Exploration Kit** contain four point electrical probes.

When a simple measurement of the electrical resistance of a test sample is performed by attaching two wires to it, one inadvertently also measures the resistance of the contact point of the wires to the sample. Typically the resistance of the point of contact (called contact resistance) is far smaller than the resistance of the sample, and can thus be ignored. However, when one is measuring a very small sample resistance, especially under variable temperature conditions, the contact resistance can dominate and completely obscure changes in the resistance of the sample itself. This is the situation that exists for superconductors.

The effects of contact resistance can be eliminated with the use of a four point probe. A schematic of a four point probe is shown in figure 2. In this diagram, four wires (or probes) have been attached to the test sample. A constant current is made to flow the length of the sample through probes labeled 1 and 4 in the figure. This can be done using a current source or a power supply as shown. Many power supplies have a current output readout built into them. If not, an ammeter in series with this circuit can be used to obtain the value of the current. A 5 Watt power supply capable of producing about 0.5 Amp is required for the experiments described for our superconducting devices.

If the sample has any resistance to the flow of electrical current, then there will be a drop of potential (or voltage) as the current flows along the sample, for example between the two wires (or probes) labeled 2 and 3 in the figure. The voltage drop between probes 2 and 3 can be measured by a digital voltmeter. The resistance of the sample between probes 2 and 3 is the ratio of the voltage registering on the digital voltmeter to the value of the output current of the power supply. The high impedance of the digital voltmeter minimizes the current flow through the portion of the circuit comprising the voltmeter. Thus, since there is no potential drop across the contact resistance associated with probes 2 and 3, only the resistance associated with the superconductor between probes 2 and 3 is measured.

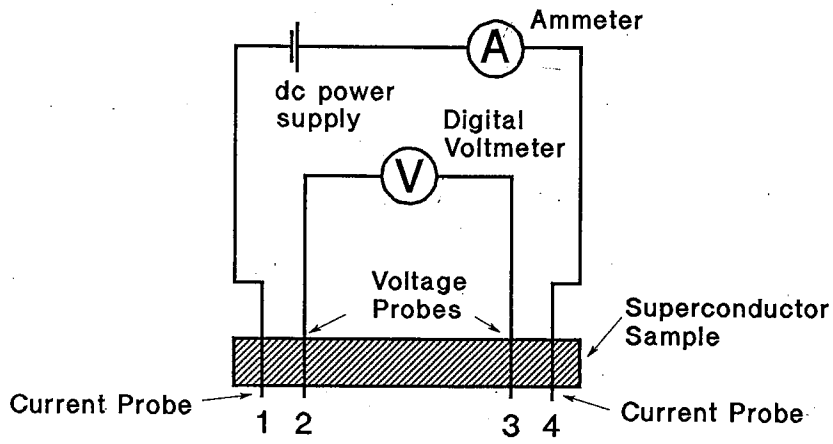

Figure 2: Schematic of Four Point Probe

The four point probe devices in the *Complete Exploration Kit* and the *Super Exploration Kit* are both encapsulated in rugged brass casings. On one side of the casing, the superconductor disk is visible. An aluminum end cap has been inserted on the back side of the brass casing to sealed and to protect the probe connections with the superconductor. Please do not attempt to remove the end cap. A matched thermocouple has also been attached to the superconductor in this casing. This thermocouple is a type 'T', and has been described in detail on page 11.

The $Bi_2CaSr_2Cu_2O_9$ superconductor four point electrical probe casing is larger than the $YBa_2Cu_3O_7$ casing. The former is stamped with a 'B' and the latter with a 'Y' for further identification.

The illustration in figure 3 below, shows the salient features of the four point probe devices. The pair of black wires are current leads for the input of current from the power supply, and have been labelled probes 1 and 4 in figure 2. The pair of yellow wires are the voltage measurement probes for measuring the voltage drop across the superconductor with the help of a digital voltmeter, and have been labelled probes 2 and 3 in figure 2. The red and blue wires are leads for the thermocouple.

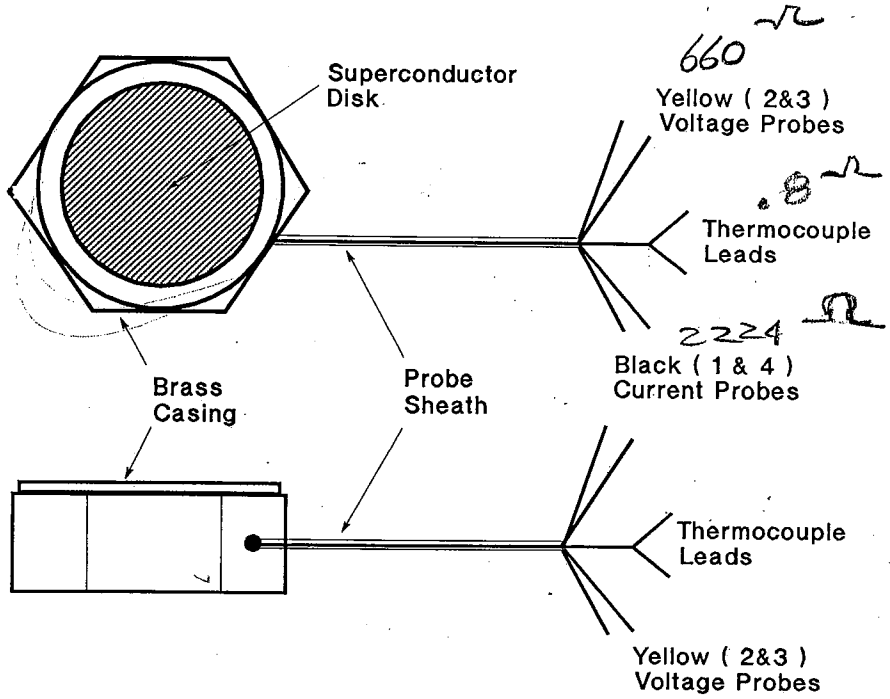

Figure 3: The Superconducting Four Point Probe